FINAL REPORT

CONTRACT NAS5-28713

SMM X-RAY POLYCHROMATOR

MAY 1988

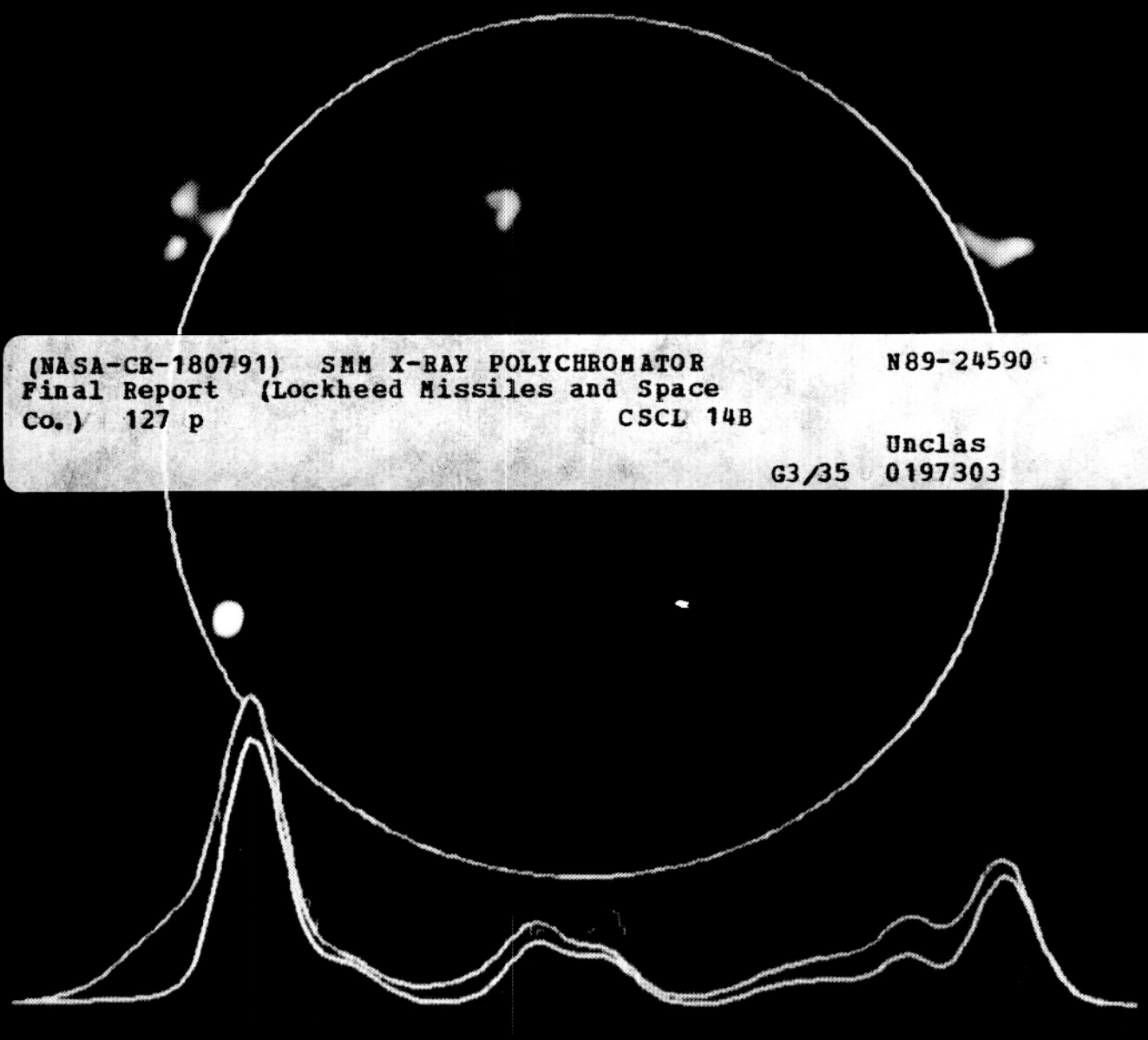

Prepared for

NASA GODDARD SPACE FLIGHT CENTER

by

LOCKHEED PALO ALTO RESEARCH LABORATORY

FINAL REPORT

Contract NAS5-28713

SMM X-RAY POLYCHROMATOR

May 1988

Prepared for
NASA Goddard Space Flight Center
SMM Project Office

by

Dr. Keith T. Strong and the XRP Team

Lockheed Palo Alto Research Laboratory
Dept. 91-30, Bldg. 255
3251 Hanover Street
Palo Alto, CA 94304

Front Cover: *The front cover contains an image of the Sun obtained with the FCS in Fe XVII. The X-ray map represents a mosaic of four arcmin square images, partly from a spacecraft raster over the whole solar disk when the Sun was quiescent, as well as from surveys of the east and west limbs of the Sun showing three new-cycle active regions during flares. Superimposed on this image is a typical BCS spectrum (shown in green) obtained during the rising phase of a flare. The solid lines represent the best fit of a two component model where one component is stationary and the other component represents the upflowing plasma. In this case, the upflowing plasma is traveling at over 300 km* s^{-1}.

This report was compiled and edited by:

Bernhard M. Haisch and James R. Lemen

Contributions were made by the following people:

L.W. Acton	M.D. Morrison
H.S. Bawa	K.J.H. Phillips
E.S. Claflin	D.T. Roethig
S.L. Freeland	S.-ur-Rehman
G.L. Slater	J.L.R. Saba
D.L. Kemp	J.T. Schmelz
G.A. Linford	K.L. Smith
D.P. Mathur	K.T. Strong
D.M. Zarro	M. Greenberg

TABLE OF CONTENTS

1. OVERVIEW

1.1 Introduction 1–1
1.2 XRP Instrument Description 1–3
1.3 XRP Support to the Solar Community 1–6
1.4 Statistics 1–7
1.5 Conclusions 1–9

2. OPERATIONS

2.1 Status of FCS and BCS 2–1
2.1.1 BCS Sequences 2–1
2.1.2 FCS Sequences 2–2
2.1.3 BCS Detectors 2–3
2.1.4 FCS Detectors 2–4
2.1.5 FCS White Light Alignment Sensors 2–5
2.1.6 FCS Gas Systems 2–5
2.1.7 FCS Crystal Drive 2–5
2.1.8 FCS Raster Drive 2–9
2.1.9 XRP Microprocessors 2–10
2.1.10 *SMM* Flare Flag 2–11
2.1.11 Alignment Activities 2–12
2.2 Planning and Evaluation 2–13
2.2.1 IOT Structure 2–13
2.2.2 Planning Observations and Command Generation 2–14
2.2.3 Streamlining and Automation of Command Generation Process . . 2–15
2.2.4 Data Processing 2–15
2.2.5 Cataloguing 2–15
2.2.6 Operations: Evaluation Process 2–18
2.2.7 Operations: Software Developments/Automation 2–18
2.3 Additional Instrument Status Figures 2–21

3. XRP SCIENCE

3.1 Introduction 3–1
3.1.1 Guest Investigator Support 3–1
3.1.2 New Observations 3–2
3.1.3 Coronal Magnetic Structures Observing Campaign (CoMStOC) . . 3–8
3.1.4 Workshops 3–10
3.1.5 Other Science Meetings 3–13

TABLE OF CONTENTS (Continued)

3.2 Science Highlights 3–13
3.2.1 Momentum Balance 3–14
3.2.2 Initial Phase of Chromospheric Evaporation 3–14
3.2.3 Gentle Evaporation 3–15
3.2.4 Density Measurements 3–15
3.2.5 Abundance Measurements 3–16
3.2.6 Active Region Studies 3–16
3.2.7 Two-Ribbon Flares and CMEs 3–17
3.2.8 Radio Studies 3–17
3.2.9 Iron K-alpha 3–18
3.2.10 Energetics of Coronal Loops 3–19
3.2.11 Spectral Atlases 3–20
3.2.12 Modelling 3–21
3.2.13 Atomic Physics 3–21
3.3 XRP-Radio Collaborations 3–22
3.3.1 University of Maryland Solar Radio Group 3–22
3.3.2 Tufts University: K. Lang and R. Willson 3–23
3.3.3 CfA: S. Habbal and VLA: R. Gonzalez 3–24
3.4 Data Analysis Software 3–24
3.4.1 Introduction 3–24
3.4.2 New File Format 3–25
3.4.3 Data Reduction and Application Software 3–26
3.4.4 Data Archiving 3–26
3.5 Data Analysis Hardware 3–30

4. ACKNOWLEDGEMENTS 4–1

APPENDICES

A. XRP Bibliography A–1
B. FCS Spectroscopic Data B–1
C. XRP Flare Catalogue C–1

1. OVERVIEW

1.1 INTRODUCTION

Following the *Solar Max Repair Mission* (*SMRM*) and with the rise in solar activity heralding the onset of cycle 22, interest in exploring high-energy solar phenomena with the *Solar Maximum Mission* X-Ray Polychromator (*SMM*-XRP) has continued to increase. This has been an unprecedented opportunity to improve and extend the XRP solar data sets and to compare coronal conditions and flare types throughout a complete solar cycle. Analysis of these data are presently under way at the Experimenters' Operations Facility (EOF), the three home institutes of the XRP experiment teams, and at many other places around the world where solar physicists are sharing this resource.

The objective of the XRP experiment is to study the physical properties of solar flare plasma and its relation to the parent active region in an attempt to better understand the flare mechanism and related solar activity. Observations have been made to determine the temperature, density, and dynamic structure of the coronal plasma as a function of wavelength, space, and time. The XRP has also determined the temperature and density structure of active regions and flare-induced changes in these regions.

In 1984 the XRP team set a goal of achieving 35 specific scientific objectives in anticipation of the *SMRM*. In the following four years we gathered data on most of these priority sequences, despite operating under solar minimum conditions most of the time (see Figure 1-1). Several of these objectives have been successfully concluded, but often the data have led not only to new scientific results but also to additional questions that require even more sophisticated observations by the XRP. Usually, we have attempted to make a particular type of observation under different conditions (e.g., disk location, flare intensity, temperature extremes), to assess the effects of different geometries, energy densities and initial conditions. We have learned (i) how to improve the observing modes of the two XRP instruments to enhance scientific return, and (ii) how to extend the range of the phenomena that can be studied. Our experience, in conjunction with vigorous collaborations with other *SMM* instrument teams, formal *SMM* guest investigators, and other members of the solar community (informal guest investigators), has led us to identify an ever-increasing list of scientific goals for the XRP.

The *SMM* was designed to make coordinated observations of the Sun simultaneously at a number of different wavelengths. The best scientific return from XRP has been obtained when used in collaboration with other *SMM* instruments

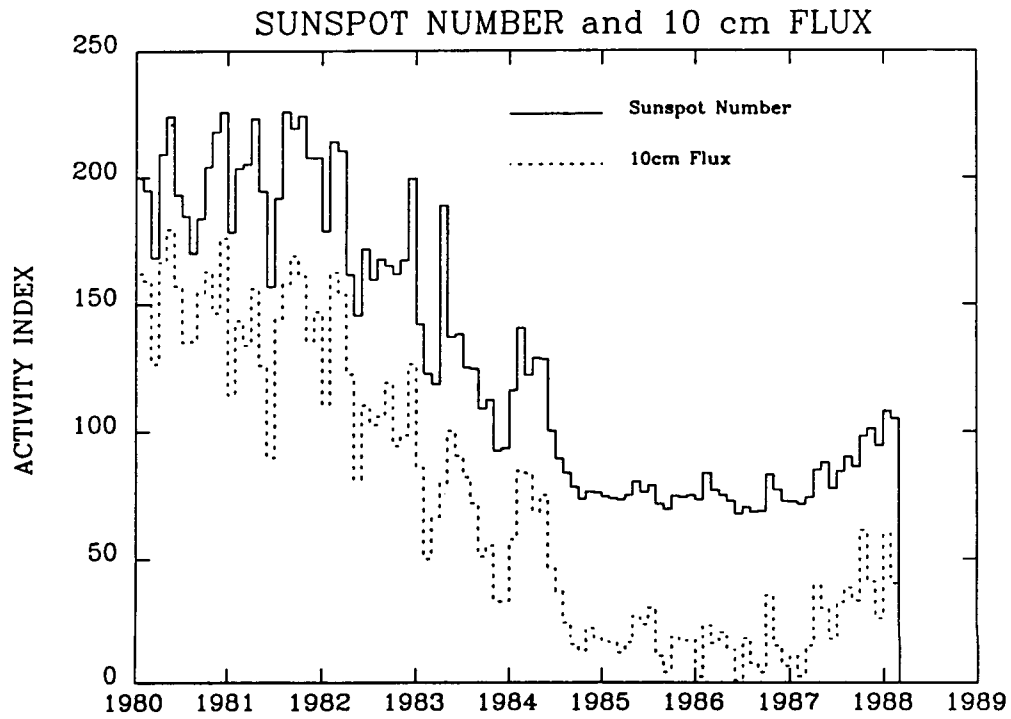

Figure 1-1. Sunspot number and 10 cm Flux variations from the launch of *SMM* to present. Note that solar minimum conditions prevailed from June 1984 until October 1986; since then there has been a rapid increase in both indexes heralding the onset of solar cycle 22.

and ground-based observatories (VLA, SPO, Clark Lake, etc.). One of the XRP team's highest priorities has been to continue this type of collaborative work. New XRP observations and the analysis of existing data will contribute to planning and defining the science objectives of future solar projects, in particular *Solar-A* and *SOHO*.

Another priority that we set in 1984 was to increase the spectroscopic data base from the FCS. In the first year of operations (1980) we obtained only four spectral scans from the FCS, an instrument designed primarily to be a spectrometer. The *SMRM* afforded an opportunity to rectify that situation as we came to understand the problems with the crystal drive mechanism which limited its use in 1980. Since the *SMRM* we have obtained over 400 new spectral scans (see Figure 1-2) which represent a wealth of information on the soft X-ray spectrum of the corona under a wide variety of conditions (from coronal holes to X flares!).

The purpose of this report is to summarize the range of new, exciting observing and analysis programs that we have accomplished with the XRP instruments during the decline of solar cycle 21 and the rise of the solar cycle 22. The document is

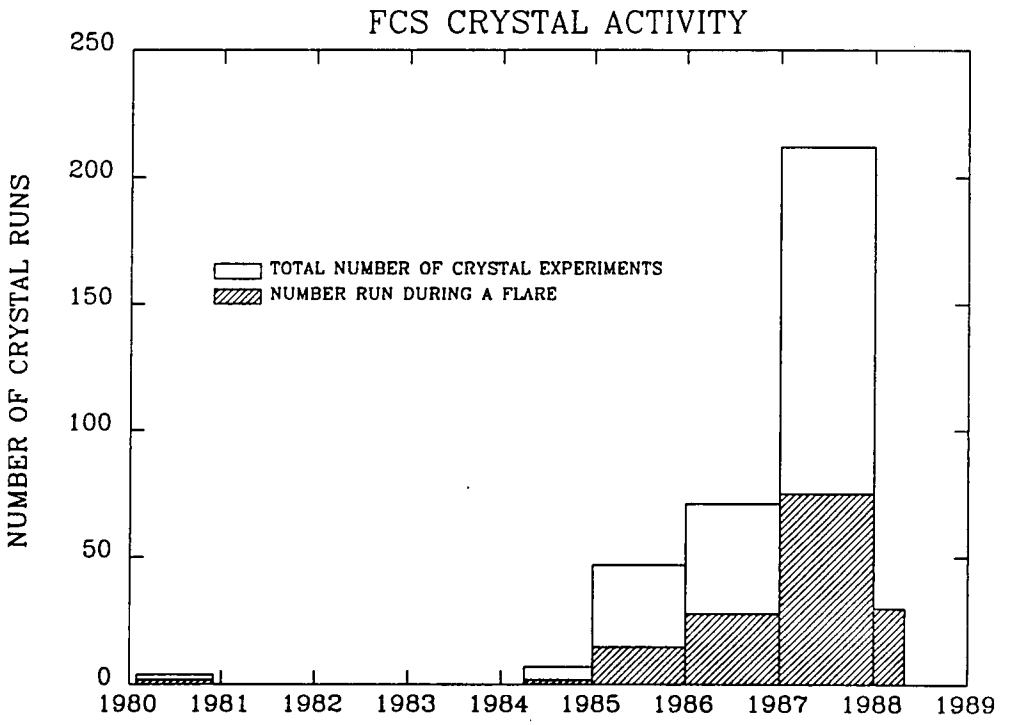

Figure 1-2. The yearly total numbers of spectroscopic scans run by the FCS. Comparing this to Figure 1-1 shows how we have learned to use the wavelength drive more efficiently even in the face of relatively low solar activity. The shaded area shows the number of spectroscopic scans run during flares.

divided into several sections. In §2 we describe XRP operations and its current status. This is meant as a guide on how the instrument is used to obtain data and what its capabilities are for potential users. The science section following (§3) contains a series of representative abstracts from recently published papers on major XRP science topics. It is not meant to be a complete list but illustrates the type of science that can come from the analysis of the XRP data. There then follows a series of appendixes that summarize the major data bases that we have available. Appendix A is a complete bibliography of papers and presentations produced using XRP data. Appendix B lists all the spectroscopic data accumulated by the FCS. Appendix C is a compilation of the XRP flare catalogue for events equivalent to a GOES C-level flare or greater. It lists the start, peak and end times as well as the peak Ca XIX flux.

1.2 XRP INSTRUMENT DESCRIPTION

The primary objective of the XRP is to study the physical conditions in the

corona for a variety of solar phenomena. This is achieved through the use of two complementary instruments (see Figure 1-3): the Bent Crystal Spectrometer (BCS), which continuously monitors the spatially integrated high-temperature flux from flares, and the Flat Crystal Spectrometer (FCS), which can image an area of ≤ 7 arcmin square with approximately 15 arcsec spatial resolution in seven bright spectral lines simultaneously or make rapid scans over a wide wavelength range or at high resolution across individual line complexes. The XRP has data during the peak of the solar cycle (February to November 1980) and during its decline (following the in-orbit repair of *SMM*, starting 24 April 1984).

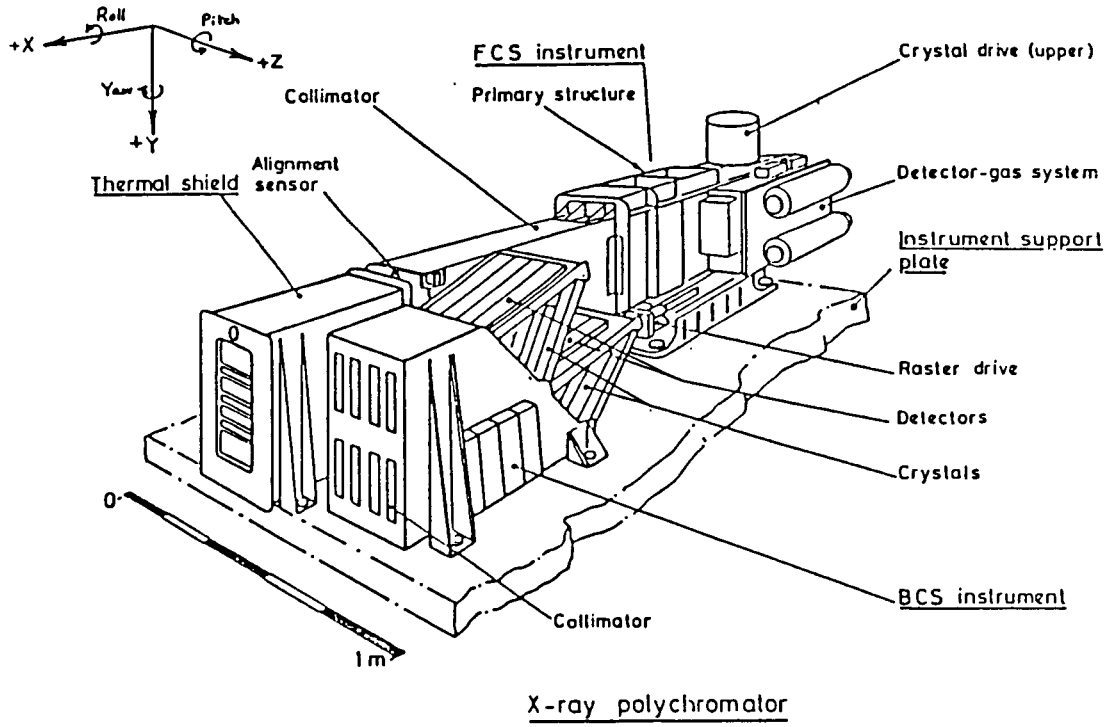

Figure 1-3. Schematic of the FCS and BCS Instruments.

The BCS has eight bent Bragg crystal spectrometers with position-sensitive detectors. It is collimated to 6 arcmin FWHM and is capable of changing its time resolution from 11 s to $\leq$0.5 s by using dynamic memory and sacrificing spectral coverage or resolution. The BCS is sensitive to the high-temperature ($T_e > 10^7$ K) component of the flare plasma; the data are used to determine electron temperature, emission measure, and the dynamics of the plasma. The basic parameters of the BCS are listed in Table 1-1.

Table 1-1. BCS Characteristics

Channel	Ion Stage Number	Wavelength (Å)	Peak T_e (10^6 K)	Resolution $\lambda/\delta\lambda$
1	Ca XIX	3.165 – 3.231	35	3463
2*	Fe^{inner}_{shell}	1.928 – 1.945	2	11206
3	Fe^{inner}_{shell}	1.839 – 1.947	2	4075
4	Fe XXV	1.840 – 1.984	50	3967
5	Fe XXV	1.866 – 1.879	50	8937
6	Fe XXV	1.854 – 1.867	50	8937
7	Fe XXV	1.842 – 1.855	50	8911
8*	Fe XXVI	1.769 – 1.796	60	7005

* Channel only has data for 1980

Table 1-2. FCS Characteristics

Ion Stage	Wavelength (Å)	Peak T_e (10^6 K)	Crystal	Scan Extent (Å)	Resolution $(\lambda/\delta\lambda)$	FOV (arcsec)
O VIII	18.969	3	KAP	13.1 – 22.4	997	16
Ne IX*	13.447	4	Beryl	10.5 – 14.9	2300	15
Mg XI	9.169	6	ADP	7.3 – 10.1	8140	14
Si XIII	6.649	10	Quartz	4.9 – 7.6	5500	14
S XV	5.039	16	Quartz	3.6 – 5.8	10300	13
Ca XIX*	3.173	35	Ge	2.3 – 3.6	5170	14
Fe XXV	1.850	50	Ge	1.4 – 2.1	25100	14

* Channel no longer operational

The FCS has seven Bragg crystal spectrometers that can be scanned in wavelength over a broad spectral range. At the "home position" of the wavelength drive, each channel can monitor the emission from a prominent soft X-ray line. The FCS is sensitive to a wide range of temperatures (2×10^6 K $\leq T_e \leq 7 \times 10^7$ K) and hence can detect everything from quiet-Sun features to flares. By scanning its wavelength drive, the FCS can access an even wider range of soft X-ray lines (see Figure 1-4) and measure Doppler broadenings and shifts. The FCS isolates specific areas in the corona for study by using its narrow collimation. The detailed characteristics of the FCS channels are listed in Table 1-2. For further details of the XRP instrument design and operational capabilities, see Acton *et al.*, Solar Physics **65**, 53, 1980.

The XRP was built by a consortium of three groups: Lockheed Palo Alto Research Laboratory, Mullard Space Science Laboratory, and Rutherford Appleton Laboratory. Research carried out using XRP data is mainly supported by NASA contracts, UK-SERC grants, and the Lockheed Independent Research Program.

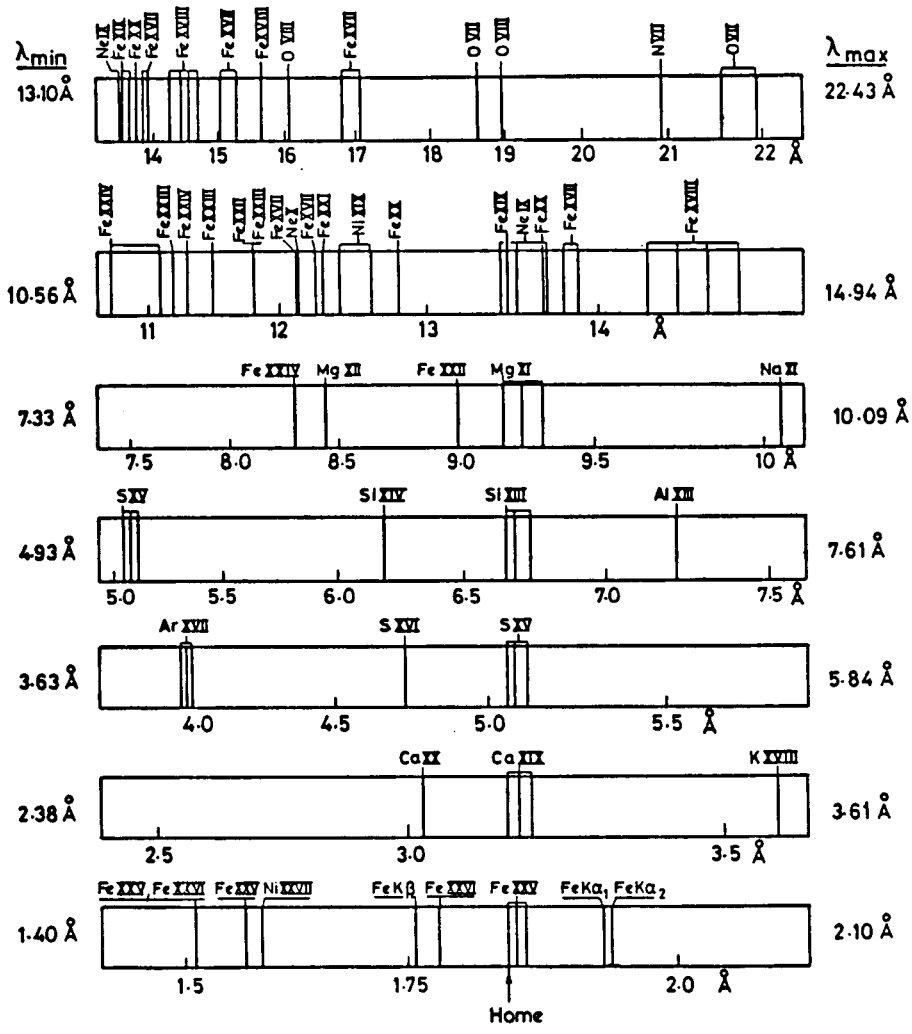

Figure 1-4. The principal soft X-ray lines observable by the FCS in each of the seven channels. Note the location of the "home position" where a strong resonance line is observed in each channel simultaneously.

1.3 XRP SUPPORT TO THE SOLAR COMMUNITY

The XRP has acted as a planning and launch support instrument for all of the *SPACELAB* missions, various rocket-borne solar payloads, and balloons. During the flights of these payloads the XRP has been used in modes to support the science objectives of the experiment. We have also strongly supported any ground-based campaigns or those of other *SMM* instruments. This has often required the expenditure of much extra time in planning and operations work, but we feel that it has

produced excellent data. We hope to continue in this role whenever the opportunity arises. Some examples of this are given below:

- **Coordination with other *SMM* experiment teams.** We have been using the UVSP bright point to identify the footpoints of loops and thus obtain electron density diagnostics and dynamics lower in the solar atmosphere. This has enabled us to initiate the sequence earlier in the flare when coronal conditions are at their extremes. We have had the highly-successful Coronal Mass Ejection Observing program with the C/P instrument to observe coronal mass ejections simultaneously in soft X-rays and white light. A number of high time resolution modes have been developed in conjunction with the HXRBS team. We continue to share data with the HXIS team on coronal arches.
- **Guest Investigator Collaborations.** The XRP has had a large and vital Guest Investigator program to date. The 1988 selection of GI's has not yet been announced, but we look forward to having an equally active program in the years to come. The XRP team has supported over 30 different GI's (official and unofficial); some of their work will be discussed in §3, and the numerous publications that they have contributed are listed in the Bibliography (Appendix A). A particularly fine example of such collaborations was the Coronal Magnetic Structures Observing Campaign (CoMStOC) which brought together over 20 Guest Investigators, ground-based observers and rocket teams to study magnetic fields in the corona.
- **Rocket and Balloon Support.** The XRP team has supported the launch of several solar rocket payloads and balloons, providing them with target information before the flight and science support, when appropriate, during the flight. Similar support was given for the *SPACELAB* Missions.

1.4 STATISTICS

The XRP experiment has taken full advantage of the opportunity provided by *SMRM*. During the 1980 *SMM* operations, which occurred just after the peak of the solar cycle there were 186 M and X class flares, of which the BCS observed only 33, and the FCS saw an even smaller proportion in a useful observing mode (e.g., only two while scanning the wavelength drive). Since the *SMRM* there has been a much lower rate of such events (150 in 4 years compared to 186 in 1980) but because there has often been only one target at a time we have observed them with far higher efficiency, seeing a total of 90 M and X flares with the BCS. The BCS observed 8 of its 10 biggest events since the *SMRM*, including some γ-ray flares (never observed in conjunction with the GRS during 1980) and some events in collaboration with the C/P instrument. The FCS has observed about 20 such large flares while running the wavelength drive. Hence, the probability of observing large flares by the *SMM*

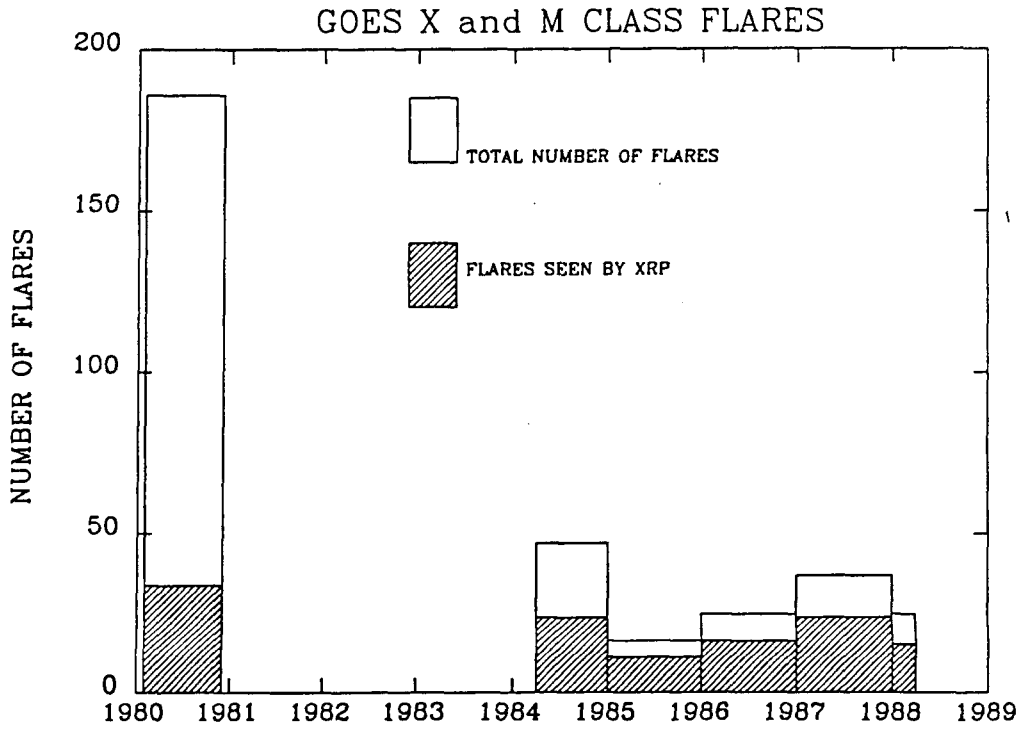

Figure 1-5. M- and X-level Flares observed by *SMM*.

pointed instruments during this solar minimum is comparable to during the last solar maximum.

Figure 1-5 illustrates the number of big flares that have occurred during *SMM*'s operational lifetime. While they tend to follow the solar cycle in numbers it is important to note that they do not completely disappear during solar minimum. However, the proportion of flares observed by the XRP has shown a marked increase (from $\leq 20\%$ to $\geq 50\%$). This is due to several factors: (i) there were fewer regions that could produce flares (often only one on the visible disk at a time compared to over ten regions at the maximum) so we missed fewer flares by being on the wrong region; (ii) the activity came in short bursts often separated by several months which gave us time to prepare for the next one during the lull (spacecraft and instrument calibrations, alignments, sequence testing, etc.); and (iii) the spacecraft and instruments had fewer technical problems which gave us longer effective observing times.

Although operations and planning have taken a major proportion of our time the XRP team and associated Guest Investigators have maintained a good publications record over the years (Figure 1-6). Over 300 publications and presentations have been made (or are submitted) since the launch of *SMM*, and a majority of these since the *SMRM*. Nearly half of these are refereed papers.

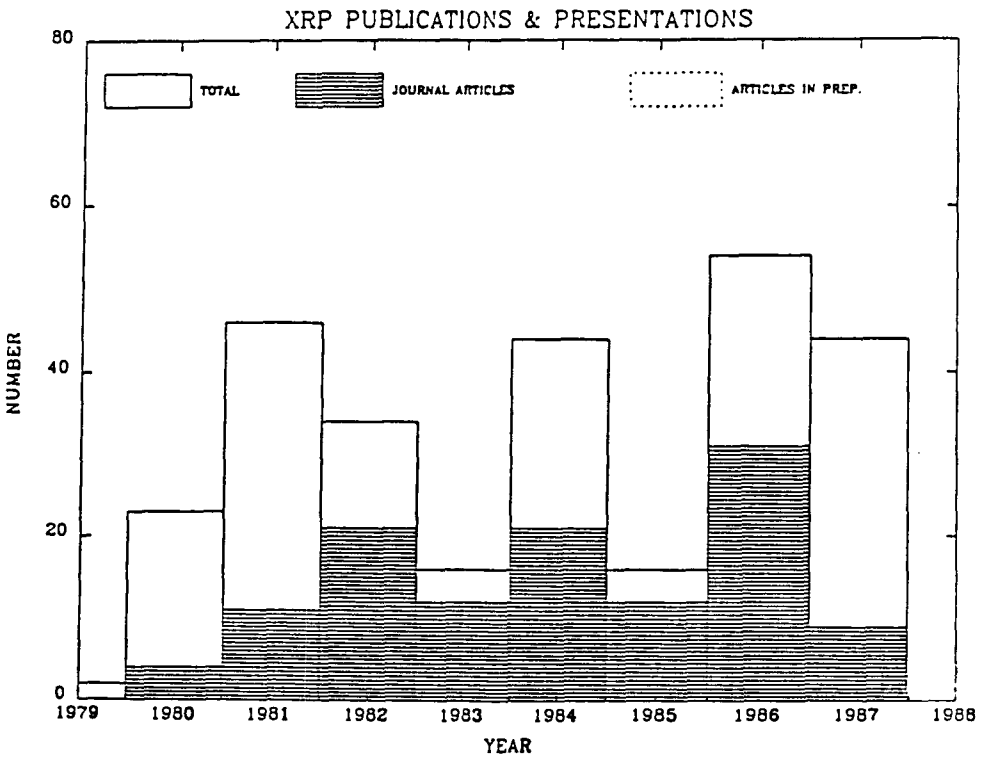

Figure 1-6. XRP Publication Record. The total number of articles and presentations is nearly 300 over the eight years of the mission (122 of which are refereed journal papers). Additional papers are in preparation or have been submitted.

1.5 CONCLUSIONS

Although the XRP has many interesting and potentially important future observations to make, it has managed to build up superb data sets on a number of coronal features; these will prove a useful resource to the whole solar community. Our "open-door" policy has made this resource available to all who ask for it. This policy has helped increase the level of interest in our data and initiated a number of worthwhile projects. More remains to be done, especially in the comparison of observations to theory, but even in this area progress is at long last being made. The XRP team continues to encourage a healthy and well-funded *SMM* Guest Investigator program.

There is a severe shortage of post-doctoral scientists trained in solar physics. This has meant that it has been impossible to hire science or technical staff that do not require extensive training. The XRP team has already trained three non-solar scientists to be productive members of the XRP team and has trained a similar number of technicians in satellite operations. We have also hired a US solar physicist back from Europe. Thus, we feel that we have contributed significantly to bringing

"new blood" into solar physics. This process must be continued if the US wishes to continue to participate in solar studies in the coming-years. Our high school work experience program has trained about 20 senior students in the last 4 years; many of these students have gone to take scientific majors at college. We believe this has been a very worth-while investment in the future of science as a whole and the US space program in particular.

The XRP team plans to continue the support of general solar objectives and the dissemination of the new XRP observations by whatever means possible. We have sponsored a recent workshop on flares and are hoping to have a follow-up session next year. We publish a quarterly newsletter and mail out *précis* of *SMM* papers under the title of "Science Briefings." Six issues have been mailed out in the last year, with four more in the draft stage. We continue to support other meetings (e.g., AAS, AGU and COSPAR) with presentations of our data. We also have a good record of publishing our results since the *SMRM* as discussed in §1.4.

We have learned how to be more efficient in operating the XRP since the *SMRM* and have reached levels of automation and sophistication that were undreamed of when the *SMM* was launched. Our engineering team is one of the most experienced in managing complex flight instruments and will be a valuable resource to the space program when scientific instruments of similar complexity become operational following the resumption of regular NASA launches. We believe that these years of observing the Sun have prepared us to take best advantage of the increase in solar activity that will occur during the rise of cycle 22. The XRP team looks forward to this challenge.

2. OPERATIONS

The X-Ray Polychromator (XRP) on the *Solar Maximum Mission (SMM)* is comprised of two spectrometers: the Bent Crystal Spectrometer (BCS) and the Flat Crystal Spectrometer (FCS). Section 2.1 describes the current status of the XRP. A description of the operations (i.e., planning, command generation, data processing, cataloguing and engineering software) performed at the Experimenters' Operations Facility (EOF) in Building 7 of Goddard Space Flight Center (GSFC) is contained in §2.2. Additional figures relevant to the instrument characteristics and status are given in §2.3.

2.1 STATUS OF FCS AND BCS

The BCS and the FCS are both micro-computer controlled instruments. Therefore, they are capable of being programmed to execute a great variety of observing sequences. General categories of the BCS and FCS sequences are given below. Figure 2-1 shows on and off periods for the BCS and the FCS detectors.

2.1.1 BCS Sequences

Commonly used sequences for the BCS are:

1. All Bins, Normal Time Resolution – This sequence collects data from all operating BCS detectors at the natural time resolution of 7.65 s. This is the most often used BCS sequence.
2. All Bins, High Time Resolution – This sequence collects data from all operating BCS detectors at twice the natural time resolution (i.e. 3.8 s). This is used as a flare response and can collect up to seven minutes of high time resolution data.
3. No Redundancy Sequence, Normal Time Resolution – The BCS detectors contain redundant coverage of some wavelengths (albeit at different spectral resolution). This sequence eliminates the high resolution coverage to obtain higher time resolution (4.3 s).
4. No Redundancy Sequence, High Time Resolution – This sequence is the flare response to the above sequence. This sequence collects up to seven minutes of 2.2 s time resolution data with no redundant spectral coverage.
5. Detectors 1 and 7, Grouped Bins, High Time Resolution – This sequence collects data for detectors 1 and 7 for up to seven minutes of 0.5 s time resolution. Limited spectral coverage for detector 7 is used. This sequence is normally used as a flare response sequence.

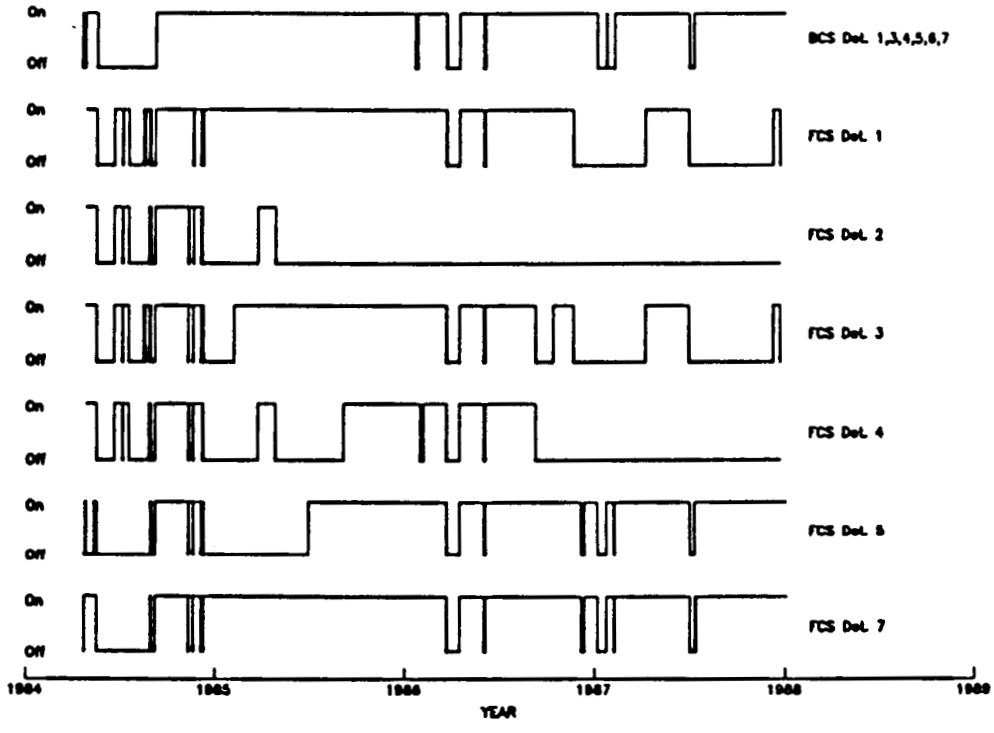

Figure 2-1. The dates when the BCS and FCS detectors were turned on and off.

6. Grouped Bins, Ultra-High Time Resolution – This sequence collects data for all operational BCS detectors with a time resolution of 128 ms. Spectral resolution is sacrificed in order to obtain this time resolution.

2.1.2 FCS Sequences

Some of the FCS observing sequences used can be categorized as follows:

1. Standard Rastering Sequences – These are the most commonly used sequences. Typical rastering sequences execute in the following ways: i) Raster continuously at a fixed size for the duration of an orbit day; ii) Raster to find an X-ray bright point and then take data at the bright point for the remainder of the orbit; iii) Raster to find a bright point and continue rastering around the bright point for the duration of the orbit; and iv) Raster continuously during orbital night for raster lubrication.
2. Survey Sequences – Surveys are similar to standard rastering sequences but require time synchronization with spacecraft repointing commands. Three main types of survey sequences are: i) Active region surveys — used for planning purposes when there is more than one active region on the disk; ii) East limb

surveys — used for planning purposes as well; the idea is to try to observe coronal structures above the limb before an active region rotates onto the disk; and iii) Diachronic surveys — a series of spacecraft repointings and rolls are used to obtain coronal X-ray data above the limb for one complete solar rotation.

3. Startup Sequences – These sequences are normally run during each orbital day. Primarily two types of sequences are used. In one sequence, data is continuously taken until a BCS Flare Flag is received. In the other sequence continuous rastering is done until a flare flag is received. At this point a new rastering or crystal scanning sequence is started.

4. Crystal Scanning Sequences – The FCS Crystal Drive is considered a limited-life resource. Therefore crystal scans occur only in cases where the probability of valuable scientific return is judged to be high by the XRP Science Staff at the EOF. Several types of FCS crystal scans are: i) Active region spectral data collection; this is initiated on a pre-programmed basis when the Science Staff believes that the X-ray emission from the region is sufficient to warrant the use of the crystal drive; ii) Flare spectral data collection sequences; these are run automatically in response of the BCS flare flag; and iii) Spectra at different lines, e.g. Home, Fe XVII, etc.

2.1.3 BCS Detectors

BCS detectors 1, 3, 4, 5, 6, and 7 are all operating normally. BCS detectors 2 and 8 failed during the *SMM* I mission. Since early 1986, the BCS detectors are being turned off during orbital nights in an effort to preserve the lifetime of the detectors. Sample spectra obtained from the operational BCS detectors are shown in Figure 2-15.

BCS Position and PHA (Pulse Height Analyzer) calibrations are done regularly. These calibrations are performed in alternate weeks. BCS PHA calibrations have shown no significant change other than the expected decrease in count rates caused by the decay of the radioactive calibration sources. Sample BCS PHA calibrations and a time history of these calibrations are given in Figures 2-16, 2-17 and 2-18. BCS position calibrations have shown spreading of the BCS calibration lines. This has been caused by the accumulation of carbon on the anode, thus changing its resistance. Calibration lines in BCS detectors 1 and 7 were lost in 1986. Because of this loss, the BCS position calibration database has been expanded to include the position of several resonance lines during the flare decays. This allows us to maintain calibration capability for the detectors. Position calibration time history and sample position calibration plots are shown in Figures 2-19, 2-20, 2-21, and 2-22. One problem with using resonance lines is that the BCS spectra may be shifted depending on where the flare occurred in the BCS field of view. Figure 2-2 shows this bin shift due to the emission offset with respect to the BCS field of view

for Channel 1 (Ca XIX). Work is currently underway to normalize the calibration database for this anomaly.

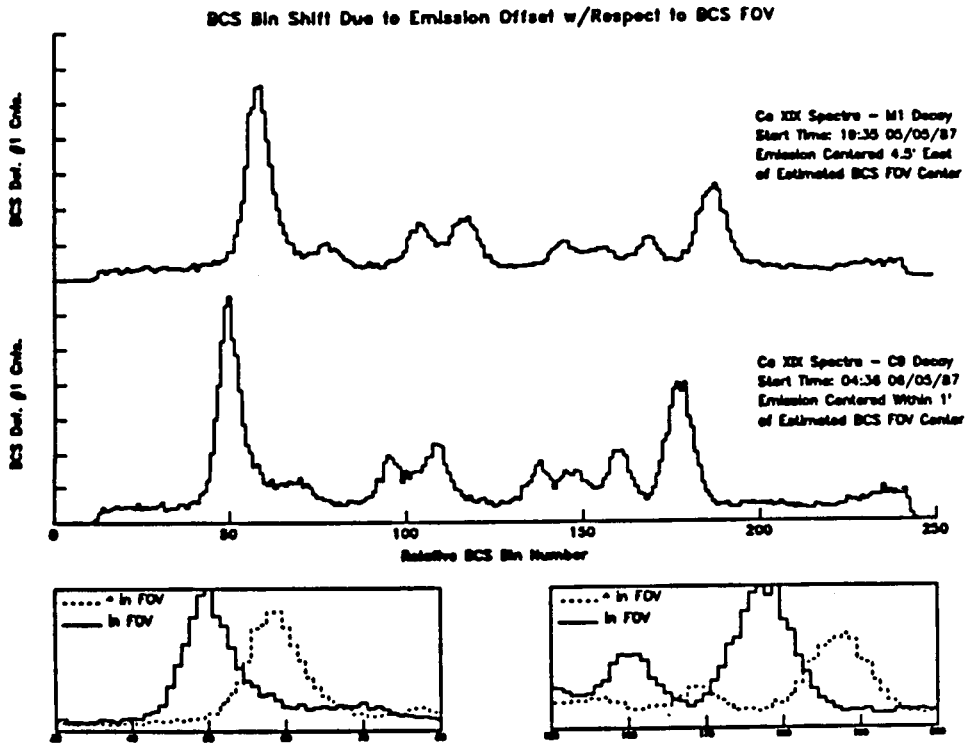

Figure 2-2. BCS bin shift due to emission offset within the BCS field of view.

2.1.4 FCS Detectors

FCS detectors 1, 3, 4, 5 and 7 are currently operational and continue to function normally. FCS detector 6 (Ca XIX) showed strong signs of impending failure toward the end of *SMM* I. A special set of tests performed in June 1983 showed that this detector had indeed ceased to function in a useful manner. FCS detector 2 (Ne IX) became useless in February 1985 after accidental turn on. It was decided to seal detector 2 by firing the pyro when the gas leakage rate increased substantially. The pyro was fired on 18 July 1985.

Unlike the BCS, FCS detectors are not calibrated on a regular basis. This is because the crystal drive has to be activated to expose the calibration sources and the gas systems have to be on. Figure 2-23 contains sample FCS PHA calibrations. The FCS PHA calibrations have also not shown significant change other than expected decrease in count rates.

2.1.5 FCS White Light Alignment Sensors

The FCS contains five white light alignment sensors (one central detector, and four limb detectors). These sensors are used to determine XRP alignment relative to the spacecraft and to other instruments on *SMM* (primarily UVSP). The white light sensors have shown a continuous degradation in their response, and early on in the mission, there was fear that this would seriously compromise the ability to determine absolute FCS pointing. Such has not been the case as the degradation rate of the sensors has decreased significantly. The degradation of the sensors has been inverse exponential. The degradation in the response of the five white light alignment sensors is given in figures 2-24 and 2-25.

2.1.6 FCS Gas Systems

The FCS thin window detectors (detectors 1 – 4) contain propane which is supplied from a pair of gas systems. Gas System A supplies the Mg XI and O VIII detectors, whereas Gas System B supplies the Ne IX and Si XIII detectors. The estimated remaining lifetime for System A is 85 days ± 20 percent and for System B is 90 days ± 20 percent. These estimates assume (a) that the gas usage rates after turn on will be unchanged from when they were turned off and (b) continuous use until the supplies are exhausted. More realistic estimates of the gas lifetime must take into account degradation as the result of cycling the gas systems. For System A, the last few cycles have each resulted in increases of 5 to 15 percent in the gas usage rate. System B has shown a much more severe cycling degradation effect. The last time it was inflated, the gas usage rate increased 60 percent over the rate prior to turn off. The previous cycling of System B caused a 40 percent increase in the rate. Figure 2-3 shows the gas rates for the two systems. Because of the limited lifetime of the two gas systems, the XRP team has had to institute strict conservation measures for the gas reservoirs supplying the FCS low-energy detectors. Recently, we have been turning off the gas flow during periods of low solar activity except to support major collaborations such as CoMStOC (Coronal Magnetic Structures Observing Campaign).

2.1.7 FCS Crystal Drive

The FCS crystal drive has been used to obtain more than 400 spectroscopic scans since the *SMM* repair. The drive has also been used to obtain calibration and engineering data a few times. All the data has been gathered with Drive B because Drive A (the prime drive) suffered a failure during check-out testing following the launch of *SMM*. Appendix B lists some of the data obtained using the crystal drive.

The large amount of crystal activity during April 1987 (50 runs) provided the Instrument Operations Team (IOT) with a large data set useful for diagnostics. The

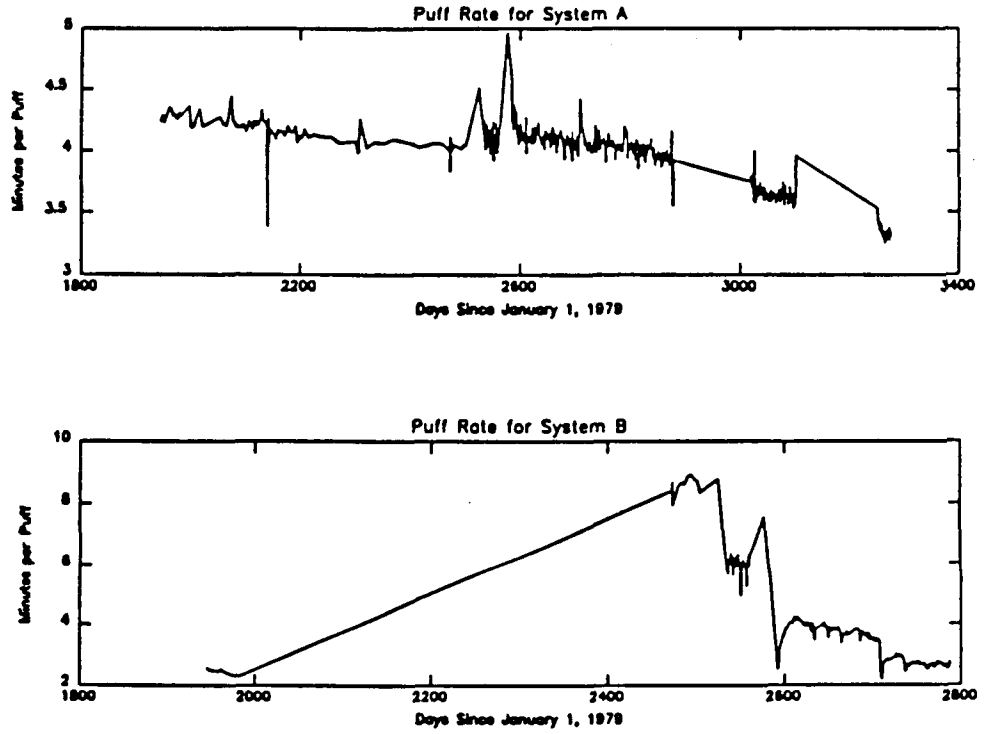

Figure 2-3. Puff rates of FCS gas systems A and B.

most interesting feature of the crystal drive has been the discovery of a relationship between the crystal drive address and the −15 volt bus voltage of the FCS. Figure 2-4 is a plot of the −15V bus voltage versus crystal address. The plot shows several well defined features indicating different voltage requirements for different areas of the drive. Figure 2-5 shows the four most well defined sub-ranges. These voltage increases indicate that the drive has more difficulty maintaining these positions.

The sub-ranges which demonstrate the largest voltage fluctuations are those associated with the heaviest crystal scan activity. This indicates mechanical or electrical changes in the drive mechanism or encoding electronics rather than a filament related problem (as experienced by Drive A). The address ranges with the increased voltage requirements include the areas where the drive loses control during movement between different scan ranges and during long flybacks. It is now thought that these voltage irregularities are also responsible for the flyback misreads long seen around the home position. The possibility exists that a fluctuation in the bus voltage caused by the crystal drive causes a flicker in the drive lamp, in turn causing the drive to temporarily read an incorrect address.

Most of the crystal drive problems have occurred during longer uncontrolled movements of the drive. Therefore dividing the long movements into shorter seg-

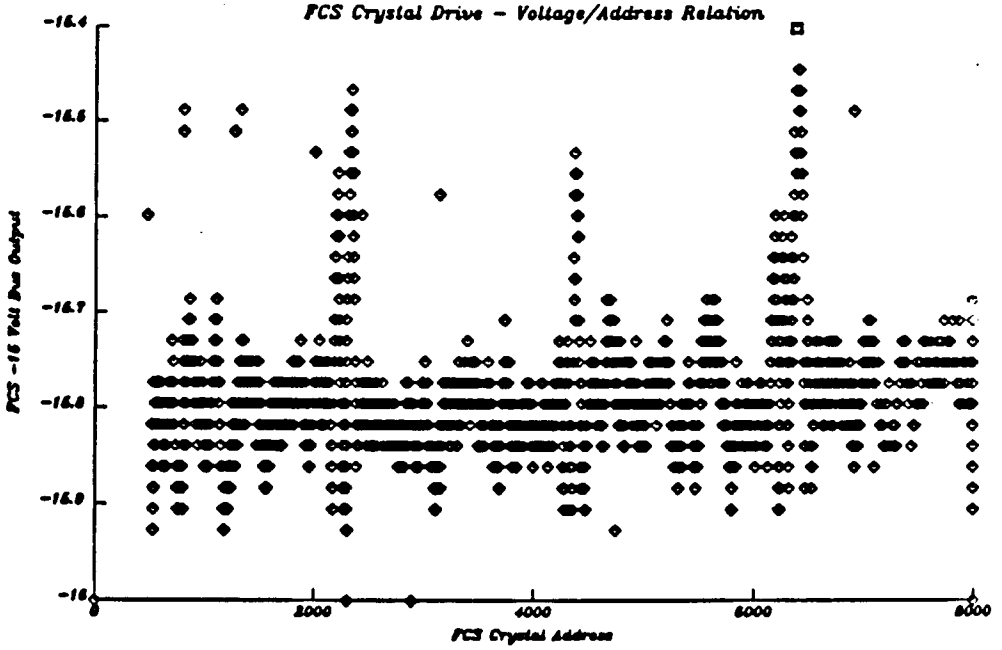

Figure 2-4. FCS crystal drive −15 V bus voltage and crystal address relationship.

ments and using more micro commands to the drive have reduced uncontrolled drive movements. The voltage/address plot is being used as a 'road map', i.e., the drive can be moved in a normal fashion between the degraded regions and movement through the affected regions requires either a fast scan or stopping above and below the area.

In July 1987, tests were performed in an attempt to differentiate between possible causes for the relationship between the FCS −15 volt bus and the Crystal Drive B address. The tests showed that changes in the voltage profile can occur in as few as 80 scans. The tests also showed that the profile is asymmetric — most likely a result of the asymmetric nature of the scan/flyback combination inherent in FCS crystal motions, and that the voltage maxima occur near the extremes of the integral scan ranges and a voltage minimum is formed toward the low end of the scan range. The tests did not fully resolve the issue of condition reversibility. That the voltage profiles showed observable changes after so few scans may be caused by the build up of lubricant near the most actively used crystal addresses.

The crystal drive started having an increasing number of problems during extensive use in November and December 1987. Most of the problems were observed

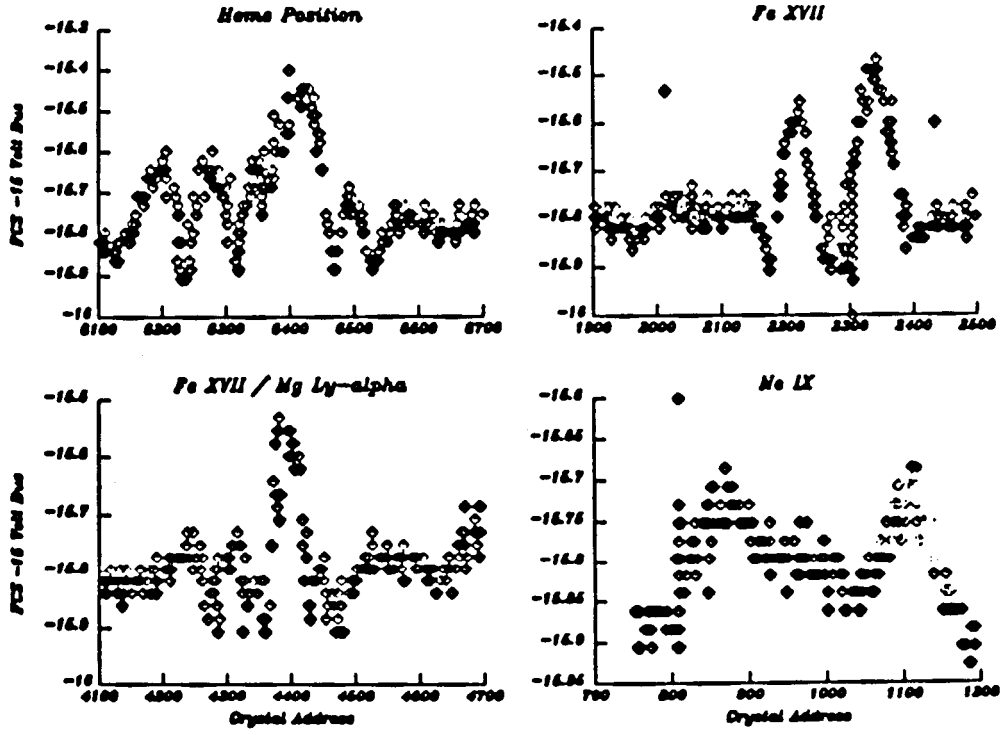

Figure 2-5. The −15 V bus voltage versus crystal address for four crystal address subranges.

during flybacks. Therefore, the IOT has decided to use a strategy of controlled scans to move the drive to the desired address. Controlled scans can be characterized as scans where the drive is never allowed to 'fly' to a new address more than 16 steps from the current position. During movements of 16 or fewer steps, the drive electronics sets the maximum speed proportional to the number of steps of the required movement.

The simplest way to avoid flybacks is to move the drive using spectroscopic scans in forward or reverse direction as needed. To save time, it is possible to selectively control the drive only during passages through the 'rough spots' by using MSS (Multiple Spectroscopic Scan) modes. These restrictions do not seriously affect scans carried out at a single raster position. When repeated scans of a wavelength region are required, two modes – one for each scan direction – within a loop can be used. If the starting position of the first mode is defined to be the same as the end position of the second mode and vice versa, no uncontrolled motion will take place during the scans. The analysis software is also not affected seriously as the forward and reverse scans are each defined by their own theta ID's which can be used to extract all the data. Current sequences using this strategy have shown no major problems.

The situation is much more complicated for scans performed within rasters. In this case, after completing the scan in one pixel, the drive will usually be far (> 16 addresses) from the starting position. For the scan in the next pixel, it will therefore 'fly' back to to the starting position with the possibility of loss of control. This problem cannot be tackled without some modifications to the FCS interpreter code. The modifications to the code can either be made in the section which positions the crystal drive at the start of a scan or in the section which performs the housekeeping at the end of a scan. The first option replaces flybacks with controlled scans. Flybacks are effectively slowed down. The second option eliminates flybacks altogether by setting the direction of the 'next' scan to be reverse of the last completed scan. The two scans may either be carried out within the same pixel or in alternate pixels. The data reduction software would need to be aware of this mode of scanning. The simplest method may be to treat such scans as multiple spectroscopic scans with different step sizes ($+n$ and $-n$) and the start and stop positions reversed. (The interpreter can not treat such scans as MSSR (Multiple Spectroscopic Scans within Raster) modes because it has only one slot for the step size for all the scans.) These modifications to the interpreter code only deal with SSR modes. MSSR modes would require much larger changes.

The actual implementation of either of the above schemes can be made in such a way that the option of bypassing them is preserved. One method would allocate a group of sequence ID's for controlled scans. The interpreter would branch to the appropriate code depending on the ID of the executing sequence. The ground software could also use the same convention to decide when to convert an SSR theta list into an MSSR list.

The operations staff has begun rewriting crystal sequences incorporating negative spectroscopic scans. For sequences requiring scans within a raster, a three staged approach has been adopted. The first stage will allow us to do forward and backward scans within the same pixel. This requires the simplest modification to the interpreter code. The second stage will let us alternate forward and backward scans in successive pixels. Finally, the third stage will implement multiple spectroscopic scans within a raster. Currently the operations staff is working towards implementing the first stage.

2.1.8 FCS Raster Drive

The FCS raster system uses a pair of motor driven cams (one each for pitch and yaw) to point the FCS collimator to a nominal accuracy of 5 arcseconds. The actual position of the collimator is determined by the output of transducers that measure the strain in each axis. The electronics system runs in an open loop manner, so when a motor does not respond properly to a step command, the planned area of observation slips in the field of view. There is a processing routine in the FCS microprocessor that corrects the field of view to the nominal boresight on every

orbit night. This was not the case during the original *SMM* mission and slips used to build up until the field of view was reset to the nominal boresight.

There have been a few major episodes of raster slips. The most extensive period of raster slips occurred during 1985. Extensive raster exercises performed during this period did not reduce raster slips. Switching the raster cams to YB and ZA did not produce any results either. The problem was finally linked to rasters larger than 5 arcminutes. Rastering exercises and discontinuation of rasters larger than 5 arcminutes finally helped alleviate the problem. Since then there have been three other periods of excessive raster slips. Raster exercises performed during these times have alleviated the problem.

2.1.9 XRP Microprocessors

Both the BCS and FCS are controlled by separate RCA 1802 microprocessors. Both processors accept commands from ground and/or the spacecraft, initiate observing modes and read science/housekeeping data. The BCS processor is primarily a data formatter in that it does not control the hardware. The FCS processor can command the FCS mechanisms but performs minimal data formatting. Since the *SMM* repair, both microprocessors have continued to work well. The BCS microprocessor has had a tendency to crash occasionally. These crashes have usually occurred during periods of increased crystal drive activity.

No changes have been made to the BCS flight software since repair, but several modifications to the FCS flight software have been made. These changes were made primarily to take advantage of telemetry which became free as two of the detectors failed. Other changes were made necessary due to modifications in the operating procedures. Another set of changes was made to change the default values of some parameters. All the changes are described below:

1. PHA Data (21 Feb 85) – This patch switched output of PHA data from FCS subcom to the channel 6 telemetry. Before this patch, PHA data overwrote DTE (Data Total Events), white light and mode information data. Normally this is not a problem as PHA data was only obtained from the calibration source during orbital nights. However as PHA data can provide an independent means of calculating background, it is useful to obtain a PHA spectrum of the solar x-rays.
2. Default Sequence (11 May 85) – The default sequence was modified to turn off the bright point seek function and BCS flare flag response. The default sequence is always run at the beginning of spacecraft night; this change prevented initiation of flare or bright point sequences, when these flags had been set during previous orbits.
3. UVSP Coordinates (17 Oct 85) – This patch outputs UVSP bright point coordinates (received with the flare flag) in channel 2 DTE slots in the FCS subcom

words. These slots became available when detector 2 became useless earlier in the year.

4. Flare Coordinates (6 Dec 85) – An error in assigning flare flag coordinates to XRP Y (NS) and Z (EW) coordinates necessitated this patch.
5. Sun Sensor Data (7 Mar 86) – After the failure of detector # 2, data from Sun sensor # 5 were switched to channel 2 telemetry. This allowed more frequent sampling and freed up space in the subcom fields for output from the other Sun sensors.
6. Raster Drive Offset (1 Apr 88) – A bug in the FCS interpreter code did not allow the raster drive to be offset 1 unit in the positive or negative Z direction depending upon the selected Z cam. This patch corrected that problem.

In addition to the above, temporary patches have been made to change the default crystal turnoff address and the default memory dump area.

2.1.10 *SMM* Flare Flag

The *SMM* On-Board Computer (OBC) has the capability of sending a flare alert to the FCS and UVSP instruments based on flare detection by the BCS. The OBC flare flag processor checks BCS flare level every second. If a specified flare threshold is exceeded, it reads the coordinates of the brightest (or the darkest, depending upon UVSP mode) pixel in UVSP image, converts them to XRP coordinates and passes them to the FCS. The OBC flare processor can also initiate one of three XRP RTS's (Relative Time Sequences). Two of these (24 and 25) RTS's are initiated if the corresponding enabling bits are set in the FCS telemetry. The third RTS (47) is initiated if the 'Super' flare threshold is exceeded. The flare thresholds, acceptable area and period for which the flare flag processor is enabled (it is usually left enabled for an indefinite period) can all be changed by modifying an OBC table.

After the *SMM* repair the OBC flare processor had to be modified substantially as HXIS (Hard X-Ray Imaging Spectrometer) flare coordinates were no longer available. However flare flag testing was delayed for a long time because it was not being delivered reliably to FCS even when FCS, UVSP and the OBC were in the correct modes. Eventually it was discovered that a bug in the CMS (Command Management System) software meant that negative coordinates were not being accepted correctly – the most significant bit was always reset to zero. Thus the field-of-view specification was always much smaller than intended and correspondingly fewer flares were meeting the flare alert criteria. Although this bug was the major cause of delay, other factors also delayed the final implementation. Other factors contributing to the delay were changes in operating method, i.e. initiation of different RTS's, and inclusion of a check of crystal drive simmer voltage prior to actual turn on (this modification was subsequently removed as it delayed start of crystal se-

quences by up to 16 s). In November 1986, the 'Super' flare code was modified to initiate RTS 47 instead of sending commands to FCS to initiate a specific sequence.

2.1.11 Alignment Activities

Co-alignment of the XRP and the UVSP instruments is performed whenever a sunspot is visible in the field of view of both the instruments. The co-alignments help the operations staff in spacecraft pointing. The scientists also use the co-alignment offsets in overlaying the XRP and the UVSP data. XRP offsets relative to UVSP are plotted in Figure 2-6. Since the middle of 1987, co-alignments are done in such a manner that the sunspot is in the center of the XRP field of view. This has been accomplished by having UVSP transfer the sunspot coordinates to XRP. On a few occasions when the XRP offsets relative to UVSP have become very large, the UVSP Co-alignment Adjustment System (CAS) has been moved to reduce the large offsets.

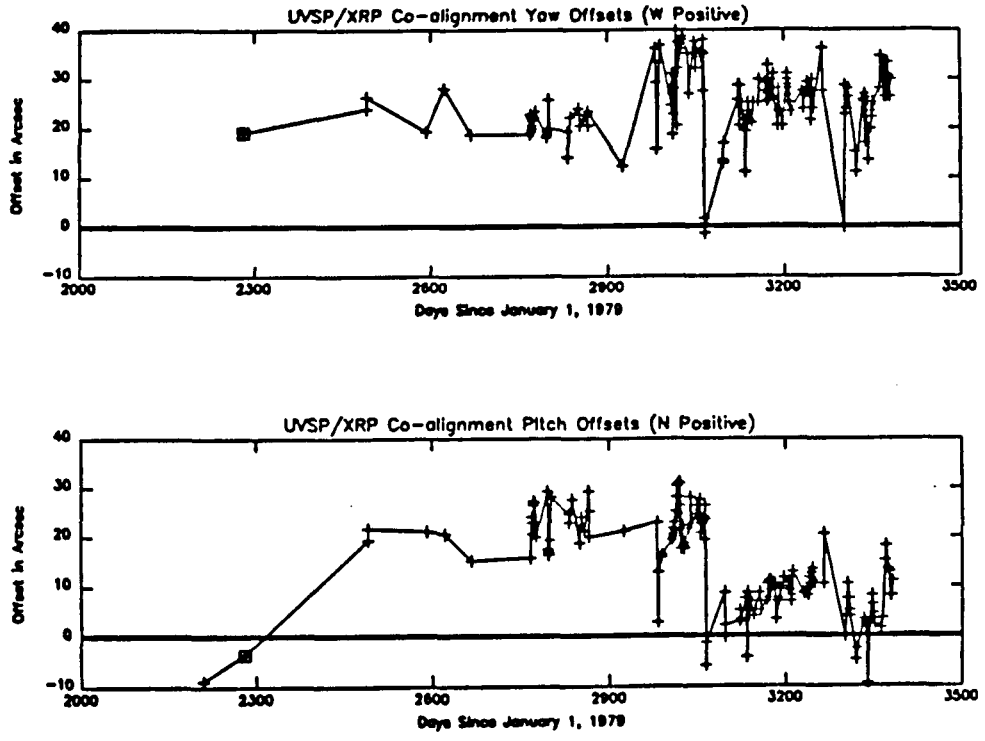

Figure 2-6. XRP/UVSP co-alignment offsets.

Co-alignments between XRP and the spacecraft have also been done at regular intervals. Figure 2-7 shows the XRP offsets relative to the spacecraft. Large XRP

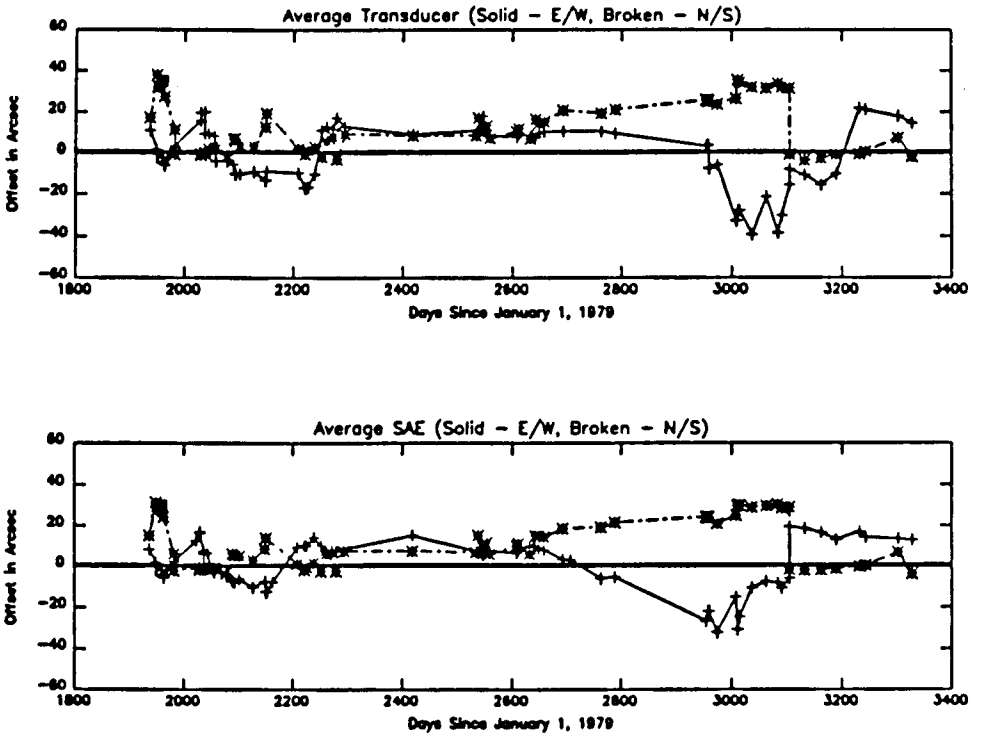

Figure 2-7. XRP/Spacecraft co-alignment offsets.

offsets relative to the spacecraft have been reduced several times by redefining the spacecraft boresight.

2.2 PLANNING AND EVALUATION

2.2.1 IOT Structure

The XRP Instrument Operations Team (IOT) was established as an independent structure from the XRP Scientific Team prior to the repair of *SMM* in order to balance the needs of smooth and safe operation of the instrument with the dynamic and often conflicting demands of the scientists. Since April 1984, the IOT has consisted of an IOT manager, a command generator, an instrument engineer, and a data analyst. The XRP Planner serves as liaison between the IOT and the scientific team.

From April 1984 until October 1986 the duties of planner were shared by representatives from the three institutions which jointly operate XRP: Lockheed, RAL, and MSSL. A representative from each institution would serve for one month out of

three. Beginning in October 1986, a permanent position was created for the XRP planner, which was filled by Lockheed.

2.2.2 Planning Observations and Command Generation

The 'XRP Planner' has the responsibility of planning and executing the observations of the XRP instruments. The cycle of planning involves several phases. There is an *SMM* planning meeting each morning presided over by the solar forecaster for that day, who presents *GOES* soft X-ray, H-alpha, magnetogram, 10 centimeter radio, and other data to summarize the state of the sun. This data is supplemented by data from the *SMM* instruments taken in the previous 24 hours. On the basis of the data and the particular goals of the various instruments, targets of observation are selected for the following day. When collaborations with other observatories, such as VLA, rocket instruments, or balloon instruments, are involved, the observations must be properly coordinated. Following the morning planning meeting, the day's schedule of XRP observations is entered into a VAX 8350 computer via a spreadsheet program. This is a high level representation of the set of instructions to be executed by the *SMM* OBC and the XRP's two microprocessors in order to carry out the days observations. The high level schedule is automatically converted into an intermediate level set of instructions by the "command generation software." It is then transferred to another computer where it is merged with the daily instruction loads of the other instruments as well as the general spacecraft commands.

It is the combination of the state of the sun, the state of the XRP instruments, and the current scientific goals for XRP that determine the observations to be done on a given day. When a new observation is requested by participating scientists or in order to fulfill a collaboration request, the planner and the scientists agree on the mode of operation of the XRP instruments which will best satisfy the observational goals. The sequence of commands for the FCS and/or BCS microprocessors must then be composed, generated, and loaded into the appropriate microprocessor. Once loaded, the sequence can be run as a subroutine in the daily instruction load. It may be necessary for the sequence to be tested one or more times to insure that it is performing as expected. Also, the effectiveness of the sequence is assessed following its execution in practice, and revisions are made where necessary.

At most times there are several concurrent observational programs being requested by various scientists. Which program is executed on a given day depends on the state of the sun. It is one of the planner's responsibilities to balance these competing requests and optimize the usefulness of the XRP instruments.

The planner is kept aware of the health of the instruments by the Instrument Operations Staff. The planner must continually assess instrument health and lifetime concerns where these affect the achievement of scientific goals and the per-

formance of observational sequences.

2.2.3 Streamlining and Automation of Command Generation Process

The primary purpose of the command generation process is to codify XRP observing plans in the form of parameter lists. These lists contain commands for the FCS "interpreter" and tables to specify FCS raster and crystal drive motions and describe how data from each channel are to be grouped into a number of 'bins' for the BCS. The command generation software allows creation and modification of all the lists mentioned above. In addition the software facilitates (i) Generation of Relative Time Sequences (RTS's) used by the *SMM* On Board Computer to command the XRP instruments; (ii) Update of the observing modes databases; and (iii) Transfer of load files to *SMM* control center for uplinking. Since the repair, the process has gradually been automated, providing the user with a menu driven command file. The command file allows access to all facilities and does not require detailed knowledge of the programs and files used by the system.

2.2.4 Data Processing

Data gathered at the EOF is for quick-look evaluation and analysis. The final data product is the set of production tapes sent by the IPD to the three XRP home institutions and the EOF. Each IPD tape contains data for a period of about 24 hours. The IPD tapes are processed at the EOF and four listings are produced as a result of the processing. Information about what sequences were run by the instruments and the status of the instruments are included in the TPSTAT listing. A listing of the raster drive status and anomalies is included in the RASDAT listing. Light curves for the period are also produced. The light curves show the photon counts registered by each detector and the status of each detector. South Atlantic Anomaly periods and day/night events are also shown on the light curves. A listing of all data gaps on the production tapes is produced. Hard copies of these listings are kept on file. Copies of light curves and backups of the other listings are sent to Rutherford Appleton Laboratory and Mullard Space Science Laboratory in England.

2.2.5 Cataloguing

The XRP Flare Catalogue is the final repository of all summary information on various flare events observed by the XRP. Each event in the listing is identified using a unique event number. The XRP Event Listing includes soft X-ray flares detected by the BCS instrument since the calendar year 1984 for which the intensity is ≥ 18 counts per second in Ca XIX. The peak count rate in Ca XIX and Fe XXV are given along with the number of peaks in an event and FCS status at the peak time. For each such event: the "Start Time", "Peak Time" and "Stop Time" are also

given. The "Start Time" occurs when the BCS Ca XIX count rate rises above 18 counts per second and the "Stop Time" occurs when the event decays back to that level. However, some event times are determined by orbital sunrise or sunset, where the flare starts before satellite day or is prematurely ended by satellite night. If the event has its "Peak Time" during orbital night or SAA, the catalogue indicates the maximum level observed during satellite day. The crystal drive "ON" indicates that a FCS Crystal Spectral Scan was made. An XRP quality code is also associated with each event catalogued in the XRP Flare Catalogue. The XRP quality code represents one of the following cases:

- Entire event observed
- Only start of event observed
- Start and peak of event observed
- Peak and decay of event observed
- Only decay of event observed
- Only rise and decay of event observed (e.g., peak lost due to radiation belts)
- No data or bad data
- No event observed (Typically shown as no listing)

Cataloguing the events is a two stage process. Stage 1 is the creation of a Single Event File (SEF) which contains the available information on a particular event observed by XRP. This file is created programmatically. However these files can be edited so that additional information (e.g. Emission Measure, comments) can be manually inserted. Stage 2 reads in one or more SEF's, generates a single record from all the records in a SEF and writes this record out to the Master Event File (MEF). When a SEF has been processed it is deleted. If new information about an event becomes available the entry for that event can be extracted from the MEF in the form of a SEF. Stages 1 and 2 are then repeated to update the MEF.

The Master Event File is an unformatted indexed file containing all the catalogued information on flares observed by XRP. All records are divided into two sections. The first section contains event data while the second is available for entering comments. Table 2-1 lists the information stored for each event in the MEF.

The catalogue management program accesses the MEF. The program can be run interactively or in batch mode and allows the user to add, delete, update, and extract single events. The program also allows the user to encode data in the MEF record format or decode data from a MEF record format. Another program is used to make a summary listing of the the Master Event File. This program lists any events within a specified time period. The program can also list events of a certain type or those meeting some specified criterion.

Table 2-1: CONTENT OF XRP FLARE CATALOGUE

Event Number	Event Start time
BCS Event End time	BCS Peak Ca Counts/sec I
BCS Peak Ca time I	BCS Peak Ca Counts/sec II
BCS Peak Ca time II	BCS Peak Ca Counts/sec III
BCS Peak Ca time III	BCS Peak Fe Counts/sec I
BCS Peak Fe time I	BCS Peak Fe Counts/sec II
BCS Peak Fe time II	BCS Peak Fe Counts/sec III
BCS Peak Fe time III	FCS Raster Id.
BCS Data Gathering Interval	FCS Detector 1 Peak time
FCS Detector 1 Peak Counts/sec	FCS Detector 2 Peak Time
FCS Detector 2 Peak Counts/sec	FCS Detector 3 Peak Time
FCS Detector 3 Peak Counts/sec	FCS Detector 4 Peak Time
FCS Detector 4 Peak Counts/sec	FCS Detector 5 Peak Time
FCS Detector 5 Peak Counts/sec	FCS Detector 7 Peak Time
FCS Detector 7 Peak Counts/sec	Crystal Scan End Address
Crystal Scan Start Address	BCS Detectors On/Off Status
HXRBS Event Number	Gain of Detector FCS 1
BCS Data Quality	Gain of Detector FCS 3
Gain of Detector FCS 2	Gain of Detector FCS 5
Gain of Detector FCS 4	Gain of Detector FCS 7
Gain of Detector FCS 6	FCS Crystal Mode
Crystal Drive On/Off Status	Spacecraft Roll Angle
FCS Detectors On/Off Status	Spacecraft Yaw Angle
Spacecraft Pitch Angle	Solar Longitude
Solar Latitude	FCS Sequence 1 Id.
Active Region Number	FCS Sequence 2 Id.
FCS Sequence 1 Time	FCS Sequence 3 Id.
FCS Sequence 2 Time	FCS Sequence 4 Id.
FCS Sequence 3 Time	FCS Sequence 5 Id.
FCS Sequence 4 Time	Last Revision Date
FCS Sequence 5 Time	Number of Y steps
FCS Raster Information	Number of Z steps
Y step size/5"	Number of Pixels
Z step size/5"	BCS Comments
Dwell per Pixel (multiple of 0.256 seconds)	FCS Comments

2.2.6 Operations: Evaluation Process

The evaluation process involves the following activities: (i) Checking instrument health and status, (ii) Comparison of the observing plan with the observing sequences actually carried out, (iii) Extraction and processing of calibration data and (iv) extraction and preliminary processing of science data for input to the planner. The above activities are carried out on a daily basis or for data of particular interest, as soon as the data become available. Since the repair of the *SMM* Spacecraft in 1984, many of the steps involved in the above process have been automated with the help of several new programs and utilities.

2.2.7 Operations: Software Developments/Automation

2.2.7.1 Monitor

This program performs the first checks on the data. It runs on the data acquisition machine (a PDP 11/34). The default mode scans data from 0000 hrs UT (Universal Time) on the previous day up to 0800 hrs UT on the current day. The program runs automatically every day and provides a log of instrument performance and abnormalities over the past 32 hours. The program works from a list of parameters to be monitored and their nominal and acceptable range values. Whenever a parameter exceeds it's range, an entry is made into a log file. The program can also be run manually. The monitor also logs all BCS events exceeding 18 counts per second. This serves as a quick look catalogue for the operations staff.

2.2.7.2 Data Transfer

The data acquisition machine is not suitable for the evaluation tasks due to it's limited processing speed and storage capacity. Thus data of interest has to be made available on the data processing computer. During the first mission this was accomplished by writing raw data to tape and reading data from tape on the other systems. However a new program to transfer data is now available. This program can be used to transfer data from several orbits. A command file on the data acquisition computer is used to construct data files for specified periods and to queue them for transfer to the processing computer. A corresponding command file on the data processing computer is used to receive data and to initiate further evaluation of the data.

2.2.7.3 Health and Status Software

The main health and safety checking programs are described below:

1. QKL: Extracts XRP data from raw telemetry and creates a disk file or writes to tape. All other evaluation programs use the files (or tapes) created by this program.

2. TRL: (i) Creates a listing of instrument status for the period covered by the input file (or tape); (ii) Produces crude light curves for all detectors; (iii) logs slips in the raster drive; and (iv) creates a crystal addresses file if the crystal drive is on. This file is used to check anomalies in the crystal drive operation.
3. ENG: A program to plot variation of any item in XRP telemetry with time. It allows tracking of critical parameters to diagnose problems.

2.2.7.4 Raster and Crystal Software

Programs exist to plot: crystal addresses as a function of time which show problems such as overshoots and sticking of the drive, the voltage level (the level is lower in problem areas), distribution of flyback speeds (the spread is a measure of encoder misreads), and a crude spectrum for evaluation. The raster software is used to make automatic entries into the raster-slips log.

2.2.7.5 Calibration and Co-Alignment Software

IDL and FORTRAN programs exist to analyze the calibration data gathered by the instrument. Software has also been written to determine the XRP offsets relative to UVSP and the spacecraft. Results of the engineering data analysis are stored in logs as mentioned below. Routines to access and update these logs also exists.

2.2.7.6 Command Files

Several command files exist both to provide utility routines and to provide batch mode processing of bulk data. The following are some of the frequently used ones:

1. FCSDISK – Receives files from the data acquisition computer, associates a comment with each file and gives the user the option of selecting a processing path – run TRL, process FCS raster data and put up images on the display device, create a file of microprocessor parameter dump, etc.
2. REFRESH – Creates a new directory for daily evaluation. Copies all the required files to the new directory (Plan form, orbit number file, default contour levels, etc.). It deletes the corresponding files which are seven days old, after saving the user-specified data files.
3. OPS – Moves to the appropriate evaluation directory given an operations day number. Optionally can provide a listing of the plans for that day and/or provide information on data files in the directory.
4. XTAL – Sets user's default directory to specified crystal data directory. If no directory or partial directory is specified, then the command file provides a listing of crystal directories available and prompts the user to select one.

5. WHATIS – Searches an archive file for a certain keyword. The archive file contains the file name, the associated comment and the directory where the file resides. The archive file is updated daily when the REFRESH command file is run.

2.2.7.7 Engineering Logs Software

Instrument parameter logs have been maintained in several different formats until recently (see next item). Software is currently under development to maintain a single engineering log file, which would have entries for all the monitored parameters. This file will be organized as an indexed file, allowing random access to a given parameter at given time(s).

2.2.7.8 Engineering Logs

A short description of each of the engineering logs kept by the Instrument Operations Staff is given below:

1. Raster Slip Log: This is an unformatted index keyed access file containing transducer and SAE readings, selected and backup cams, orbit number, time, and sequence id. Slips are logged at the time the FCS interpreter is turned off (usually at LMS). The log runs from approximately six months from the repair up to the present. FORTRAN software exists to access the log.
2. Crystal Log: This is an ASCII file containing the following information for every crystal run: time, address at turn on, temperatures of both bearings, address range covered, number of misreads and the FCS sequence id. The log is complete from repair up to March 1988. Software for automating crystal log updates has been worked on but is incomplete.
3. Calibration Data: Two calibration data logs exists. One file has the BCS position calibration data. The other file contains BCS and FCS PHA calibration data. Both files are organized as ISAM files. FORTRAN and IDL software exists to access and update both files. Both files contain data since *SMM* repair.
4. Pointing Offset: Offsets between XRP and Spacecraft boresights are stored in this file. The data are saved in a keyed access file containing transducer and SAE values and offsets at each limb. FCS White Light Alignment Sensors values are also stored in this file. The log is complete since repair. 1980 data is available in a paper file. IDL analysis and access software exists for this file.
5. Co-alignment: XRP-UVSP co-alignment data is stored in this file. This is an ISAM file which contains solar position, roll angle, size of raster, step size and the calculated offset. IDL software exists to update and access the log.

6. Pointing: This is the spacecraft pointing log. It is an "as planned" log. The actual pointing is determined from a file which is created when telemetry data are reformatted. The file is accessed and updated using FORTRAN software.
7. Gas Systems and Temperatures Log: This log contains the puff counter for the two gas systems. Gas system leakage rate and lifetime are calculated using this information. The log also contains six critical instrument temperatures. IDL software to access and analyze this information exists.
8. Background Values: This log contains information about the background in the XRP detectors. The data analysis software uses this information to subtract the background from the observed data.

2.3 ADDITIONAL INSTRUMENT STATUS FIGURES

In this section we give several additional figures which characterize the the calibration information about the FCS and BCS spectrometers, the white light alignment sensor response, and the co-alignment of the pointing between the FCS and the UVSP, and the FCS and the spacecraft. Several of these figures are referred to in the preceding sections.

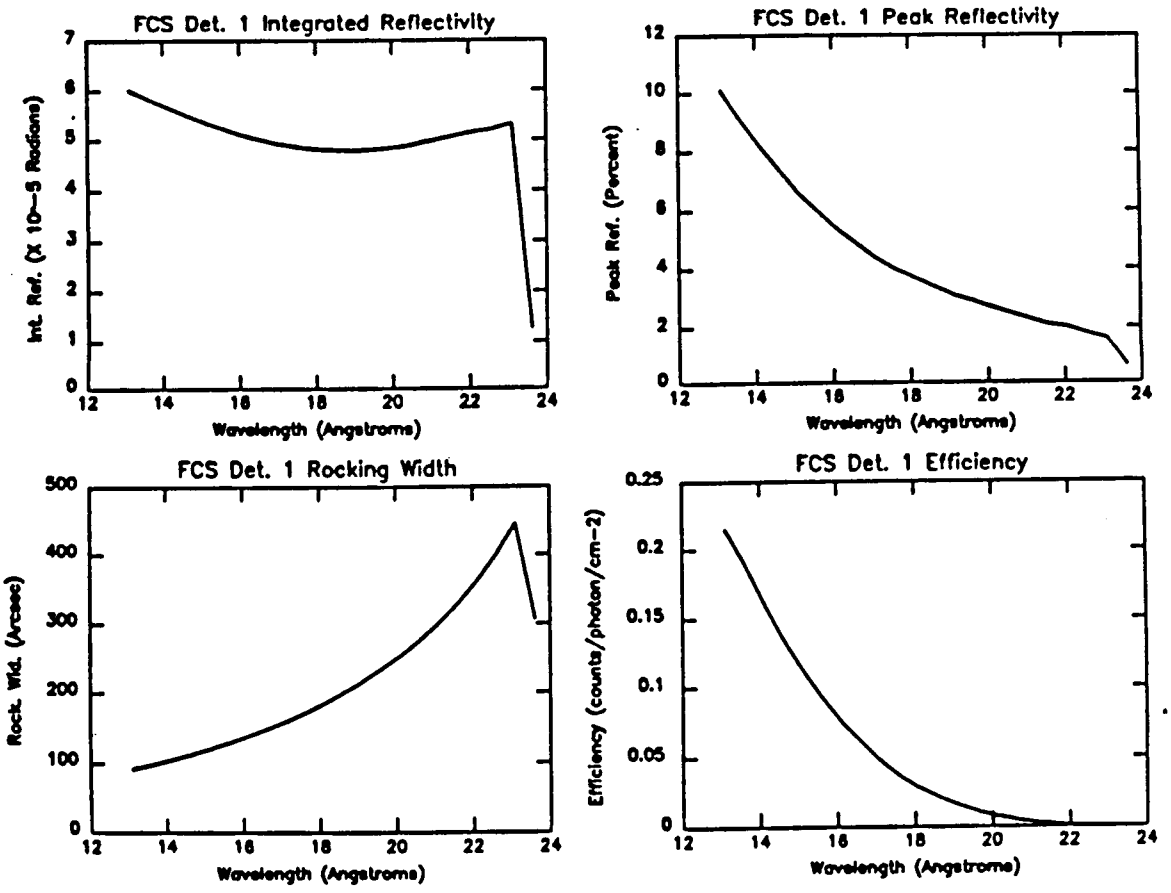

Figure 2-8. FCS spectrometer characteristics: Channel 1.

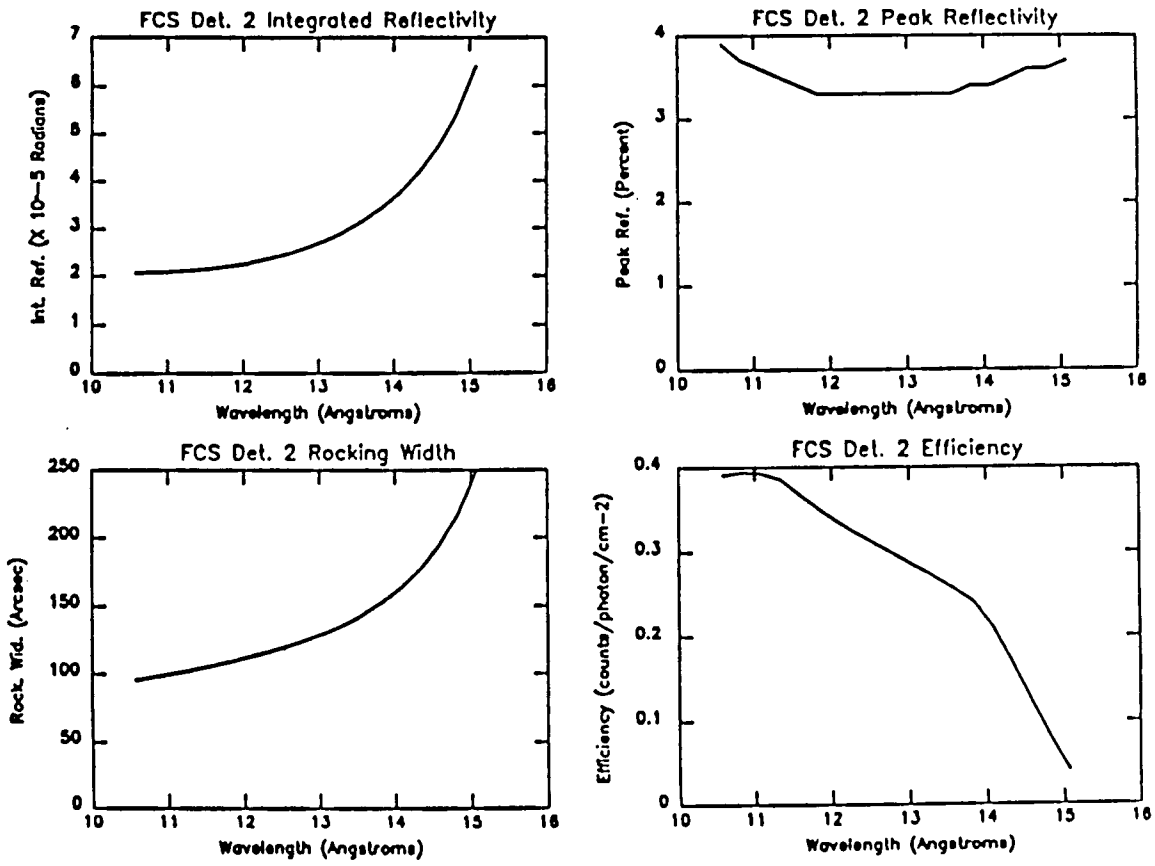

Figure 2-9. FCS spectrometer characteristics: Channel 2.

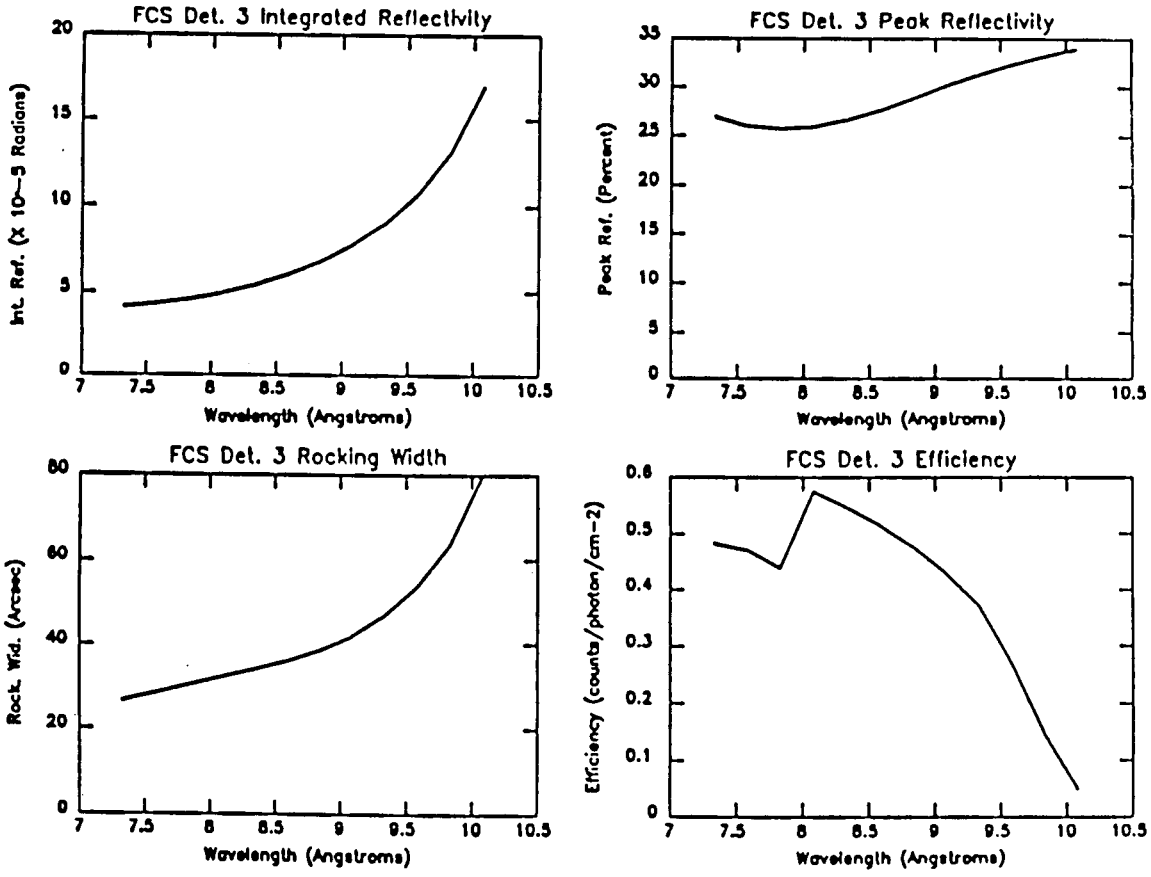

Figure 2-10. FCS spectrometer characteristics: Channel 3.

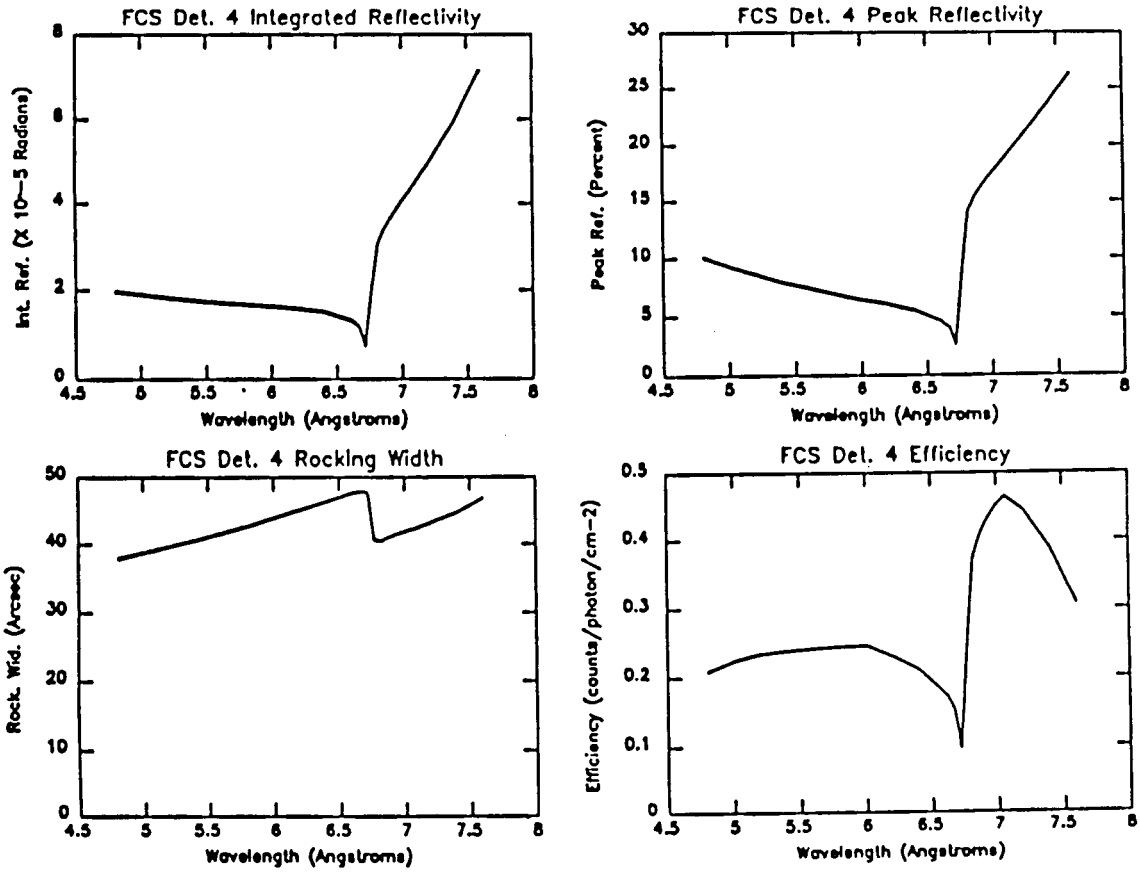

Figure 2-11. FCS spectrometer characteristics: Channel 4.

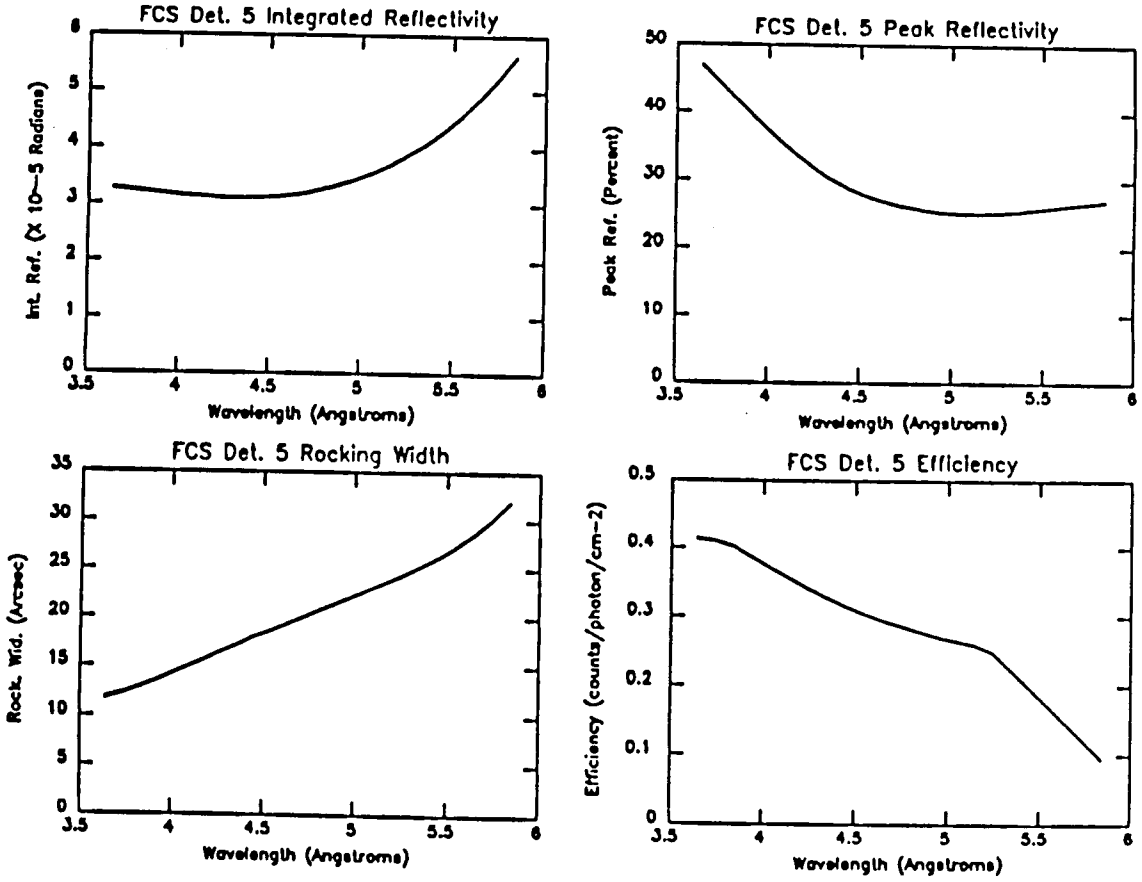

Figure 2-12. FCS spectrometer characteristics: Channel 5.

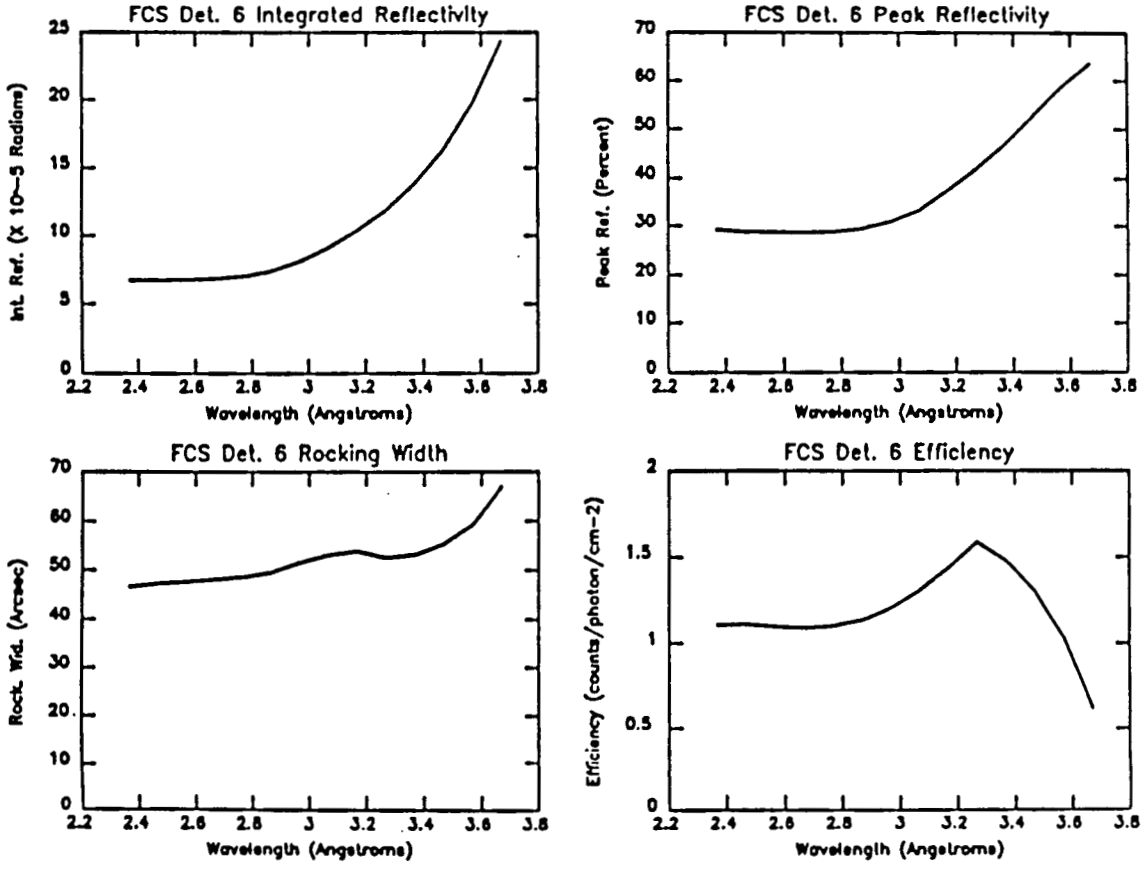

Figure 2-13. FCS spectrometer characteristics: Channel 6.

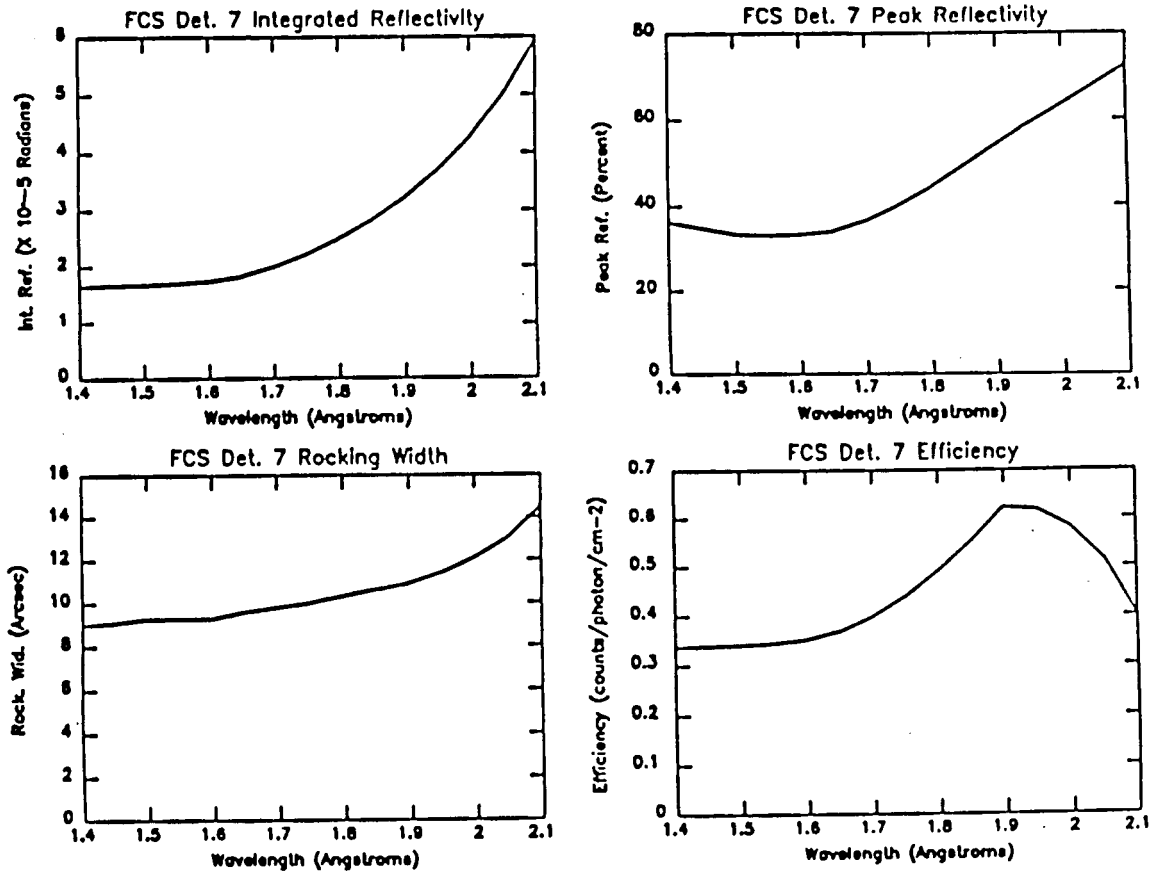

Figure 2-14. FCS spectrometer characteristics: Channel 7.

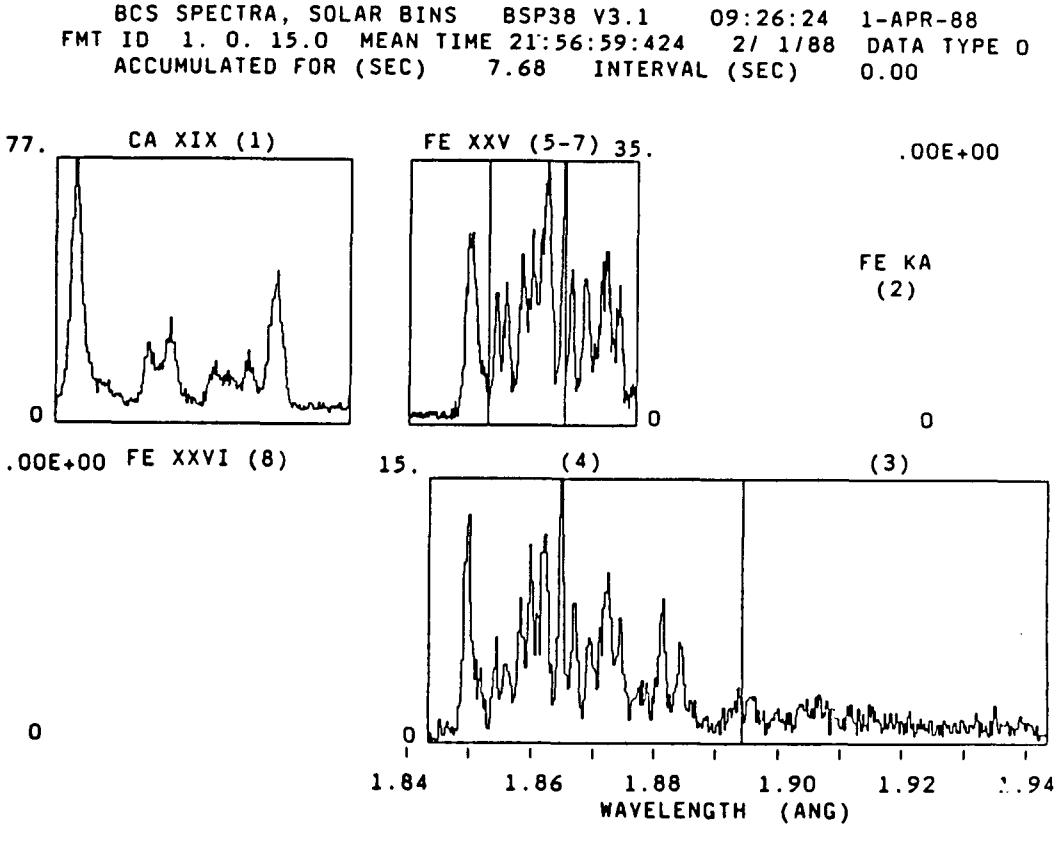

Figure 2-15. BCS sample spectra. Channels 1 and 3 to 7 are displayed. Channels 2 and 8 were not operational during the *SMRM*.

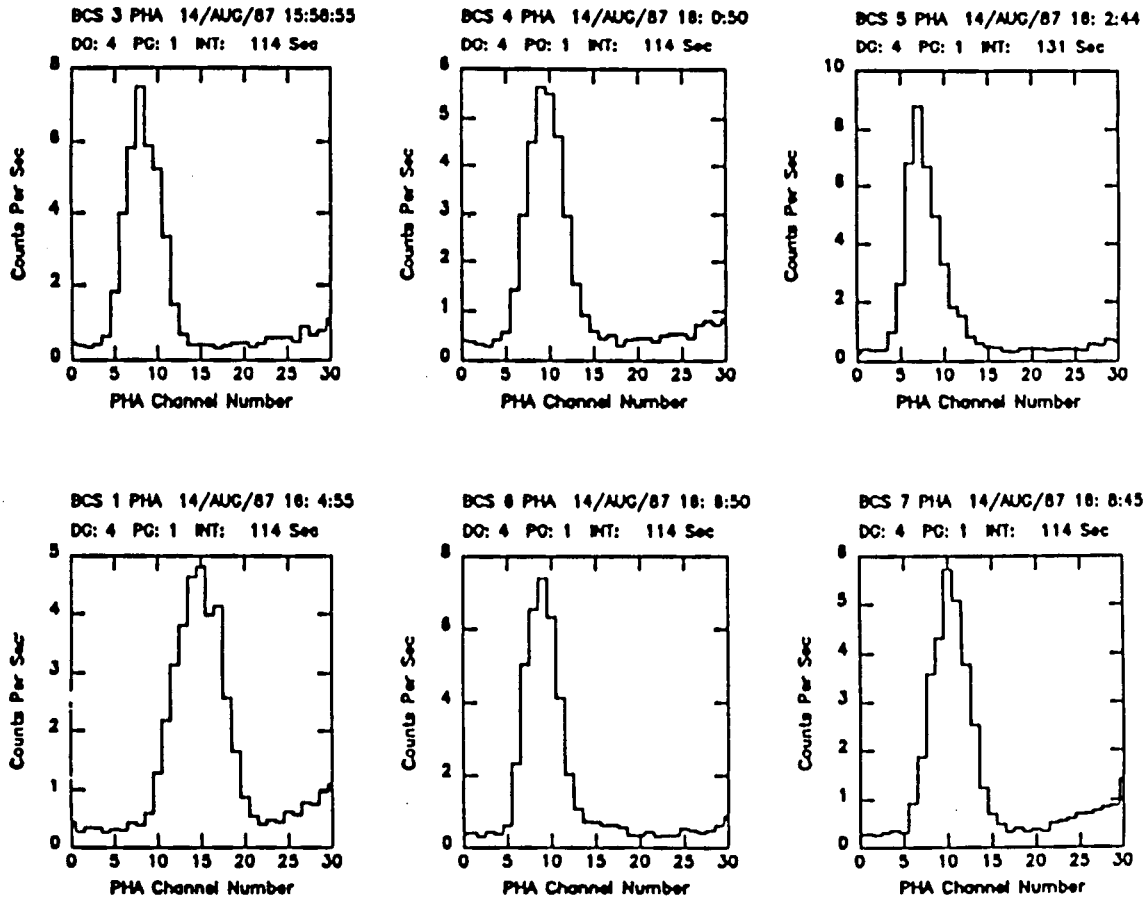

Figure 2-16. Sample BCS PHA calibration data obtained in channels 1 and 3 to 7 using a $^{+55}$Fe radioactive source.

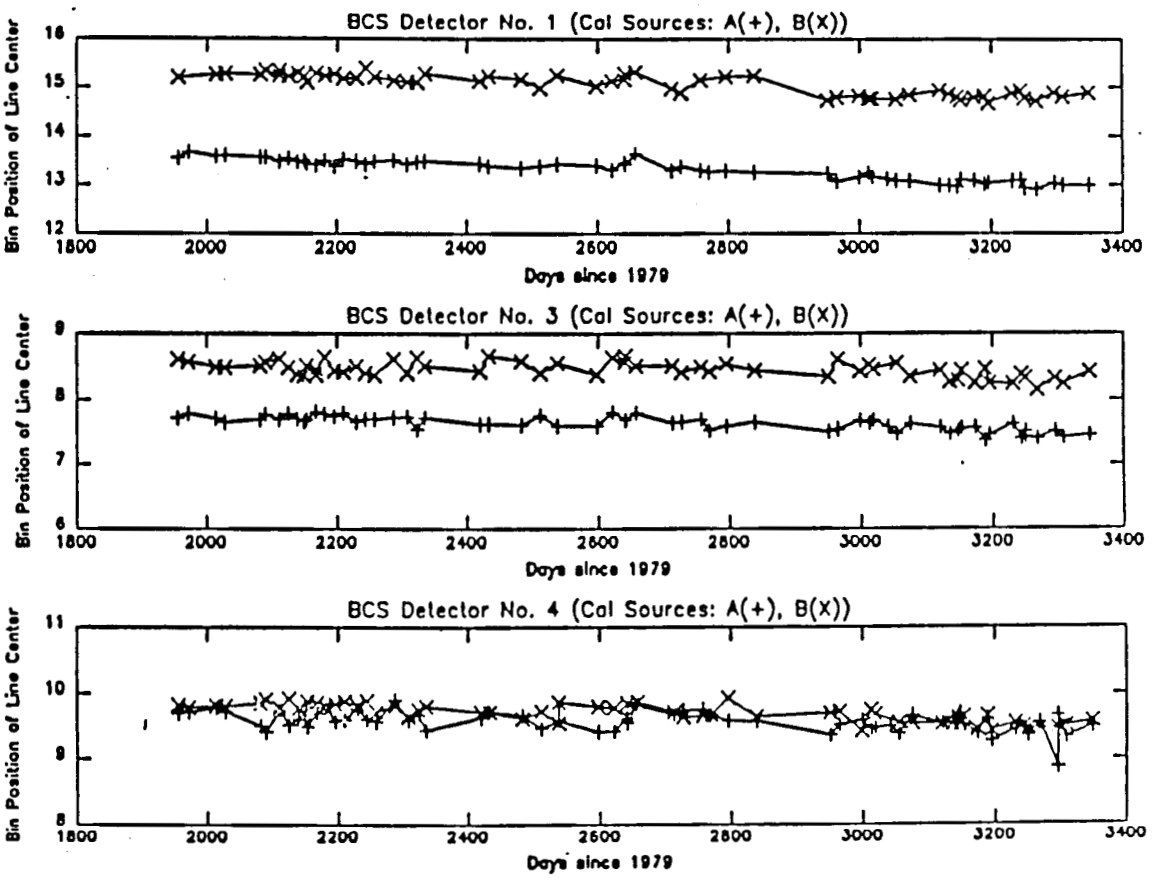

Figure 2-17. Time history of the BCS PHA calibration data. Channels 1, 3 and 4 are displayed. These data indicate the stability of the detector gains as a function of time.

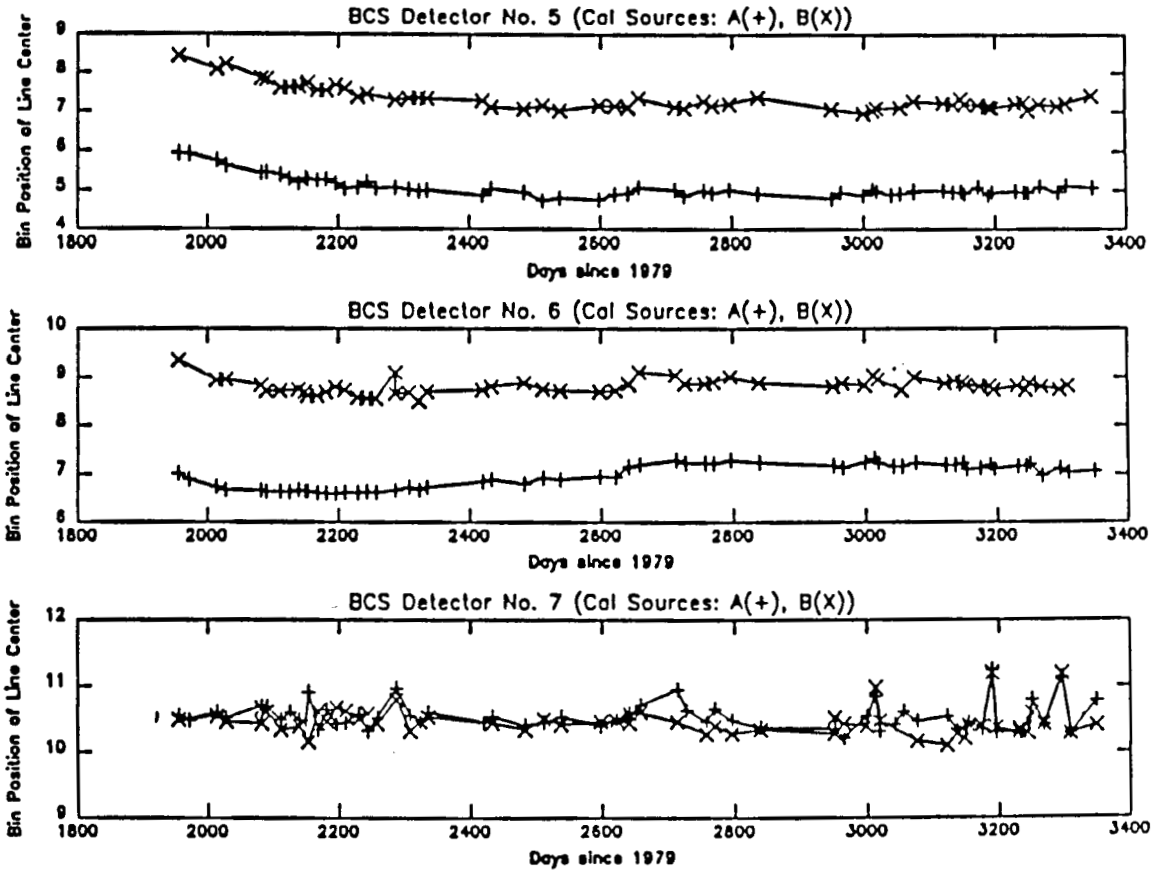

Figure 2-18. Time history of the BCS PHA calibration data. Channels 5, 6 and 7 are displayed. These data indicate the stability of the detector gains as a function of time.

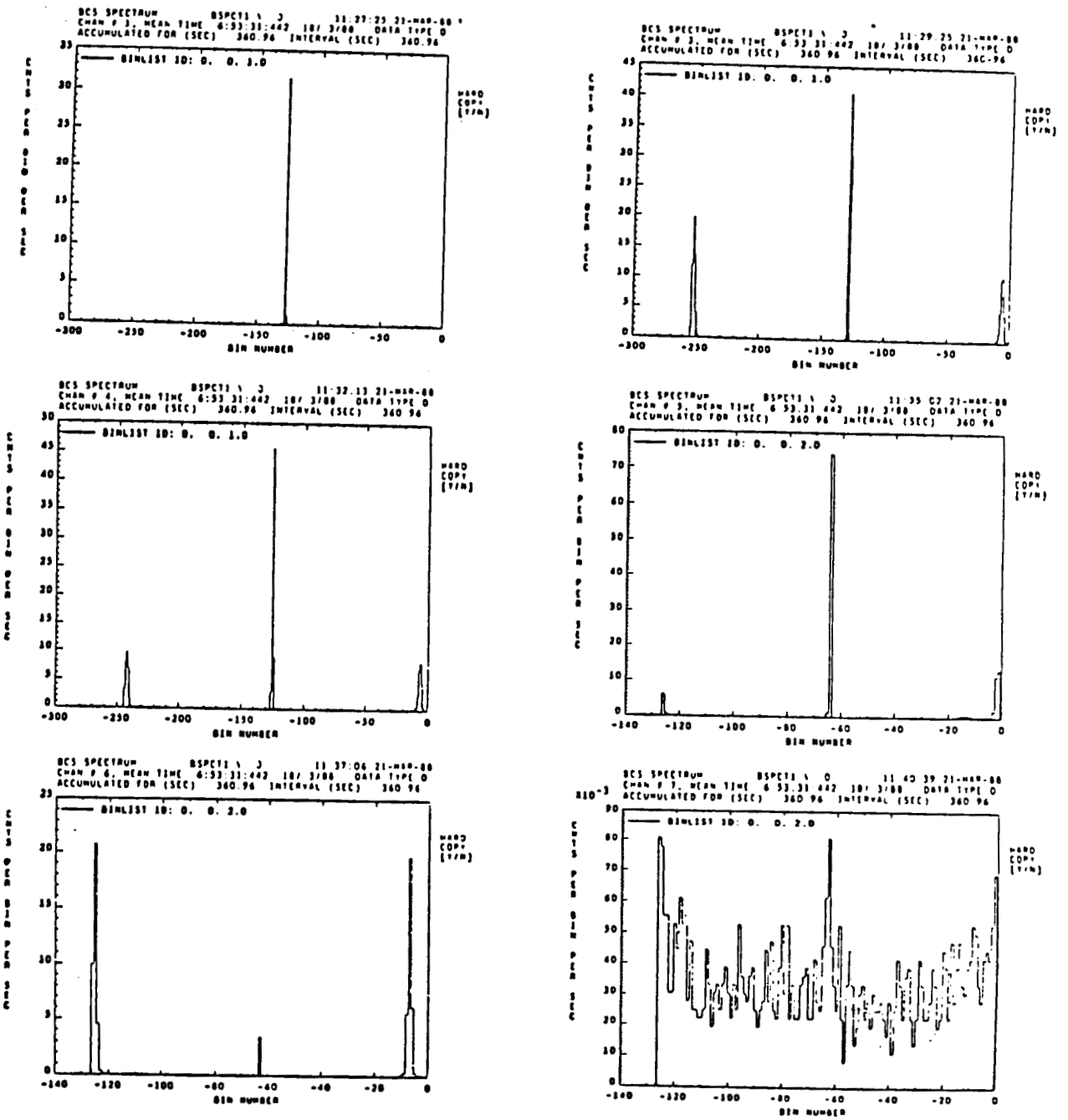

Figure 2-19. An example of BCS data obtained during a position calibration.

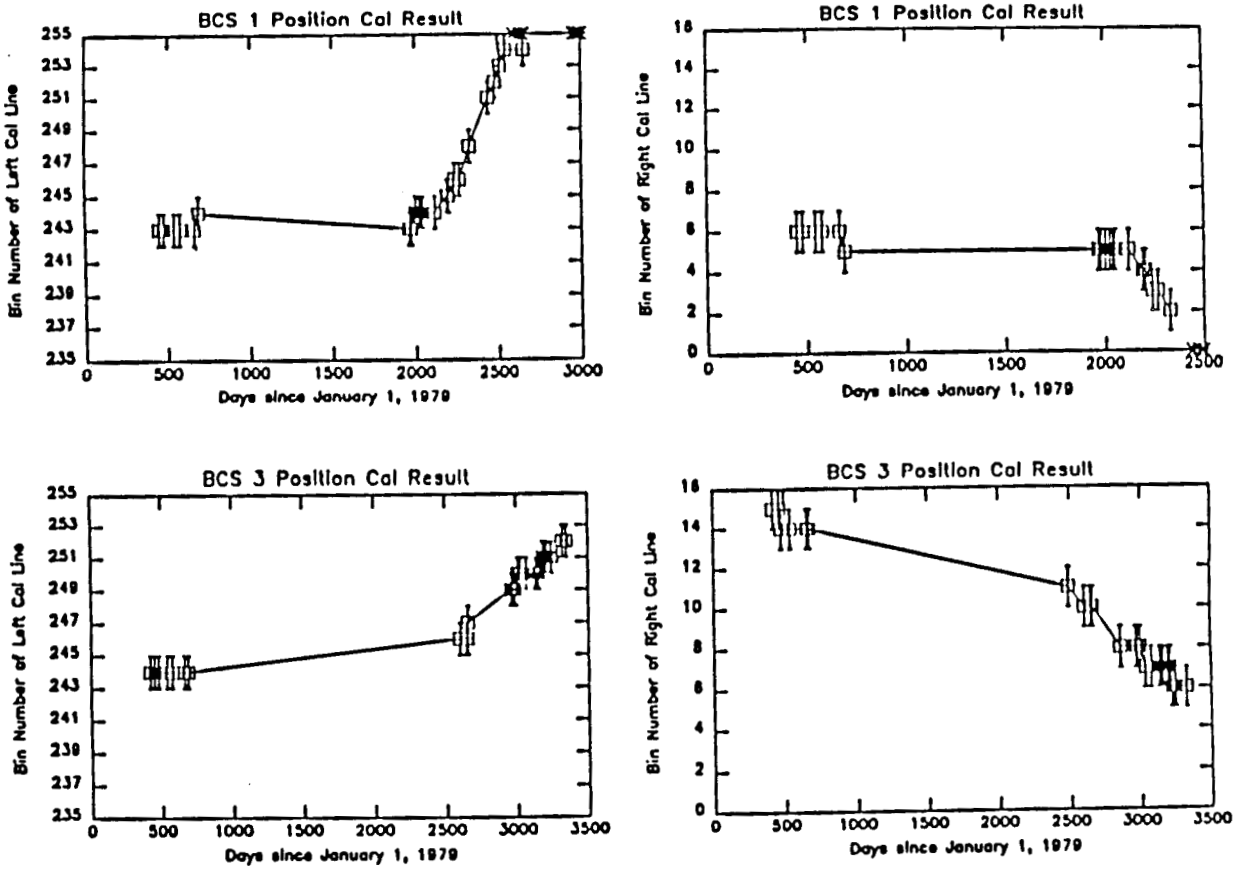

Figure 2-20. Time history of the BCS position calibration data for channels 1 and 3.

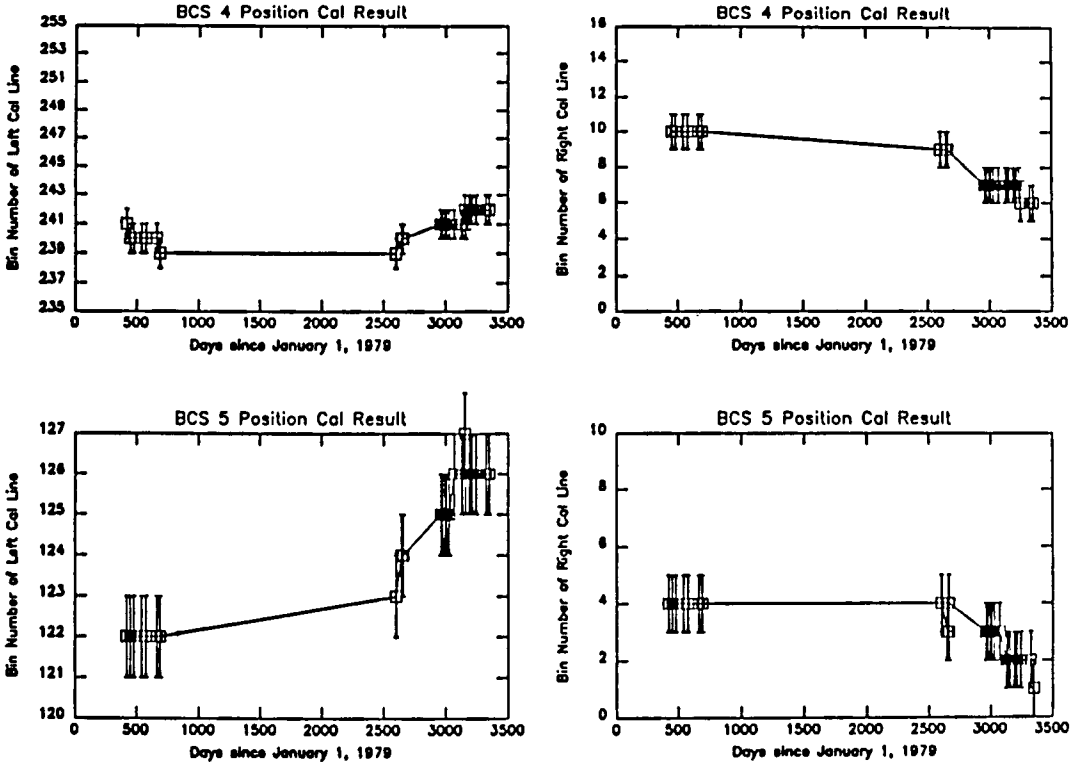

Figure 2-21. Time history of the BCS position calibration data for channels 4 and 5.

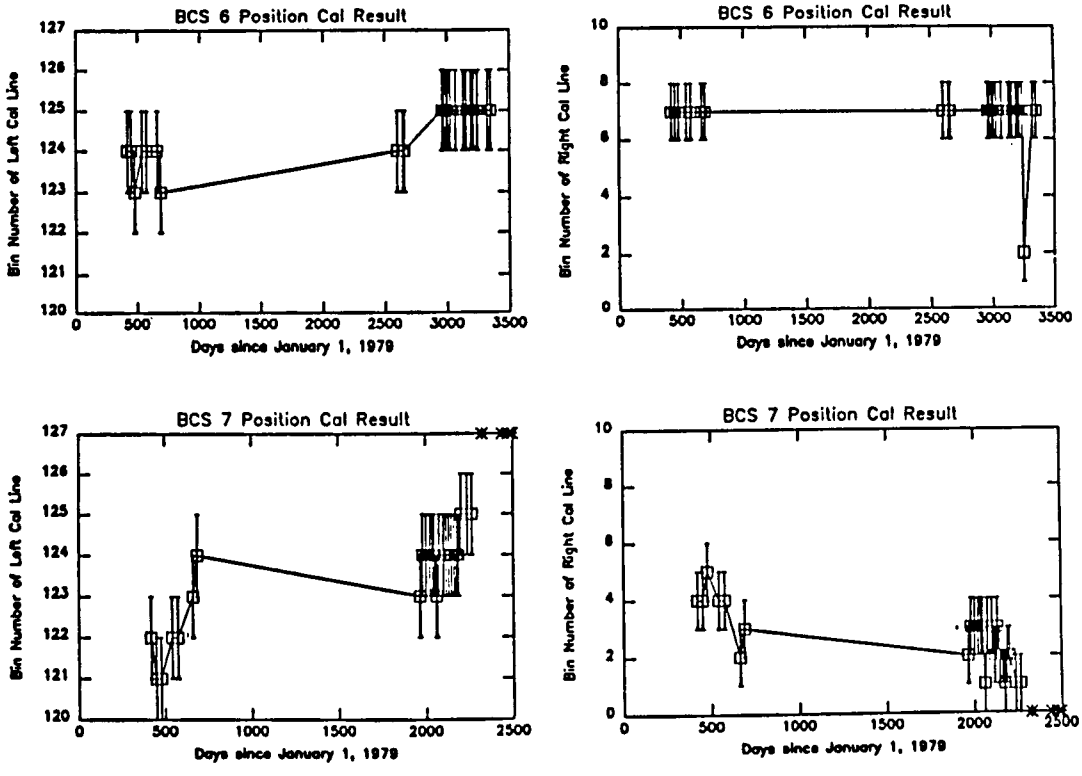

Figure 2-22. Time history of the BCS position calibration data for channels 6 and 7.

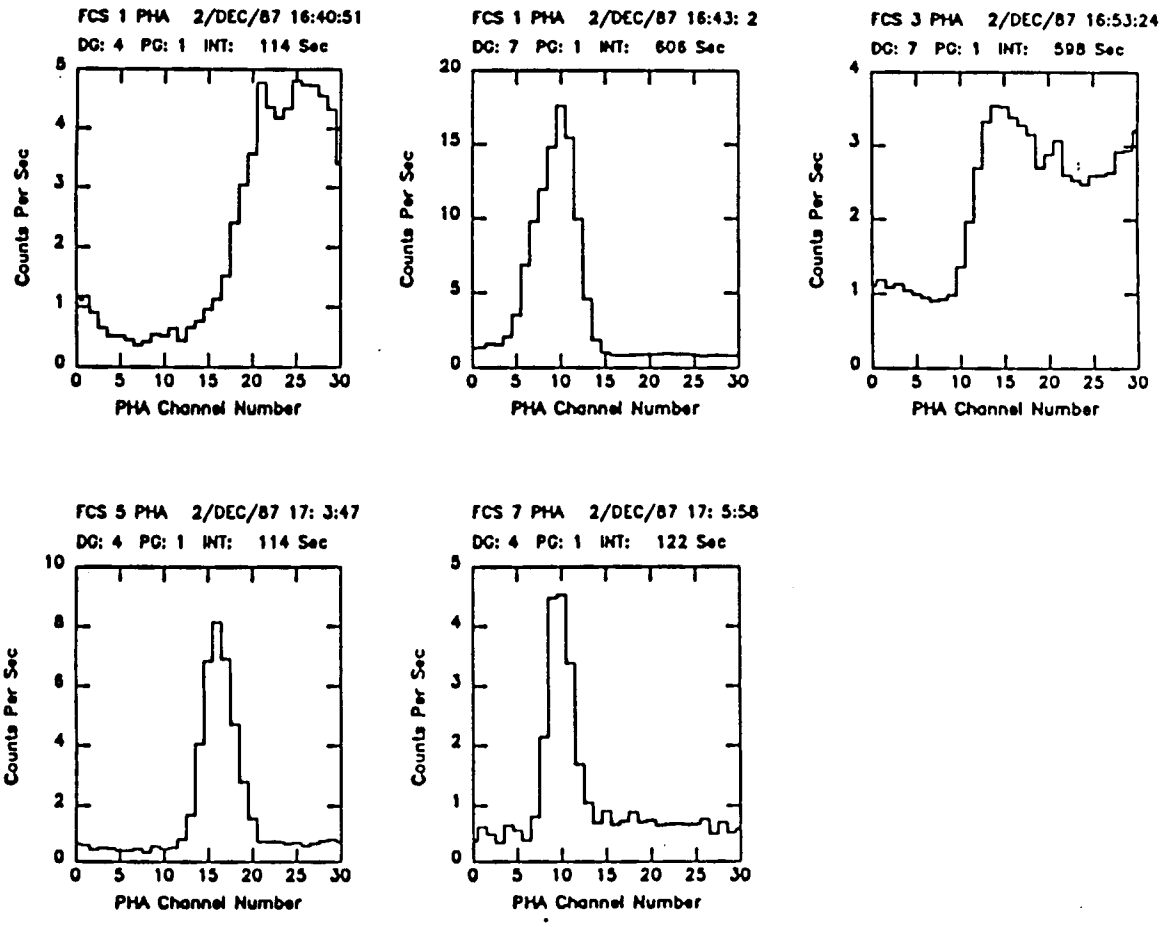

Figure 2-23. An example of FCS data obtained during a PHA calibration using a $^{+55}$Fe radioactive source.

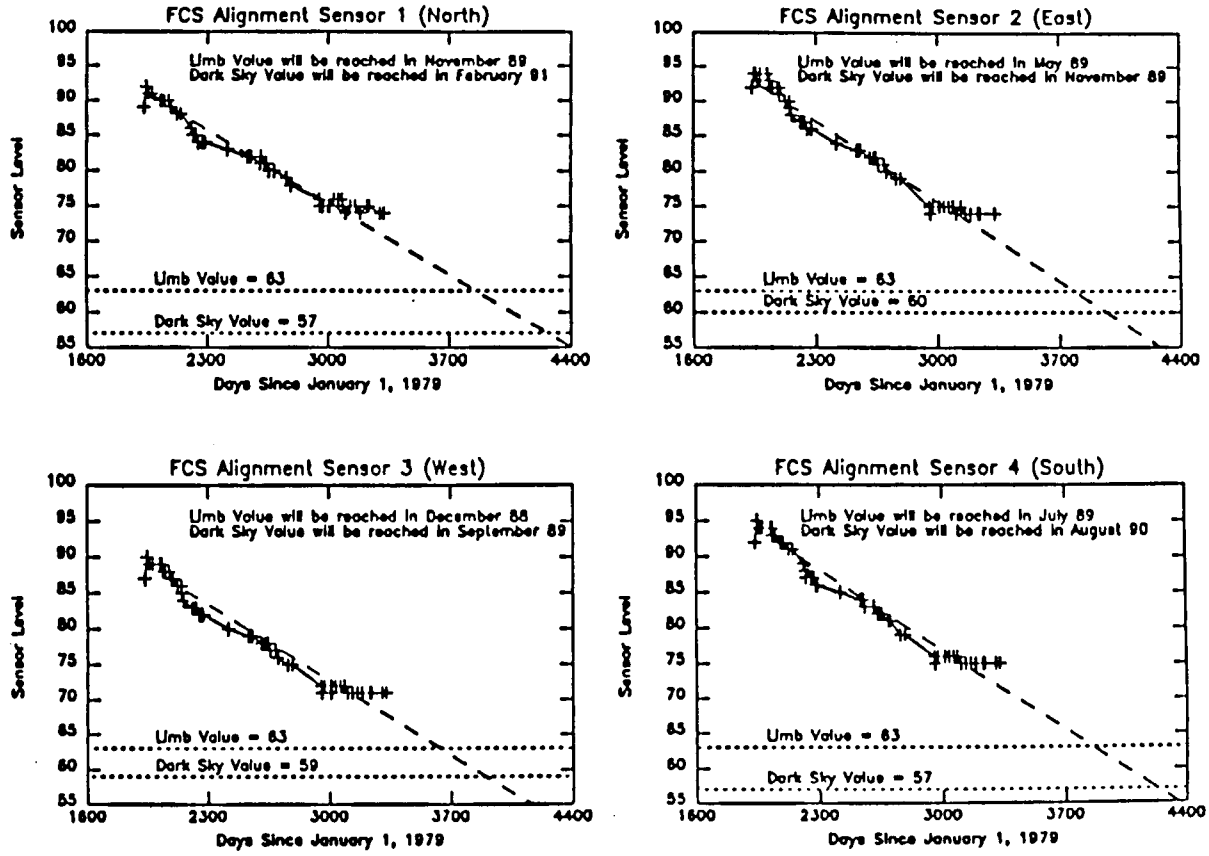

Figure 2-24. The responses of the four limb White Light Alignment Sensors as a function of time.

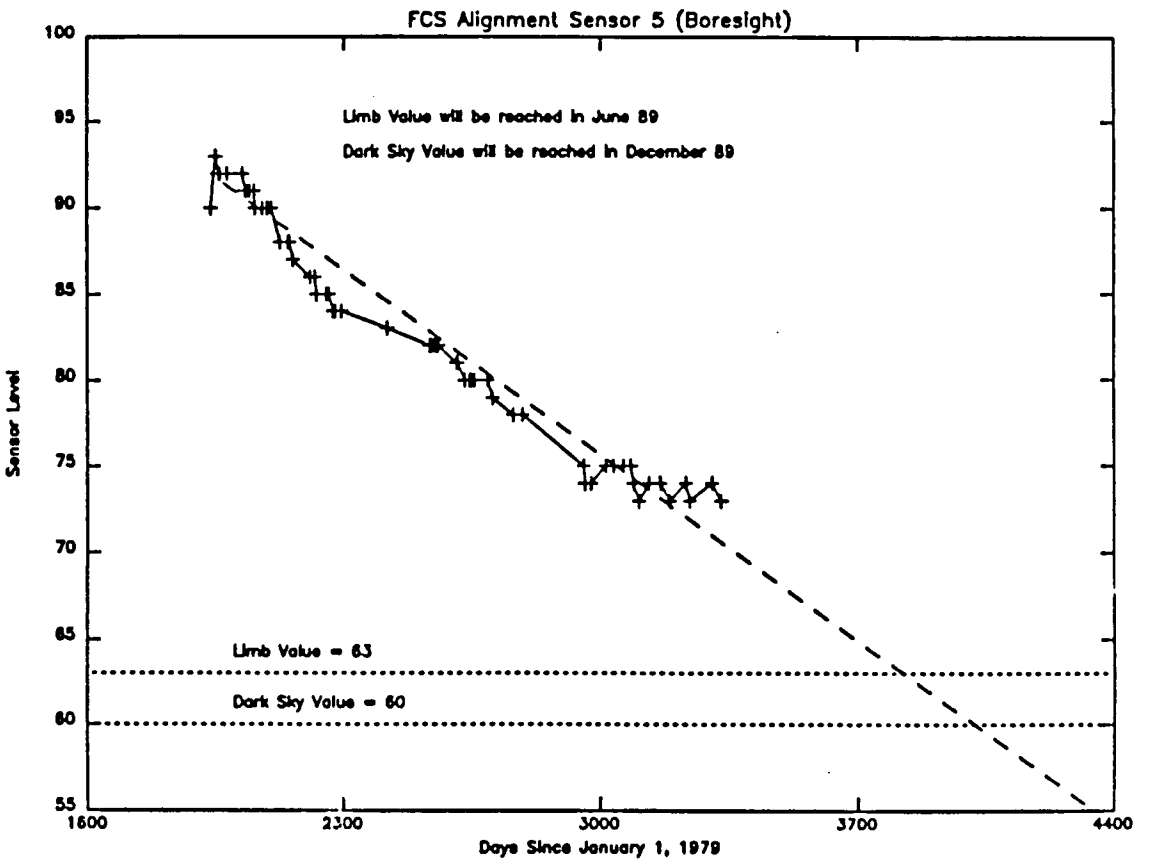

Figure 2-25. The response of the boresight White Light Alignment Sensor as a function of time. The end of useful life has been estimated as June 1989.

3. XRP SCIENCE

3.1 INTRODUCTION

3.1.1 Guest Investigator Support

The Guest Investigator (GI) Program has been pivotal in the development of new scientific results obtained with the XRP. The program has nurtured many productive collaborations between Guest Investigators and XRP scientists in which there is substantial cross-fertilization of ideas and expertise between various disciplines. For example, XRP observations are used to support joint VLA microwave observations (cf. CoMstOC), Sacramento Peak Hα observations, rocket-based observations, and balloon-borne hard X-ray experiments. This sharing of information, particularly across different wavelengths, provides greater physical insight into complex solar phenomena than could be derived from a single instrument. The productivity of the GI program is further enhanced by the availability and accessibility of processed XRP data to the GI. Often, an XRP experiment designed for a specific purpose (such as the imaging of coronal loops on the solar limb) may provide the necessary data for an independent study (such as initial conditions leading to a coronal mass ejection). These data are delivered by XRP staff to the GI in the required format, or are processed by the GI working directly with XRP, thus stimulating further collaboration.

The extensive list of multi-author publications in Appendix A is strong testament to the fruitful nature of the GI program. Several abstracts of these joint papers are given in Section 3.2. In addition to encouraging collaboration, the GI program often serves as a useful mechanism for graduate students to utilize unique soft X-ray data in their research projects. Two examples of this student involvement follow.

Z. Svestka (SRON, Utrecht) and student P. Hick have been investigating the phenomenon of post-flare arches, discovered initially with HXIS. Using the imaging capability of the FCS, they have found new evidence for X-ray structures with similar characteristics (5×10^4 km altitude, 3×10^9 cm^{-3} density, several hour longevity) to the coronal arches observed by HXIS. Since these observations were obtained with a different type of instrument, they provide independent confirmation of the physical reality of the arch phenomenon. Using the temperature diagnostic capability of the FCS, they have derived physical parameters in different parts of the arch that are complementary to those derived by HXIS.

R. Canfield (Institute for Astronomy, University of Hawaii) and graduate student T. Metcalf are investigating the nature of flare heating of the temperature

minimum region (TMR) by examining intensity enhancements in Mg I lines. Their data are unique in several respects. Unlike past optical studies, the Mg I preflare data extends well before the onset of all five events studied. Second, coincident hard X-ray observations enable a determination of the relative timing between the hard X-ray impulsive phase and the TMR heating, placing limits on any direct heating or ionization caused by impulsive phase processes such as nonthermal electron beams and EUV radiation. Further, simultaneous XRP observations can be used to place limits on heating by soft X-ray irradiation.

3.1.2 New Observations

New and innovative observations are always difficult to obtain. Recently, however, a variety of novel XRP experiments have been performed which have provided greater insights into solar phenomena. The success of these new observations is a direct consequence of the ever increasing expertise of XRP staff, particularly in the area of sequence writing and debugging.

Footpoint Observations

A case in point is the observation of a compact C4 flare which occurred on 24 May 1987. This observation had several notable firsts:

(1) FCS spectral scans were controlled by a new first run sequence which consisted of Mg XI triplet scans (to infer electron density at flare onset), successive home position profile scans (to infer plasma velocities), followed by Ne IX triplet scans (to monitor the evolution of electron density during the cooling phase).

(2) The flare was observed with the FCS pointed at the UV brightpoint coordinate provided by the UVSP. The facility to transfer UVSP data coordinates (only recently available through software improvements to the *SMM* central onboard computer) enabled the initiation of FCS wavelength scanning much earlier during the impulsive phase than would have been achieved with internal flare flags (such as BCS Ca XIX count levels).

(3) Previous FCS scans have been performed at sites of enhanced coronal soft X-ray emission such as Mg XI or Fe XVII. Consequently, these observations were spatially biased to the upper apex regions of the coronal loop(s). However, by positioning at the UV brightpoint – a proxy indicator of heating sites in the flare transition region – the new FCS scan sequence was operated in the vicinity of the loop footpoint, where chromospheric evaporation signatures of soft X-ray blueshifts and high densities are predicted to be greatest.

(4) Preliminary analysis of the data has revealed an initially high electron density ($> 10^{12}$ cm^{-3}) and a pronounced blue asymmetry in the low-temperature (for a flare: 6×10^6 K) Mg XI line. Fits of synthetic Mg XI profiles indicate a

blueshift velocity of about 200 km s^{-1} to account for the asymmetry. Velocities of this magnitude have been predicted by simulations of chromospheric evaporation (e.g. Pallavicini *et al.* 1983, *Ap. J.*, **270**, 270), and have been observed in *high-temperature* lines such as Ca XIX (i.e. formed above 10^7 K). The present observation is the first detection of such a large evaporation velocity signature in a *low-temperature* soft X-ray line during the impulsive phase. The above result highlights the usefulness of coordinated XRP/UVSP observations of flares, particularly in providing new spectral data to constrain and test models of chromospheric evaporation.

Spectroscopy

There continues to be great interest in lines of highly ionized He-like ions. Atomic physicists are able to calculate line intensities with considerably greater accuracy now than a few years ago. Previously, line intensities were derived from collision strengths that varied smoothly with electron energy. More elaborate computer codes now accurately compute the effect of auto-ionizing resonances, producing large changes in the calculated intensities in some cases. One theory group working in this area is that at Queens University, Belfast (QUB), who have produced results for a large number of He-like ions. These ions are of great interest to XRP as they are very intense in active region and flare spectra and, in some cases, yield diagnostically important density- and temperature-sensitive ratios. The following results involve data from the FCS instrument:

(1) He-like Ne IX is in a crowded region of the spectrum, but the intruding lines are basically due to one ion, Fe XIX, and in a still-to-be-published work (Bhatia, Lemen, Mason, Phillips, 1988, *M.N.R.A.S.* to be submitted) these lines are calculated and compared with FCS and other active region and flare data. Meanwhile, the QUB work for Ne IX is found to agree extremely well with data, and electron densities have been derived throughout the course of at least one flare.

(2) Other QUB calculations for He-like Mg, Al and S have been compared with FCS data, and again the results are very satisfactory. There is, however, no density dependence for S. For Al, recent RAL work indicates that this line is a most useful diagnostic for temperature and perhaps density owing to the interesting fact that the region of the Al XII lines contains a Mg XI line with very similar $G(T)$ to Al, giving a tight constraint on temperature.

(3) QUB are now doing calculations for He-like Si (high-n) and Ar. Ar in particular is a favoured ion for the FCS as it can be observed with the non-thin window channel 5 (i.e. does not depend on limited gas supplies). Preliminary spectra during flares have already been obtained but not yet fully analyzed; they will be compared with calculations when these are available.

(4) Finally, several lines in FCS channel 3 were observed for the first time during an intense flare in July 1985. These were between 7 and 10 Å and for a few months after the spectra were obtained provided a source of some puzzlement. A few of the more intense lines had been seen previously and partly identified. In a paper by Fawcett, Jordan, Lemen and Phillips (*M.N.R.A.S.* **225**, 1013, 1987), these were finally identified, using laboratory data and Hartree-Fock calculations, as $n = 2 - 4$ transitions in Fe XIX – XXII. We are quite excited by the possibility that some of these lines could be density-dependent, but full atomic calculations do not yet exist. Two of the most intense of these mystery lines are seen in second order in FCS channel 1 spectra, explaining two long-standing puzzles, one a satellite to the O VIII home-position resonance line.

High-Time Resolution Studies

In addition to FCS observations, new BCS observations are being undertaken. Beginning in January, 1988 a new BCS sequence was written to take advantage of the 128 msec time resolution of which the BCS micro-processor and electronics are capable. Prior to this, the highest resolution which had been used was 0.5 s. Furthermore, in previous attempts to observe at high time resolution, the high time resolution mode was initiated only after the flare reached C1 level, by which time the impulsive phase was well under way, if not over. Thus this new sequence fills a crucial gap in the observational phase space accessible to the BCS instrument. The sequence has been run successfully on a very limited basis during several flares of varying magnitudes. The primary goal of the observations is to search for the soft X-ray counterpart to the rapidly varying hard X-ray bursts which are frequently observed by HXRBS during the impulsive phase of solar flares. B. Dennis and A. Kiplinger of the HXRBS experiment have suggested that observing these variations in soft X-rays would lend support to the nonthermal explanation of the hard X-ray features. During 16–18 March 1988 the sequence was run in coincidence with high time resolution Hα observations at Sacramento Peak Observatory. Six candidate flares were observed simultaneously at 128 msec resolution by BCS and HXRBS. These data are being examined for evidence of rapid fluctuations.

Active-Region Studies

In 1980 the FCS made many observations of active regions in its polychromatic ("home position" – HP) mode. These data were used to determine plasma characteristics of the corona in such regions. However, the analysis, without information on the line shape or centroid, required many assumptions to interpret the data. Only two spectral scans of active regions were made in 1980, and so there were few data on which to base those assumptions. Hence, some of our earliest observations following the *SMRM* were spectral scans of active regions in order to establish a good data base on the HP lines. Several interesting and novel themes have emerged from active-region studies:

(1) **Active-Region Dynamics.** The line profiles of quiescent active region plasma in some cases show line widths that exceed the expected thermal Doppler width by an amount equivalent to a turbulent velocity of over 50 km s^{-1}. This is being investigated as a possible source of coronal heating. We are also looking for directed flows in the coronal loops.

(2) **Characteristic Temperatures of Active Regions.** With the added flexibility afforded by the use of the FCS wavelength drive, we were able to expand the number of lines observed. Hence, we can use more accurate temperature diagnostics than those available with the HP lines. For example, we can use line ratios from different ions of the same element (independent of relative abundances which are generally poorly known). It is even possible to do differential emission measure studies on active regions using the FCS data to establish whether a single electron temperature can truly represent the coronal emission from an active region, as is often assumed.

(3) **Theoretical Simulations of Active Region Spectra.** Using the published atomic data and the known instrument characteristics, we are now able to simulate the soft X-ray spectrum in any of the XRP wavelength bands. Figures 3-1, 3-2, and 3-3 illustrate the simulated spectra for a variety of typical coronal conditions in each of the remaining FCS channels. These simulations can be compared with an observed scan of the same spectral region by a least squares technique to determine the most probable characteristic temperature and emission measure. Such comparisons between theory and data are shown in Figure 3-4. Note that several of the lines seem anomalously bright or faint, and some are missing entirely. The differences represent problems in the atomic data (ion balance, oscillator strength, the wavelength of the line, and/or the elemental abundances). Hence, these spectral atlases, taken under a variety of coronal conditions, have proved to be useful in identifying such problems in the theory.

(4) **Long-Term Evolution of Active Regions.** The XRP data base now contains a wealth of data on active region evolution. With the additional observing time that the *SMRM* has afforded us, we have observed the birth, growth, and decay of many active regions. We have been able to observe regions transit the solar disk and even make several returns. Hence, it is now possible to determine how these regions change throughout their lifetimes. We can also compare typical plasma parameters for active regions at different times in the solar cycle. The XRP team were the first to note the time of solar minimum and the onset of the new cycle regions based on the switch of X-ray-emitting and flare-producing regions from the equatorial bands to high solar latitudes ($\geq 30°$).

There are a host of other topics associated with active region and quiet Sun studies by the XRP that could be discussed here. Lack of space forbids more

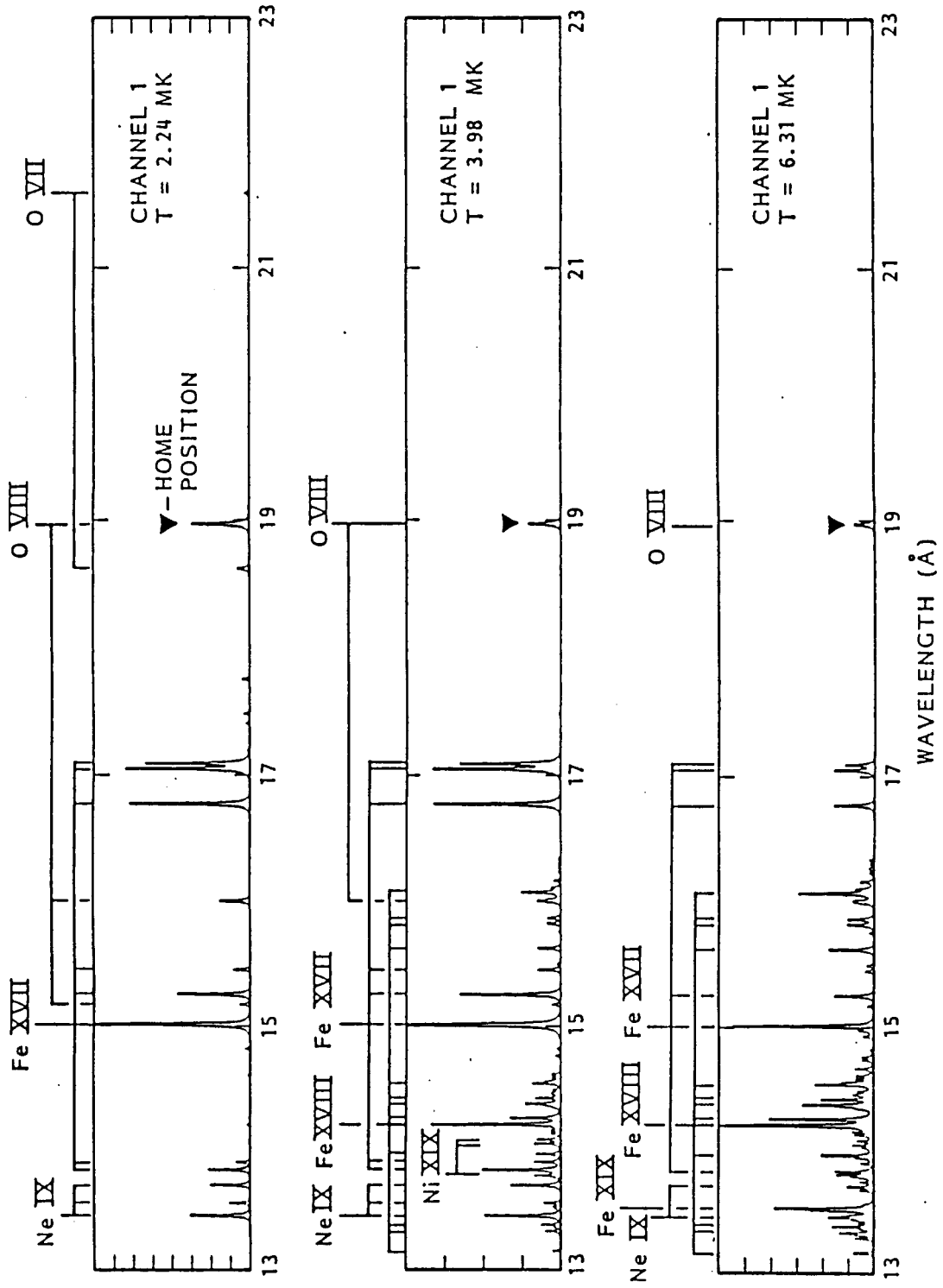

Figure 3-1. Simulation of FCS Channel 1 spectra at temperatures of 2.24, 3.98, and 6.31 MK. Principal spectral lines are marked along the top of each graph. The O VIII resonance line is the home position for Channel 1 (see arrow).

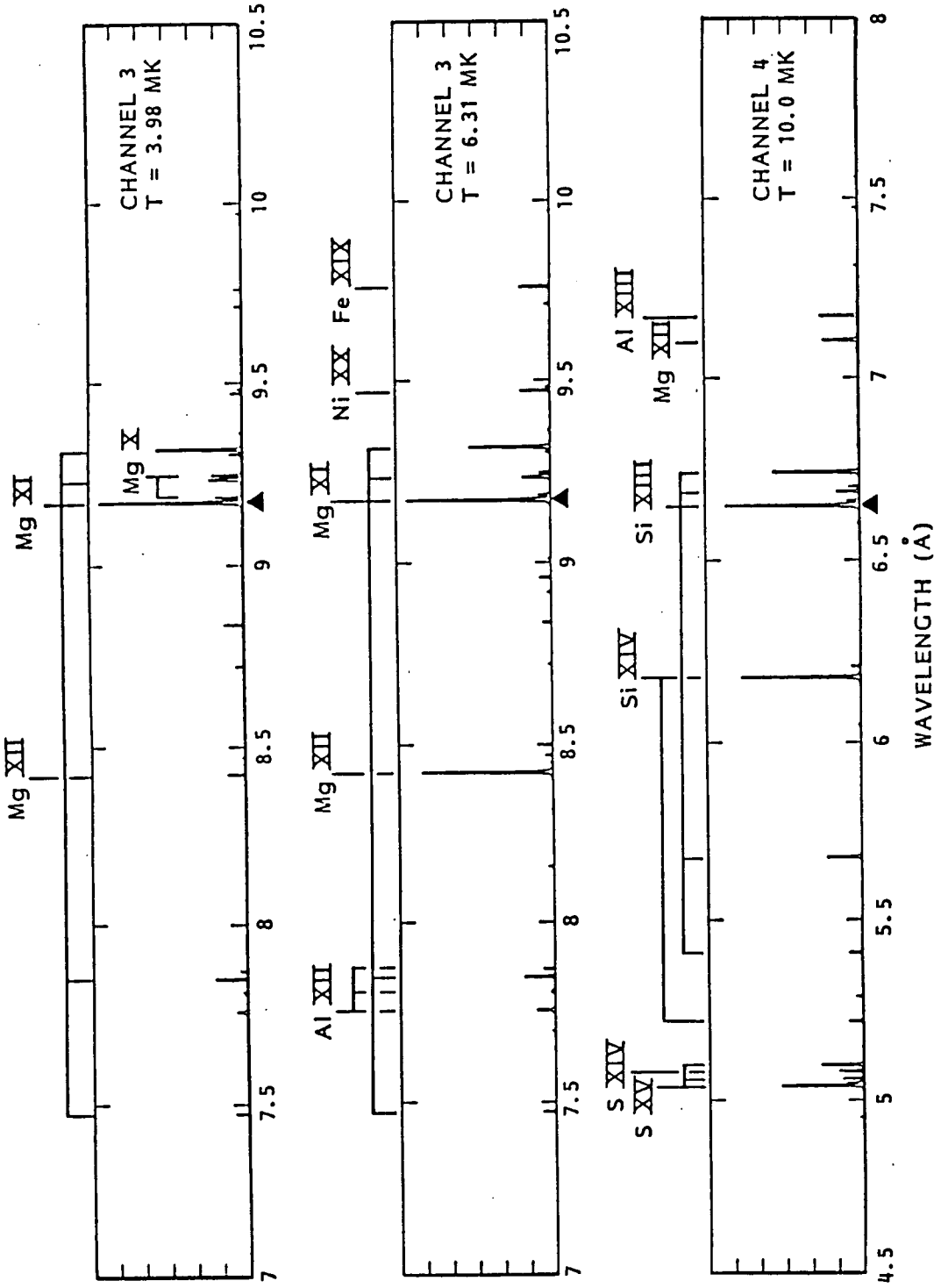

Figure 3-2. Simulation of FCS Channel 3 and 4 spectra. Channel 3 is simulated at 3.98 and 6.31 MK and Channel 4 at 10.0 MK.

extensive discussions, but it should be noted that, although active region and quiet Sun studies may be less spectacular than those of flares, they may very well represent one of the longest lasting legacies of the XRP program.

3.1.3 Coronal Magnetic Structures Observing Campaign (CoMStOC)

The Coronal Magnetic Structures Observing Campaign (CoMStOC) was organized by the XRP science team and *SMM* Guest Investigator Gordon Holman. This campaign required intensive coordinated multi-wavelength observations over a three week block of time to achieve a detailed study of active region coronal loops. Key elements in the campaign were the spatial resolution and spectral information available at cm wavelengths with the Very Large Array (VLA) and the soft X-ray plasma diagnostics provided by the FCS. The combined VLA and XRP observations should separate the contributions of the two microwave emission mechanisms — thermal bremsstrahlung and gyroresonance — and provide the only method of measuring the magnetic field strength in the solar corona.

The XRP low-energy detectors were turned on for a period of 26 days, beginning on 25 November 1987, in support of CoMStOC. These detectors have thin-aperture windows and a gas flow system. The gas reserves are now running low and are used only for blocks of a few weeks at a time, during a large collaboration or for major episodes of solar activity.

The XRP team wrote or renovated several FCS active region crystal sequences specifically for the CoMStOC thin-window turn-on. These sequences consist of maps at the peaks of various bright resonance lines to determine plasma parameters across the region and wavelength scans in the X-ray brightest portion of an active region where there are enough counts to do spectroscopy. A brief description of each sequence appears below.

AR Velocities: designed to study the occurrence and location of nonthermal line broadening in quiescent active regions. Line profiles for four bright resonance lines are scanned; electron temperatures are determined from ratios of the line strengths and the "excess line widths" above the electron Doppler values can then be used to estimate velocities from turbulent motions.

AR Densities: concentrates on the density measurement available from the ratio of the forbidden to the intersystem lines in the Ne IX triplet.

Quintmap: this is the most general sequence for determining plasma parameters such as electron temperature, emission measure and (unit filling factor) density across an active region from different line ratios.

AR Atlas: scans a wide range of active region lines at the brightest Fe XVII pixel, providing detailed spectroscopic information on plasma properties.

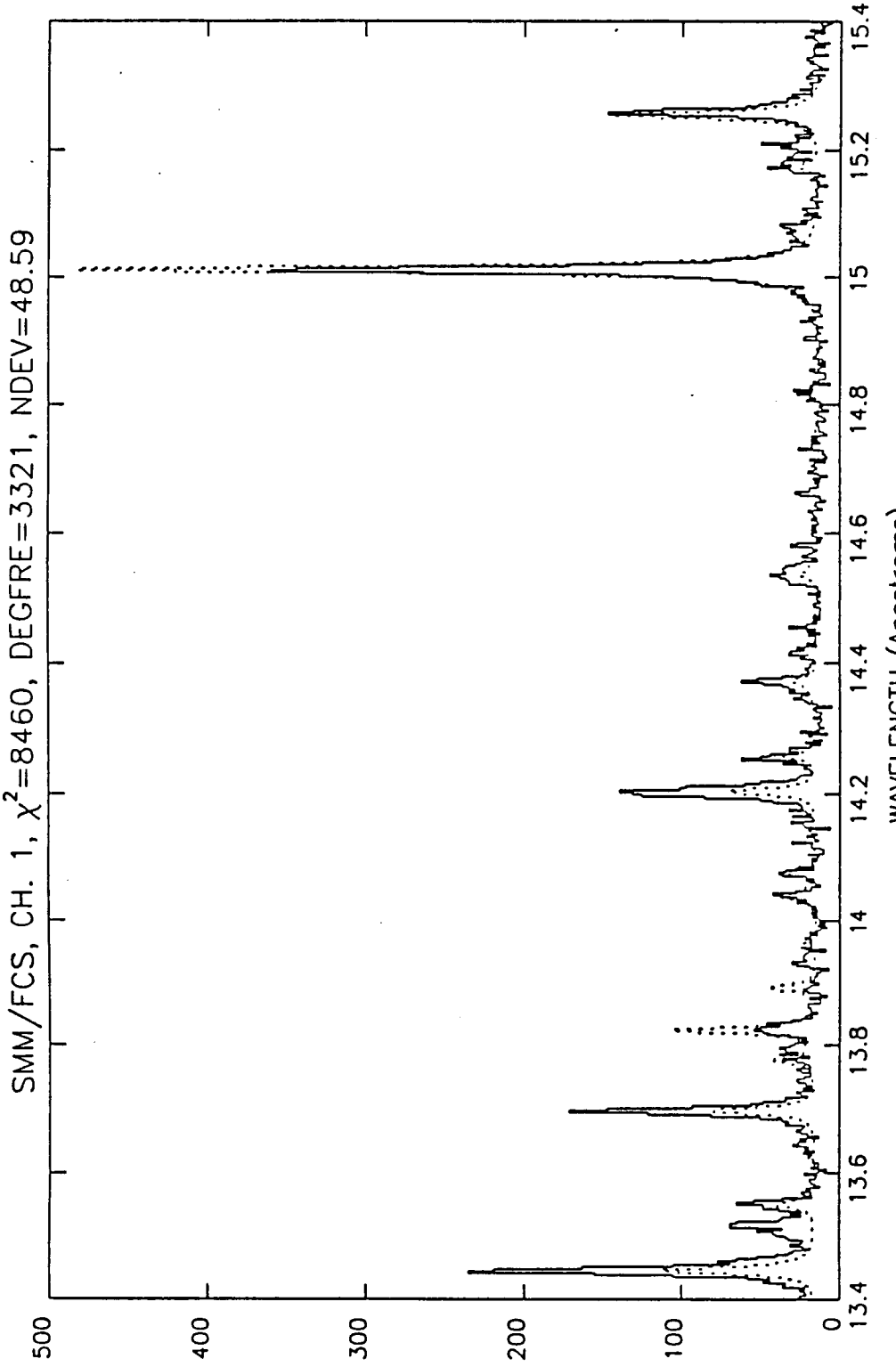

Figure 3-3. Simulation of FCS Channel 5 and 7 spectra. Channel 5 is simulated at 15.8 MK and Channel 7 at 25.1 and 39.8 MK.

Critical information for CoMStOC planning and analysis was received throughout the period from participating observatories: Owens Valley, the SOON sites, Big Bear Solar Observatory, Haleakala, Marshall Space Flight Center, Kitt Peak, Sac Peak, HAO, and UVSP. The Goddard *SMM* Solar Forecasting Center did a fantastic job of coordinating this flood of information.

Saturday, 28 November 1987, the first VLA day, N. Nitta and N. Gopalswamy of the University of Maryland observed AR 4896 (S33W91 at 1800 UT) and AR 4891 (S21W81 at 1800 UT), two active regions near the west limb of the solar disk. Good quality three-element data were obtained from Owens Valley; the spectrum evolved significantly over a two hour period, in a manner consistent with the progressive occultation of the stronger coronal fields as the region disappeared over the limb.

Friday, 4 December 1987, Joan Schmelz of XRP and Ray Gonzalez of the VLA observed AR 4899 (N31W02 at 1800 UT) which was close to central meridian but rather weak and stable. The GOES background was flat at the A5 level with only minor fluctuations.

Friday, 11 December 1987, Rob Willson of Tufts University observed at the VLA; AR 4901 (S32W61) was on the southwest limb during the observing time. Both the AS&E soft X-ray rocket and the NRL EUV rocket flew successfully from White Sands.

Friday, 18 December 1987, the last CoMStOC VLA day, Rob Willson observed AR 4906 which was at S32E13 at 1800 UT. This was the return of AR 4896, the region observed on the west limb on the first CoMStOC VLA day. The GOES background was again flat and stable at the B1 level.

3.1.4 Workshops

The XRP team has hosted two science workshops and plans to host a third later this year. These workshops are briefly described in this section.

SMM-TNT Workshop

The *SMM*-sponsored Workshop on "Thermal/Nonthermal Interactions in Solar Flares" (TNT) was hosted by the XRP team at the Sheraton Hotel in New Carrollton, Maryland during the week of 23–27 March 1987. The conference was organized by Applied Research Corporation personnel under subcontract from Lockheed. Keith Strong chaired the conference and the XRP team at Goddard supplied most of the technical support leading up to and continuing through the conference. The meeting was centered on an ongoing poster session and was complemented by review talks and meetings of subgroups which reported on progress and goals in plenary sessions. On the last day, the Workshop culminated in a session discussing

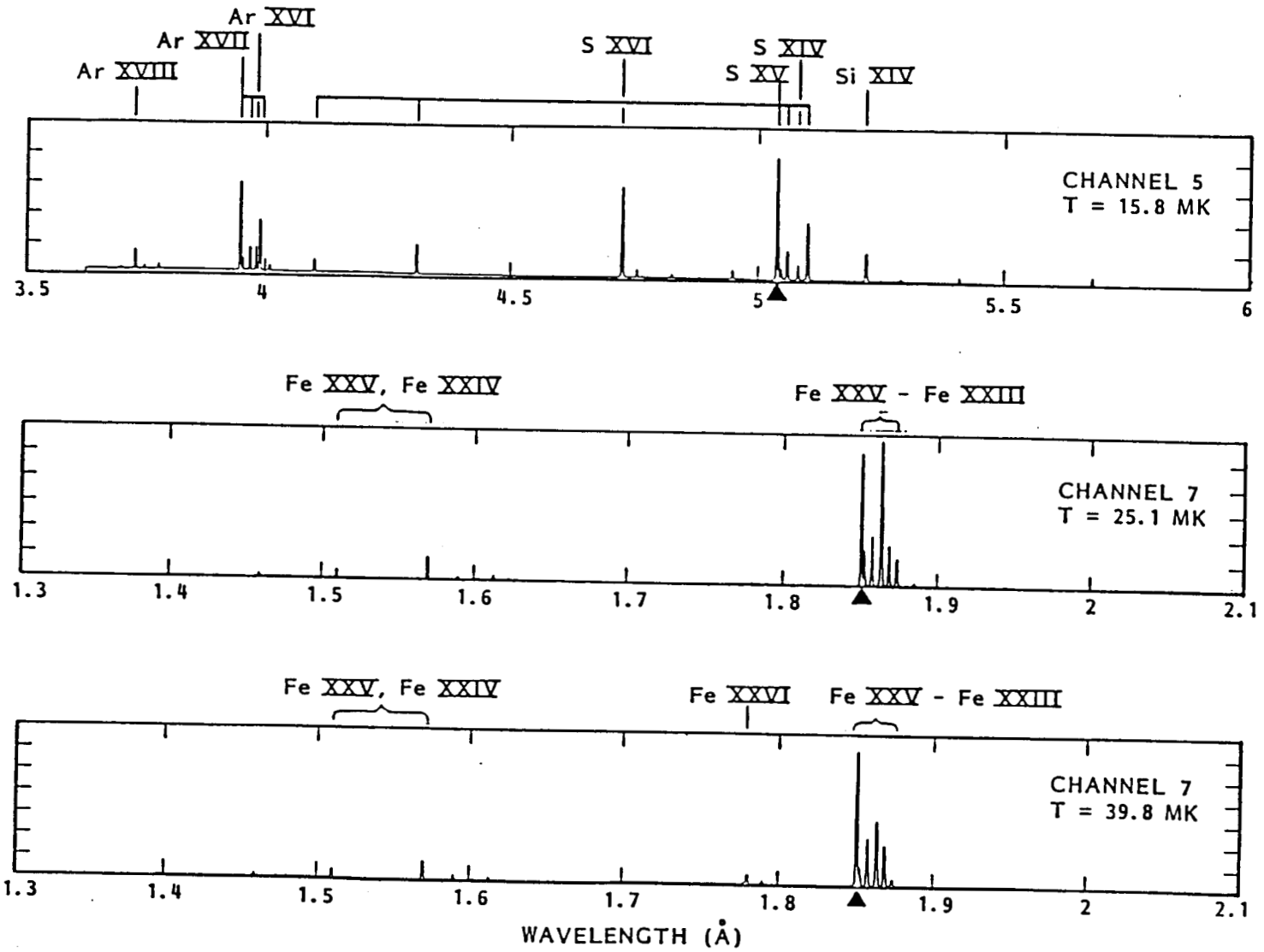

Figure 3-4. Comparison of an FCS active region spectrum (solid line) from Channel 1 for 13 February 1986 with a 3.16 MK simulated spectrum based on the work of Mewe *et al.*, 1985. The simulated spectrum (dashed line) includes a linear background term and was fitted over 13.09–22.27Å. Units of the ordinate are counts/0.256 s. Acquisition time for the data shown was three minutes. Emission measure derived from the fit is 5.8×10^{47} cm^{-3}.

opportunities for solar physics over the next few years to the space station era. The meeting had 80 attendees representing much of the international solar physics community. In addition to "observers" from *SMM*, NASA Headquarters, and *Solar-A*, there were 72 active participants, divided into four study groups that looked at problems in the areas of: (i) large scale magnetic field phenomena, (ii) flare dynamics, (iii) energy release and deposition, and (iv) global energy balance. A number of collaborations were forged at the meeting which, if successful, should produce progress in a number of vital areas for flare research. There are plans for a second follow-up workshop (TNT II) in England, to bring together results from work begun at the first. A workshop publication is being deferred until TNT II. The cost of the Workshop was approximately $43,000.

CoMStOC Workshop

An informal workshop on the Coronal Magnetic Structures Observing Campaign (CoMStOC) was hosted by the XRP team on 23–25 March 1988 at Goddard Space Flight Center (GSFC). The workshop was both organized and chaired by Joan Schmelz, the XRP/Radio observations liaison. The goal of CoMStOC was to obtain the detailed coronal loop plasma and magnetic field measurements needed to improve substantially our understanding of active region coronal loop structures. At the workshop, participants in the campaign met to share both the data gathered as part of CoMStOC and their knowledge of the observations and equipment required by the campaign. There were 25 workshop participants in all, including representatives of the XRP science team, the *SMM* Solar Forecast team, the GSFC Laboratory for Astronomy and Solar Physics theory group, the Big Bear Solar Observatory, the Owens Valley Radio Observatory, the Haleakala vector magnetograph, the NRL HRTS and the AS&E soft X-ray rocket teams, and the Very Large Array (VLA), as well as solar radio observers from U. Maryland, Tufts U., Cal Tech, Center for Astrophysics (Harvard), and JILA (U. Colorado). Costs to the *SMM* workshop budget amounted to $2000 in travel expenses to bring two key participants to the workshop who otherwise could not have attended. Refreshments were kindly provided by the *SMM* Project office.

IAU Colloquium No. 104

IAU Colloquium No. 104, "Solar and Stellar Flares," is being organized, in part, under the sponsorship of the XRP Workshop budget; additional funding is being provided by the IAU, ESA, COSPAR, Lockheed, and a separate NASA grant to Stanford University. The motivation for this five-day meeting, to be held during the week of August 15–19, 1988, at Stanford University, is to bring together both solar and stellar researchers, and both theoretician and observers, to explore the flare phenomenon from all possible perspectives. Meeting Co-chairmen are Bernhard M. Haisch from the LPARL *SMM* Team, and Marcello Rodono, director of the Catania

Observatory. *SMM* data and observing programs will be prominently featured at this symposium. The proceedings will be published by Reidel as a special edition of *Solar Physics*; this will also be marketed as a book. An enthusiastic response followed the First Announcement in August of 1987, and at this point we expect more than 250 participants from around the world to take part. $45,000 has been allocated in the *SMM* Workshop budget to sponsor this meeting.

3.1.5 Other Science Meetings

Scientific results involving XRP data have been and continue to be presented at numerous local (Solar Neighbourhood), national (American Astronomical Society), and international meetings (COSPAR, IAU). The diversity of topics addressed by these presentations is illustrated by the great variety of papers in Appendix A – many of which have evolved into publications in refereed journals.

In addition to the above well-known astronomy and astrophysics meetings, XRP results are now presented regularly at meetings of the American Geophysical Union (AGU). Until recently, the AGU was considered predominantly a forum for earth science and interplanetary research. This situation has changed dramatically as the geophysical community have, through their exposure to *SMM* data, become keenly interested in solar research and its relevance to their own terrestial work.

3.2 SCIENCE HIGHLIGHTS

The scientific contribution of the *SMM* to the understanding of solar processes is abundantly evident from the numerous publications that have been produced since the launch in 1980. This statement is no less true when applied to the XRP. Many publications feature work which depend principally on XRP data or have used XRP data in conjunction with data acquired by other space-based or ground-based instrumentation. In some cases, XRP data have been the stimulus for new modelling or theoretical studies. Most of this work has been or is due to be published in refereed journals. A selection of work has also been presented at several important conferences and workshops. A complete bibliography of papers relating to the XRP is given in Appendix A.

In this Final Report we have chosen to highlight approximately a dozen topics in which the XRP has played a significant role in providing insights to key questions. In the following sections we reproduce important abstracts of published papers and in several cases give an abridged list of additional references. Many more topics have been addressed in the literature and Appendix A should be consulted for a complete listing of publications. In Section 3.3 a discussion of the XRP-Radio collaborative work is described.

3.2.1 Momentum Balance

"Explosive Plasma Flows in a Solar Flare," D. M. Zarro, R. C. Canfield, K. T. Strong, and T. R. Metcalf, *Ap. J.*, **324**, 582, 1988.

Solar Maximum Mission soft X-ray data and Sacramento Peak Observatory Hα observations were combined in a study of the impulsive phase of a solar flare. A blue asymmetry, indicative of upflows, was observed in the coronal Ca XIX line during the soft X-ray rise phase. A red asymmetry, indicative of downflows, was observed simultaneously in chromospheric Hα emitted from bright flare kernels during the period of hard X-ray emission. Combining the velocity data with a measurement of coronal electron density, we show that the impulsive phase momentum of upflowing soft X-ray emitting plasma equalled that of the downflowing Hα emitting plasma to within an order of magnitude. In particular, the momentum of the upflowing plasma was 2×10^{21} g cm s^{-1} while that of the downflowing plasma was 7×10^{21} g cm s^{-1}, with a factor of two uncertainty on each value. This equality supports the explosive chromospheric evaporation model of solar flares, in which a sudden pressure increase at the footpoint of a coronal loop produces equal and oppositely directed flows in the heated plasma.

Additional References: Gunkler *et al.*, *Ap. J.*, **284**, 839, 1984; Antonucci *et al.*, *Ap. J.*, **287**, 917, 1984; Bentley *et al.*, *Astron. and Astrophys.*, **154**, 255, 1986; Doyle and Bentley, *Astron. and Astrophys.*, **155**, 278, 1986; Zarro *et al.*, *Adv. Space Res.*, **6**, 61, 1986.

3.2.2 Initial Phase of Chromospheric Evaporation

"Initial Phase of Chromospheric Evaporation in a Solar Flare," E. Antonucci, B. R. Dennis, A. H. Gabriel, and G. M. Simnett, *Solar Phys.*, **96**, 129, 1985.

In this paper we discuss the initial phase of chromospheric evaporation during a solar flare observed with instruments on the Solar Maximum Mission on May 21, 1980 at 20:53 UT. Images of the flaring region taken with the Hard X-ray Imaging Spectrometer in the energy bands from 3.5 to 8 keV and from 16 to 30 keV show that early in the event both the soft and hard X-ray emissions are localized near the footpoints, while they are weaker from the rest of the flaring loop system. This implies that there is no evidence for heating taking place at the top of the loops, but energy is deposited mainly at their base. The spectral analysis of the soft X-ray emission detected with the Bent Crystal Spectrometer evidences an initial phase of the flare, before the impulsive increase in hard X-ray emission, during which most of the thermal plasma at 10^7 K was moving toward the observer with a mean velocity of about 80 km s^{-1}. At this time the plasma was highly turbulent. In a second phase, in coincidence with the impulsive rise in hard X-ray emission during the major burst, high velocity (370 km s^{-1}) upward motions were observed. At

this time, soft X-rays were still predominantly emitted near the loop footpoints. The energy deposition in the chromosphere by electrons accelerated in the flare region to energies above 25 keV, at the onset of the high-velocity upflows, was of the order 4×10^{10} ergs s^{-1} cm^{-2}. These observations provide further support for interpreting the plasma upflows as the mechanism responsible for the formation of the soft X-ray flare, identified with chromospheric evaporation. Early in the flare soft X-rays are mainly from evaporating material close to the footpoints, while the magnetically confined coronal region is at lower density. The site where upflows originate is identified with the base of the loop system. Moreover, we can conclude that evaporation occurred in two regimes: an initial slow evaporation, observed as a motion of most of the thermal plasma, followed by a high-speed evaporation lasting as long as the soft X-ray emission of the flare was increasing, that is as long as plasma accumulation was observed in the corona.

3.2.3 Gentle Evaporation

"Conduction-Driven Chromospheric Evaporation in a Solar Flare," D. M. Zarro and J. R. Lemen, *Ap. J.*, (in press), 1988.

We present observations of gentle chromospheric evaporation during the cooling phase of a solar flare. Line profiles of the low-temperature ($T \sim 6 \times 10^6$ K) coronal Mg XI line, observed with the X-Ray Polychromator on the *Solar Maximum Mission*, show a blueshift that persisted for several minutes after the impulsive heating phase. This result represents the first detection of an evaporation signature in a soft X-ray line formed at this low temperature. By combining the Mg XI blueshift velocity data with simultaneous measurements of the flare temperature derived from Ca XIX observations, we demonstrate that the upward flux of enthalpy transported by this gently evaporating plasma varies linearly with the downward flux of thermal energy conducted from the corona. This relationship is consistent with models of solar flares in which thermal conduction drives chromospheric evaporation during the early part of the cooling phase.

3.2.4 Density Measurements

"Properties of an Impulsive Compact Solar Flare Determined by *SMM* X-ray Measurements" G. A. Linford and C. J. Wolfson, *Ap. J.*, (in press), 1988.

We have analyzed soft X-ray, hard X-ray, magnetogram, and Hα data for an impulsive compact flare which occurred on 21 May 1985. The X-ray observations were from the X-Ray Polychromator (XRP) and the Hard X-Ray Burst Spectrometer on board the *Solar Maximum Mission* satellite (*SMM*). Observations from the XRP instrument included images during the pre-flare period and the impulsive phase, and soft X-ray spectra of helium-like ions during the remainder of the flare. The

impulsive phase images show a flare loop with hot loop legs. The derived flare loop dimensions are $\sim 2 \times 10^4$ km (length) and ~ 150 km (diameter).

Measurements of line ratios from the Mg XI ion indicate that the plasma density varied from about 4×10^{12} cm^{-3} early in the flare to about 10^{12} cm^{-3} during the flare decay. The temperature of this plasma is shown to be about that for maximum emission (7×10^6 K) and varied only during the late decay phase of the flare, dropping to about 5×10^6 K. The average measured value of the Mg XI G ratio supports a theoretical formulation that includes both dielectronic and radiative recombination. When all of the observations are combined, the simplest interpretation of the event is one in which the source of the soft X-ray flare emission was confined to a thin loop of very high density. The very short timescales, high pressure and density, and small volume for this event place it beyond the extremes of the classical compact flare characteristics as described by Pallavicini *et al.* (1977).

Additional References: Wolfson *et al.*, *Ap. J.*, **269**, 319, 1983; Svestka *et al.*, *Adv. Space Res.*, **6**, 253, 1986.

3.2.5 Abundance Measurements

"Determination of the Calcium Elemental Abundance for 43 Flares from *SMM*-XRP Solar X-Ray Spectra," J. R. Lemen, J. Sylwester, and R. D. Bentley, *Adv. Space Res.*, **6**, 245, 1986.

The helium and lithium-like X-ray transitions of Ca XVIII–XIX have been used to make an absolute measurement of the coronal calcium elemental abundance relative to hydrogen (A_{Ca}) in solar flares. Cooling phase spectra of 43 flares obtained in channel 1 of the Bent Crystal Spectrometer (BCS) on the *Solar Maximum Mission* have been analyzed. The abundance is determined from the intensity ratio of the Ca XIX resonance line ($^1S_0 - ^1P_1$) and nearby continuum. A large variation is observed in the values of the derived abundances, ranging up to a factor of 2.5 between the extreme cases. This confirms the earlier results of Sylwester, Lemen, and Mewe (1984), who investigated a smaller sample of flares. In addition to the variability of A_{Ca} observed between different flares, it was suggested that A_{Ca} varies during the heating phase of some flares. We neglect this phenomenon in the present work, and concentrate on the cooling phase during which A_{Ca} appears to remain constant for any individual flare. Attempts to correlate the A_{Ca} measurements with other observable features are discussed.

Additional References: Sylwester, Lemen, and Mewe, *Nature*, **310**, 665, 1984.

3.2.6 Active Region Studies

"Evidence for Coronal Turbulence in a Quiescent Active Region," J. L. R. Saba and K. T. Strong, *Adv. Space Res.*, **6**, 37, 1986.

The first evidence for nonthermal broadening of X-ray lines in a quiescent active region was based on a single observation of a limb active region by the Flat Crystal Spectrometer (FCS) on the *Solar Maximum Mission* (*SMM*) satellite (Acton *et al.*, *Ap. J. (Lett.)*, **244**, L137, 1980). With the renewal of *SMM* operations, the FCS has been used to investigate this phenomenon further. On 28 April 1984, a map of Mg XI resonance line profiles was made of a bright area in NOAA Active Region 4474 during a nonflaring period. The narrowest line profiles are consistent with the nominal instrumental width plus a thermal width equivalent to about 3×10^6 K, the temperature derived from line ratios of O VIII, Ne IX, and Mg XI. The broadest line profiles are consistent with the instrumental width plus a thermal width equivalent to about 7×10^6 K, but a substantial amount of plasma at this temperature would result in much greater flux in the FCS higher temperature channels than was seen. If the excess width is attributed solely to plasma turbulence, the corresponding velocity is about 40 ± 10 km s^{-1}. If associated with energy dissipation, such turbulent motions could have important consequences for coronal heating. Correlations of line widths and intensities with magnetic and Hα structures are investigated.

Additional References: Haisch, *Adv. Space Res.*, **6**, 45, 1986.

3.2.7 Two-Ribbon Flares and CMEs

"The X-ray Signature of Solar Coronal Mass Ejections," R. A. Harrison, P. W. Waggett, R. D. Bentley, K. J. H. Phillips, M. Bruner, M. Dryer, and G. M. Simnett, *Solar Phys.*, **97**, 387, 1985.

The coronal response to six solar X-ray flares has been investigated. At a time coincident with the projected onset of the white-light coronal mass ejection associated with each flare, there is a small discrete soft X-ray enhancement. These enhancements (precursors) precede by typically ~20 minutes the impulsive phase of the solar flare which is dominant by the time the coronal mass ejection has reached an altitude above 0.5 $R_\odot$. We identify motions of hot X-ray emitting plasma, during the precursors, which may well be a signature of the mass ejection onsets. Further investigations have also revealed a second class of X-ray coronal transient, during the main phase of the flare. These appear to be associated with magnetic reconnection above post-flare loop systems.

Additional References: Svestka *et al.*, *Sol. Phys.*, **108**, 237, 1987; Hick *et al.*, *Sol. Phy.*, (in press), 1988.

3.2.8 Radio Studies

"Solar Active Region Physical Parameters Inferred from a Thermal Cyclotron Line and Soft X-ray Spectral Lines," K. R. Lang, R. F. Willson, K. L. Smith and K. T. Strong, *Ap. J.*, **322**, 1044, 1987.

We present simultaneous high-resolution observations of coronal loops at 20 cm wavelength with the VLA and at soft X-ray wavelengths with the *SMM* FCS. The images at 20 cm and soft X-ray wavelengths have nearly identical sizes and ellipsoidal shapes, with a linear extent of about 5×10^9 cm. This emission stretches between and across regions of opposite magnetic polarity in the underlying photosphere. Complete X-ray coronal loops can therefore be imaged at 20 cm, and the VLA maps describe the radio wavelength counterpart of X-ray coronal loops. X-ray spectral lines were used to obtain values of electron temperature $T_e = 2.6 \pm 0.1 \times 10^6$ K and electron density $N_e = 3.1 \pm 0.3 \times 10^9$ cm^{-3} averaged over the emitting area. These parameters are used with plausible estimates for the loop thickness, magnetic scale height, and magnetic field strength to show that the plasma is optically thin to thermal bremsstrahlung, but that it might be optically thick to thermal gyroresonance radiation at 20 cm. The absence of detectable circular polarization is consistent with an optically thick plasma. The observed brightness temperature was roughly equal to the electron temperature of the coronal plasma. The VLA maps at 10 closely spaced frequencies between 1440 and 1720 MHz describe the same coronal loops or arcades of loops. A plot of the maximum brightness temperature of these loops as a function of observing frequency exhibits a linelike feature with a central frequency of 1650 MHz and a half-width of 80 MHz. This spectral feature is attributed to a thermal cyclotron line and indicates that the optical depth of thermal gyroresonance radiation must be greater than that of thermal bremsstrahlung at these frequencies. The X-ray values for T_e and N_e are combined with plausible values of magnetic scale height and optical depth for gyroresonance absorption to show that the harmonic of the gyrofrequency is 4. The central frequency and narrow width of the thermal cyclotron line are combined with this harmonic to show that the magnetic field strength of the coronal loops is 147 ± 5 G.

Additional References: (See section 3.3 for additional references.)

3.2.9 Iron K-alpha

"The Excitation of the Iron K-alpha Feature in Solar Flares," A. G. Emslie, K. J. H. Phillips and B. R. Dennis, *Sol. Phys.*, **103**, 89, 1986.

We evaluate the relationship between the hard X-ray photon spectrum and the flux of iron Kα emission in a thick-target electron bombardment model. Results are presented for various power-law hard X-ray spectra. We then apply these results to two events observed with the Hard X-Ray Burst Spectrometer and the Kα channel of the X-Ray Polychromator Bent Crystal Spectrometer on the *Solar Maximum Mission* satellite. For one of the events, on 29 March 1980 at 09:18 UT, the Kα flux predicted for a thick-target non-thermal process is significant compared to the background fluorescent component, and the data are indeed consistent with an enhancement of the predicted amount. For the other event, on 14 October,

1980 at 06:09 UT, the hard X-ray spectrum is so steep that no significant Kα flux is predicted for this process, and no enhancement is seen. We conclude that the agreement between the predicted Kα flux and the observed magnitude of the Kα enhancement above the fluorescent background at the time of the large hard X-ray bursts lends support to a thick-target non-thermal interpretation of impulsive hard X-ray emission in solar flares.

Additional References: Parmar *et al.*, *Ap. J.*, **279**, 866, 1984.

3.2.10 Energetics of Coronal Loops

"Active Region Coronal Loops: Structure and Variability," Bernhard M.Haisch, Keith T. Strong, Richard A. Harrison and G. A. Gary, *Ap. J. Suppl.*, in press (October issue), 1988.

We have studied X-ray images of a pair of active region loops (which are in all likelihood, of course, each ensembles of finer scale loops) which show significant, short timescale variability in the line fluxes of O VIII (18.97 Å, $T \approx 3 \times 10^6$ K), Ne IX (13.45 Å, $T \approx 3 \times 10^6$ K), and Mg XI (9.17 Å, $T \approx 6 \times 10^6$ K) during four orbits as observed by the Flat Crystal Spectrometer onboard the Solar Maximum Mission (*SMM*) and in 3.5 – 11.5 keV soft X-ray bands as observed by the *SMM* Hard X-ray Imaging Spectrometer (*HXIS*). The FCS Spectroheliograms have a spatial resolution of 10″ over a 3′ × 3′ area; HXIS images span 6.4′ × 6.4′ with coarser, 3″, resolution.

Vector magnetograms and high resolution ultraviolet images obtained by a rocket experiment that day (23 September 1980) have been used to model the three-dimensional characteristics of the loops. Although similar in appearance in projection on the FCS spectroheliograms, it appears from the field line models that the northern (N-) loop is long and high ($L \approx 1.3 \times 10^5$ km, $h \approx 6 \times 10^4$ km), whereas the southern (S-) loop is shorter and too low to determine a reliable vertical height ($L \approx 4 \times 10^4$ km).

X-ray light curves have been generated from the 25 FCS spectroheliograms and from HXIS maps spanning four consecutive orbits for both loops individually; and for the higher resolution FCS images light curves of the loop tops and brightest points have been generated as well. The largest variations involve flux changes of up to several hundred percent on time scales of ten minutes. However no significant $H\alpha$ flare activity was reported, and loop temperatures (below) remained in the $T \approx 4 - 6 \times 10^6$ K range. Temperatures and emission measures were derived from Mg XI/Ne IX line ratios and absolute emissivity/flux ratios respectively, and these too show significant variability.

Application of the Rosner, Tucker and Vaiana (1978) scaling law ($T = 1.4 \times 10^3 (pL)^{\frac{1}{3}}$) to the quiescent phases of both loops results in reasonable densities ($n_e \approx$

$2 - 5 \times 10^9$ cm^{-3}), which, however, are inconsistent with the EM's, resulting in far too large a volume, V, or column height, h for either loop compared to what is observed. We find that the densities must be about an order of magnitude higher than predicted by the scaling law, and we take this as evidence that the RTV analysis fails because steady-state conditions do not prevail in these systems.

Examination of the decay phases of several events adds to the inconsistency in that relatively low densities are suggested there as well, resulting in the anomaly that $n_e(quiet) > n_e(active)$. We reject this possiblity and conclude that the decay phases of the light curves indicate radiative cooling, inhibition of conduction, and some type of "continued heating," which we interpret as resulting from ongoing, underlying activity at still lower energy levels: the *microflare* level. We interpret the large-scale variations we have observed as falling somewhere between the (conventional) flare and the microflare in a continuous energy spectrum of discrete coronal heating processes.

These two loops together made up a significant fraction of the solar X-ray luminosity: the average S-loop luminosity was $L_x \approx 2 \times 10^{28}$ ergs s^{-1}. Fluctuations of the sort reported herein would therefore constitute measureable variability for the Sun observed as an (X-ray) star. This behaviour is in fact very similar to *Einstein* and *Exosat* observations of stellar microflaring. We conclude that the coronal loops discussed herein are the solar analogs of the stellar microflare, both in the energies involved and in the timescales.

Additional References: Simnett and Strong, *Ap. J.*, **284**, 839, 1984; Bornmann, *Ap. J.*, **293**, 595, 1985; MacNeice *et al.*, *Sol. Phys.*, **99**, 167, 1985; Cheng *et al.*, *Ap. J.*, **298**, 887, 1985; Simnett, Phillips, and Bentley, *Adv. Space Res.*, **6**, 109, 1986; Strong, *Adv. Space Res.*, **6**, 257, 1986.

3.2.11 Spectral Atlases

"New Spectral Line Identifications in High Temperature Flares," B. C. Fawcett, C. Jordan, J. R. Lemen, K. J. H. Phillips, *M.N.R.A.S.*, **225**, 1013, 1987.

A solar flare spectrum in the wavelength region between 7.8 and 10.0 Å, recorded by the Flat Crystal Spectrometer on *Solar Maximum Mission* during a flare on 1985 July 2, is presented. It includes several spectral emission lines not hitherto reported. Most are identified through comparison with wavelengths either measured in laser-produced spectra or calculated *ab initio*. It is found that they are mainly due to n = 2–4, 5 transitions in Fe XIX to Fe XXIII. In a few cases, previous identifications are corrected. The more intense lines appear in second order in another channel of the spectrometer. The potential of line-intensity ratios for temperature and density diagnostics is discussed.

3.2.12 Modelling

"A Numerical Hydrodynamic Model of a Heated Coronal Loop," P. MacNeice, *Sol. Phys.*, **103**, 47, 1986.

The fluid equations describing a fully ionized single temperature (i.e., electron and proton temperatures assumed identical) hydrogen plasma in a coronal loop subject to a transient heating pulse (2×10^9 ergs cm^{-2} s^{-1}) centered about the loop apex have been solved numerically. An adaptive regriding scheme was used to ensure adequate spatial resolution throughout the transition regions, and due regard paid to the numerical time constants. Because of the fine gridding made possible by this scheme these results represent the first reliable simulation of the impact of a downward propagating conduction front on the transition region, and the early stages of the development of the downward moving compression and upward ablation. Intensities in the O V (1371 Å) transition region line were calculated from the model results. Finally estimates have been made of the importance of the downward-streaming collisionless high-energy tail of the distribution in the transition region resulting from the very steep temperature gradients. It is shown that the mass and energy densities are not substantially altered by the non-Maxwellian tail except in so far as they are coupled to higher moments of the distribution function such as the heat flux through the fluid equations.

Additional References: Gary *et al.*, *Ap. J.*, **314**, 782, 1987; Fludra and Sylwester, *Sol. Phys.*, **105**, 323, 1986; Haisch and Claflin, *Sol. Phys.*, **99**, 101, 1985; Mewe *et al.*, *Astron. and Astrophys.*, **152**, 229, 1985.

3.2.13 Atomic Physics

"Inner-Shell Transitions of Fe XXIII and Fe XXIV in the X-ray Spectra of Solar Flares," J. R. Lemen, K. J. H. Phillips, R. D. Cowan, J. Hata and I. P. Grant, *Astron. and Astrophys.*, **135**, 313, 1984.

New calculations for the dielectronically excited $n = 2p$ Fe XXIV and $n = 2l$, $3l$, $4l$, $5l$ and $6p$ Fe XXIII satellites are presented and compared with solar-flare spectra obtained with the Bent Crystal Spectrometer instrument on board the *Solar Maximum Mission* spacecraft. Excellent overall agreement is achieved between the calculated and observed spectra. The calculations show that high-n satellites in Fe XXIII tend to converge in wavelength on the Fe XXIV transitions of the type $1s^2 2s - 1s2s2p$. For example, the diagnostically important line q, which in the past has been used as an indicator of the lithium- to helium-like ion balance $N(\text{Fe XXIV})/N(\text{Fe XXV})$, is shown to have a contribution from the Fe XXIII satellites amounting to about 10% of its total. Three different ionization balance calculations are considered (Jacobs *et al.*, 1977; Shull and van Steenberg, 1982; Doyle and Raymond, 1981). Implications for the use of the Fe XXIII–XXV spectrum as a diagnostic of solar flares are discussed.

Additional References: Lemen *et al.*, *J. of Appl. Phys.*, **60 (6)**, 1960, 1986; Mewe, Lemen, and van den Oord, *Astron. Astrophys. Suppl. Ser.*, **65**, 511, 1986; McWhirter and MacNeice, *Sol. Phys.*, **107**, 323, 1987; Antonucci *et al.*, *Astron. and Astrophys.*, (in press), 1986.

3.3 XRP-RADIO COLLABORATIONS

Collaborations with XRP and various solar radio astronomy groups continue to produce intriguing data on both solar features and flare phases. These radio observations have been made using the Very Large Array (VLA), Clark Lake, and the Westerbork Synthesis Radio Telescope (WSRT). A description of the work done in collaboration with the University of Maryland Solar Radio Group, K. Lang and R. Willson of Tufts University, and S. Habbal (CfA) and R. Gonzalez (VLA) appears in this section. Radio collaborations for the Coronal Magnetic Structures Observing Campaign (CoMStOC) are described in section 3.1.

3.3.1 University of Maryland Solar Radio Group

Preflare Buildup:

Coronal signatures of preflare energy buildup as seen in X-rays, UV, and microwaves have been compared and contrasted for a large number of events during an extensive study in the *SMM* workshop. Schmahl, Strong and Waggett examined background-corrected BCS light curves to look for flare onset times, and found that X-rays start rising 5–10 minutes before the impulsive phase. Similar onset profiles are seen in the microwave flux curves. This result suggests a thermal origin for the first phase of flares. However, spatially resolved observations (FCS, VLA) show complex structures that indicate differences between the gradual preflare and postflare phases. (Schmahl, Webb, Woodgate, Waggett, Bentley, Hurford, Schadee, Schrijver, Harrison and Martens, NASA CP 2439, 1986.).

In collaboration with the XRP group, it was shown that type III bursts mapped at Clark Lake appeared about an hour before the onset of a flare, implying that nonthermal electrons are generated during flare buildup. Soft X-ray emission during the preflare and preflash phases showed an increasing trend in temperature. We have suggested that nonthermal electrons generating type III bursts may also be responsible for the soft X-ray emission through plasma heating. (Kundu, Gopalswamy, Saba, Schmelz and Strong, *Solar Phys.*, in press, 1988)

Flares and Mass Ejections:

Simultaneous observations were made in microwaves and soft X-rays of the X-flare of 19 May 1984. The high brightness temperature of the post flare phase at

6 cm (50×10^6 K) as compared with the electron temperature determined by the X-ray observations (Schmelz *et al.*, BAAS, 1987) suggests that there was a nonthermal component to the "post-flare" emission. The flare structures seen at 6 cm and in X-rays had common centroids, but different shapes. This poses interesting questions regarding the post-flare energization processes. (Schmahl, Kundu, Schmelz, Saba and Strong, BAAS, 1987).

Coronal mass ejections, as seen in radio, white light and X-rays were examined in detail during the *SMM* workshop. Gergely presented examples of Type II (shocks) and Type IV (plasmoids) bursts associated with CME's. Phillips, Waggett and others examined BCS time profiles for determining onset times of the CME precursors. (Hildner *et al.*, NASA CP 2439, 1986).

Active Regions:

Strong, Alissandrakis and Kundu (*Ap. J.*, **277**, 865, 1984) compared WSRT maps of an active region observed in X-rays using the FCS instrument. They found that the ring structure seen at 6 cm wavelength above a large sunspot could be explained by reduced electron temperature above the sunspot.

The active region which produced the X-flare of 19 May 1984 was also mapped on the preceding day at 6 cm and 20 cm using the VLA. Preliminary examination of XRP images for the two days shows that the region was partially occulted by the limb on the 18th of May. The data provide an excellent way to determine the relative heights of emission in the two wavelength domains (Schmahl, Kundu, Schmelz, Saba *et al.*, in preparation).

3.3.2 Tufts University: K. Lang and R. Willson

Comparisons of high resolution images of solar active regions at 20 cm wavelengths (VLA) and in soft X-rays indicate that the structure and dominant radiation mechanisms of the coronal loops are complex and inhomogeneous (Lang *et al.*, 1987, *Ap. J.*, **322**, 1035; 1044). The data suggest that there are both cool and hot active region radio plasmas that are not detected at X-ray wavelengths, and that there is X-ray emission that remains invisible at 20 cm wavelengths. To understand the relative importance of gyroresonance and thermal bremsstrahlung radiation mechanisms and determine the magnetic field strength in the solar corona, simultaneous microwave and soft X-ray images must be taken and compared with theoretical models. Also, computer techniques are used to extrapolate the photospheric magnetic field results from Kitt Peak and MSFC to coronal heights; these result will be compared with the magnetic field derived from the XRP/VLA observations.

3.3.3 CfA: S. Habbal and VLA: R. Gonzalez

Simultaneous observations of the Sun were made on 1–2 November 1986, in the Fe XVII line with XRP, at 90, 20 and 6 cm radio wavelengths with the VLA, and in Hα and Ca I 6103 Å lines at Big Bear Solar Observatory. The simultaneous observations were made at disk center where there were two spot groups. A type I radio noise storm was observed at 90 cm. Radio synthesis mapping, together with photospheric magnetic field data provided, for the first time, solid evidence for the association of radio noise storms with active regions. The data also showed that a population of a few keV electrons was being continuously produced even 24 hours after the peak of the storm. Comparison with the Fe XVII line observations from the XRP showed that the density of these nonthermal electrons was not high enough to produce X-ray emission. This comparison also established a very good correspondence between temperatures inferred from the Fe XVII line and the 20 cm brightness temperatures ranging from 2 to 3.5×10^6 K. A very good spatial correlation between the bright regions of emission in Fe XVII and at 6 and 20 cm was also found. The goal of the ongoing collaboration is to compare the dynamical behavior of the emission from this active region at the cm radio and X-ray wavelengths.

3.4 DATA ANALYSIS SOFTWARE

3.4.1 Introduction

This section describes the important XRP data files and the software that is used to reduce the data contained in these files. There are two paths for the analysis of XRP data: BCS data files and associated software and FCS data files and associated software. These two paths begin at the "reformatter" which reads the IPD-supplied production tapes and creates the first set of BCS and FCS data files. From this point onward the BCS and FCS data analysis are handled separately.

In 1987, the data files and analysis software for BCS and FCS were revamped to simplify the data reduction process. The development of new analysis software is still in progress and is expected to be completed by Autumn 1988. This effort has led to a reduction in the number of primary data files — from 12 files to 7. For analysis software, the number of FCS programs will decrease by a factor of 2, with the number of BCS programs remaining about the same. Details of the older data files and programs are given in several of the monthly reports and XRP Newsletters between the dates of 1985 and 1987. The new programs are outlined in Section 3.4.3.

The XRP software is written in two languages: VAX FORTRAN and Interactive Data Language (IDL). All of the data reduction software is written in VAX

FORTRAN and most of the graphics and application software are written in IDL. Software developed from these languages will run on DEC equipment (VAX and MicroVax). Other computers which support the FORTRAN 77 compiler will also be able to run the FORTRAN software, with some minor revisions.

3.4.2 New File Format

The new file format was created to reduce the number of files and to reduce the complexity of the data reduction software (Table 3-1). Complete documentation on the new file format is given in the "XRP File Format Control Document" which is currently being prepared. At the first level of processing, the new format version BCS and FCS files contain all the information from the older files for data, data indices, pointing, and instrument status. For FCS data reduction, the software is simplified by combining all types of data (imaging, spectral, and sit and stare) into a single file. The task of reading data from these files and creating images, spectra, and light curves is handled by a single application program. Furthermore, data reduction such as summing and interpolating images, spectra, etc., is also handled by a single program called "SumFIS." This change represents a large decrease in the number of programs necessary to reduce the FCS data. The programs associated with BCS analysis will remain unchanged.

Table 3-1: OLD AND NEW FILE NAMES

File Type	Prefix	Old Prefix
BCS Raw Data	BDA	BCSDA, BCSIX
BCS Spectroscopic Data	BSR	BRR
BCS Fitted Spectra File	BSF	SPC
BCS Calibration Parameters File	BPC	CAL
BCS Fit parameters file	BPF	FIT
FCS Raw Data	FDA	FCSDA, FCSIX
FCS Image and Spectroscopic Data	FIS	FRRDA, FRRIX, FSSxx, FSSsu
FCS Spectral Fitting Parameters	FSM	FSM
Spacecraft Pointing & BCS Subcom File	SPS	SPSUB
PHA Data	PHA	PHADA
The following files shall become redundant:		
BCS Original Data Files	–	BORG
BCS Spectra File	–	BSP
FCS Image File (IDL)	–	(free format)

The general structure of the primary XRP files is shown in Figure 3-5. The intent of this new structure is to include all the information necessary for the analysis of the data in a single file. This includes the information necessary to reconstruct the observing sequence, the data from the experiment, and the status of the instrument at the time of the observation. The only exception to this rule occurs at the first level of processing (BDA and FDA files) which allows the data reduction to occur independently of mode definitions. After the first level of processing, all subsequent files contain a complete set of information.

3.4.3 Data Reduction and Application Software

The processing steps for the first level of analysis of BCS and FCS data is outlined in Figure 3-6. The input files for this initial stage of processing are: the data file from the IPD tape, and the instrument status from the engineering log file. These files are then accessed by the "reformatter" program which in turn produces the primary XRP data files, BDA and FDA. The next level of processing involves these data files and the mode data base files. One uses either the "MKFIS" (FCS) or the "BCSBSR" (BCS) programs to process these data files and create the final data reduction files, FIS and BSR.

There are several application programs which can be used to produce spectral fits, to estimate temperature and density for a given area of an image, and to characterize line profiles, etc. Table 3-2 lists several of these application programs and their primary purpose.

Table 3-2: XRP APPLICATION SOFTWARE

Program	Language	Purpose
VoigtFit	FOR	Fit FCS spectra (Bevington stats.)
Fast	FOR	Fit FCS spectra via Batch (Bevington plus)
PlotFCS	FOR	Plot FCS data and spectral fits
VOIGTBSS	FOR	Fit BCS lines
SPCFIT	FOR	Fit two component thermal model to BCS spectra
CALBSS	FOR	Calibrate BCS wavelength dispersion
FCSArray	IDL	FCS image processing for images $< 10'$ square
EWLimb	IDL	Limb survey and full sun image processing

3.4.4 Data Archiving

XRP data will be archived in three main formats. The different formats represent data processed to different degrees, from raw telemetry data to image and spectral data corresponding to individual observational modes. In addition to these,

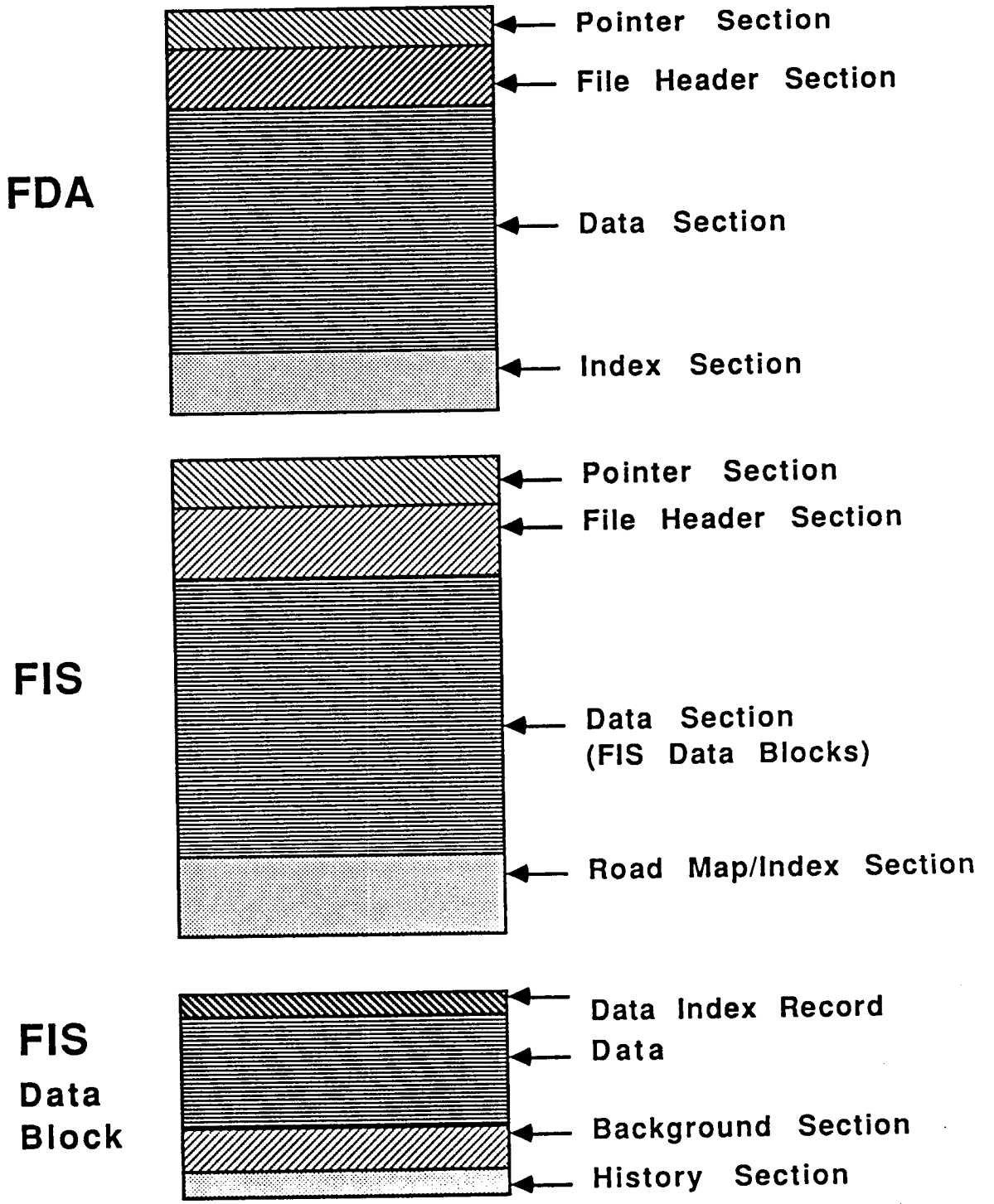

Figure 3-5. A block diagram of the primary FCS data files: the FDA and FIS files. Also shown are the details of the FIS data block.

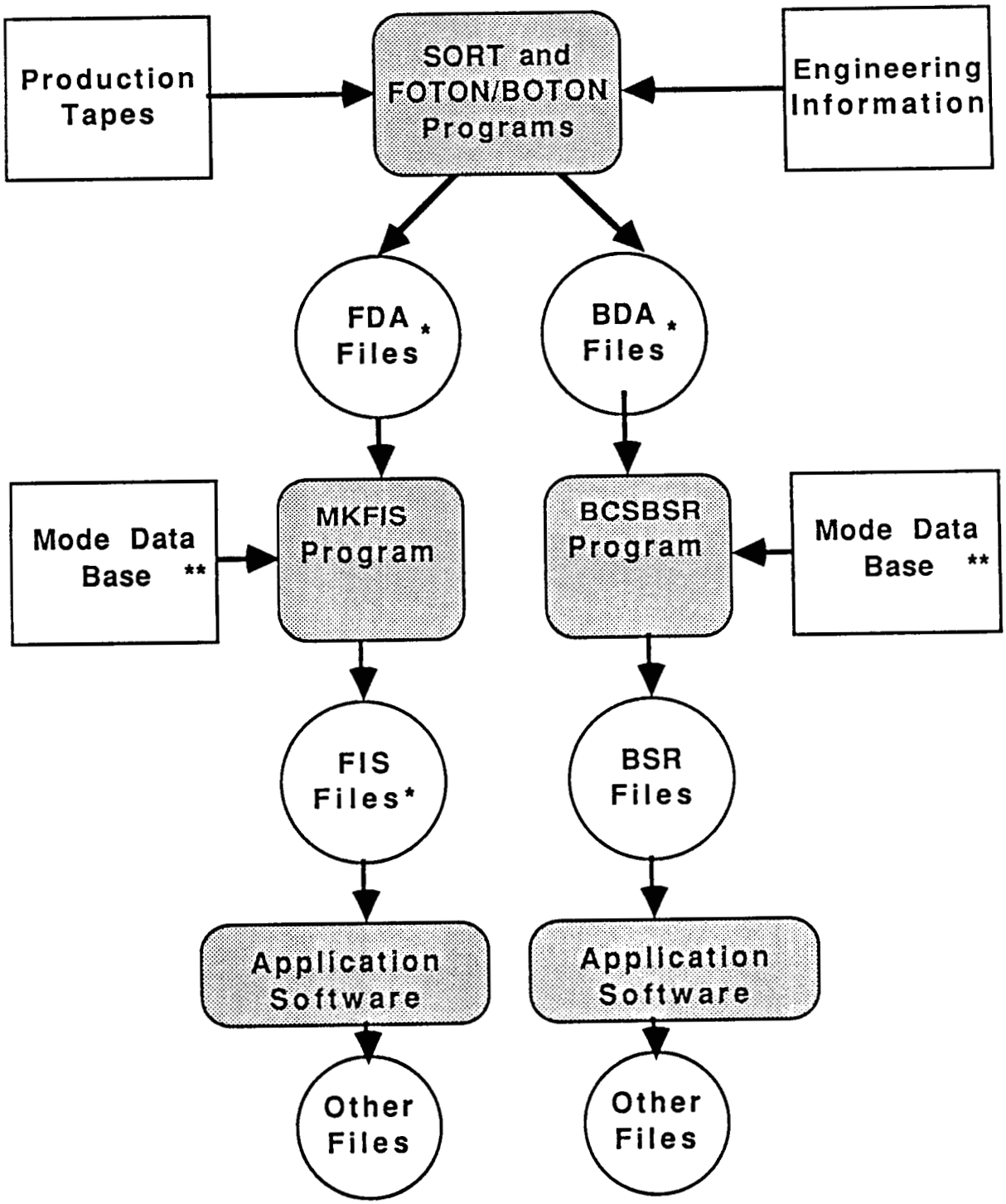

Figure 3-6. The primary *SMM*-XRP data reduction flow chart. The files marked by an (*) will be archived and the files marked by an (**) are prepared during command generation.

selected data, primarily for large flares, FCS crystal runs, collaborative data etc., will make up another archived data set.

Together with the observational data, several other types of data will be included with each of the above archived data sets. These will include instrument design parameters, engineering parameters log, observational modes description data base, atomic coefficients, and emissivity functions. The software to access the data will also be included with each archived data set.

Selected processed data sets will be archived first, since much of these data have already been processed to level suitable for archiving. This will be followed by the raw telemetry archive, the reformatted data archive and finally the processed data archive. Each of these archived data sets is described in more detail below.

Selected Data Archive

This will consist primarily of reformatted data files (in some cases processed files may be available) for the following data sets:

(1) Data for all catalogued XRP flares – generally all flares, which register more than 18 counts s^{-1} in the BCS Calcium XIX channel (above the *GOES* C level) are catalogued. The reformatted data from both BCS and FCS instruments, for the entire orbits during which the flare was observed, will be included;

(2) The data obtained during FCS crystal runs. Some of this data will be included in (1) above. However, FCS spectroscopic data has also been obtained in several 'stand alone' runs, observing active regions;

(3) Collaborative data sets – data obtained as part of a collaboration, such as CoMStOC or CMEO, etc.

Raw Telemetry Archive

This is essentially a copy of the raw data tapes on optical disks. The On-Board Computer data that is not required for XRP data analysis will be discarded, reducing the storage requirements. This archive will be available for any processing which may be required.

Reformatted Data Archive

Reformatting represents the first level of processing. Raw telemetry data for short periods (typically an orbit) is processed into files which allow access to data by specifying observing modes. The archive will consist of FCS reformatted data from every orbit during the mission when the instrument was pointed at the Sun and was in a valid science data collection mode and BCS pre-flare, flare and post-flare data.

Processed data archive

This will cover the same periods as "Raw Telemetry Archive" above but the data will be processed into images and spectra. For most purposes the user will only need to access this archive.

3.5 DATA ANALYSIS HARDWARE

The new XRP computer system was shipped to LPARL in mid-March and the system was installed by the end of March. The XRP computer system consists of a Digital Equipment Corporation MicroVAX II. This system implements the 32-bit VAX architecture and a modular version of the VAX/VMS operating system so that it is compatible with the larger VAX 8350 system at Goddard Space Flight Center. It will allow programs that were developed on those systems and those at Lockheed in support of XRP to be run on the MicroVAX II. The system is configured with 16 megabytes of memory, two disk drives — one for operating-system modules and another larger 456 megabyte unit for data storage, and two computer magnetic tape units: one "streaming" cassette drive for system functions and the other a 9-track 6250/1600 bpi for data storage and retrieval. Table 3-3 gives a list of the equipment which comprises the XRP computer system.

Some parts of the new computer system had not yet been delivered at the time this report was prepared. The computer has been purchased to support the following activities: scientific research of XRP data by LPARL personnel; preparation of data for *SMM* Guest Investigators; archiving of XRP data onto optical disk in order to meet the requirements of data submission to the NSSDC. The computer system will have graphics and image display capabilities and will be used in the preparation of papers for publication and conferences.

Communication with other computers and terminals at LPARL has been established with Ethernet DECnet and EIA RS-232C communications protocols — the hardware and software to support these communications were purchased for this machine. LPARL provides and maintains the physical links and network on other associated VAX machines. Most of the scientific personnel working on the XRP project at LPARL have terminals located in their offices and will be provided the option of connecting to the XRP MicroVAX II as well as to the other computers on the SPAN and Lockheed networks. Figure 3-7 shows the components of the *SMM* MicroVax computer and its network link.

The major components of the MicroVAX II, the central processor, the tape and disk drives, modem communications, and system console are located in an established computer room housing additional LPARL VAX systems. This facility provides an environment site which matches local legal and DEC recommended requirements. These include, for example, power and air conditioning, fire and

Table 3-3: XRP COMPUTER SYSTEM

The microVAX II system (purchased under contract number NAS5-28713 and assigned Digital reference number 88A47641X) was delivered to LPARL in mid-March 1988.

MicroVAX II System	DH-630Q5 FA
— 16 Mb Memory	
— TK70 Cartridge Tape	
— KDA50 Disk Controller	
— DHQ11 8 lines	
— DELQK Ethernet	
— ZNAEC5	
— (2) BA23 Cabinet	
456 Mb Disk Drive	RA81.HA
RD and RX Drive Controller	RQDX3-AA
71 Mb Disk Drive	RD53A-AA
Dual 400 KB DRIVE	RX50-AA
Tape Drive	TU81F-DA
System Console Terminal	LA100-BA
Ethernet Transceiver	H4000
Integral Modem - Qbus interface	CK-DMV11-CF
Integral Modem	DMV11-N
RA81 Cable	BC26B-6D
Ethernet Cable	BNE3M-20
VMS 8 USER LICENSE	QZ002-C5
— Media & Documentation	QZ002-H5
— Update service (12 Mo.)	QZ002-35
DECNet License	QZD04-UZ
— Media & Documentation	QZD04-H5
— Update Service (12 Mo.)	QZD04-35
FORTRAN	QZ100-UZ
— Media & Documentation	QZ100-H5
— Update Service (12 Mo.)	QZ100-35
*Terminal Server (8 Lines)	DSRVB-AA
— Licence	Q0Z06-UZ
— Software	Q0Z06-H5
*VAXstation II/GPX RD54	SV-LV59B-EK
— 5 Mb Memory	
— TK50 Cartridge Tape	
— 19" colour monitor	
*Ascii/Postscript Laser Printer	LN03R-AA

(*)Items were yet to be delivered when this report was prepared

temperature overload protection, acoustically treated surroundings, and emergency lighting.

LPARL has provided a terminal/analysis room where commonly used peripherals will be located. The terminal/analysis room is a $13' \times 24'$ carpeted room with indirect lighting, and a $7' \times 7'$ acoustically controlled area to accommodate noisy peripherals. Appropriate terminal communication lines will be placed between this room and the main computer.

The XRP team also utilizes a Toshiba model 3100 laptop IBM PC/AT clone with integral modem to support personnel in the field with communications and remote storage and entry of data.

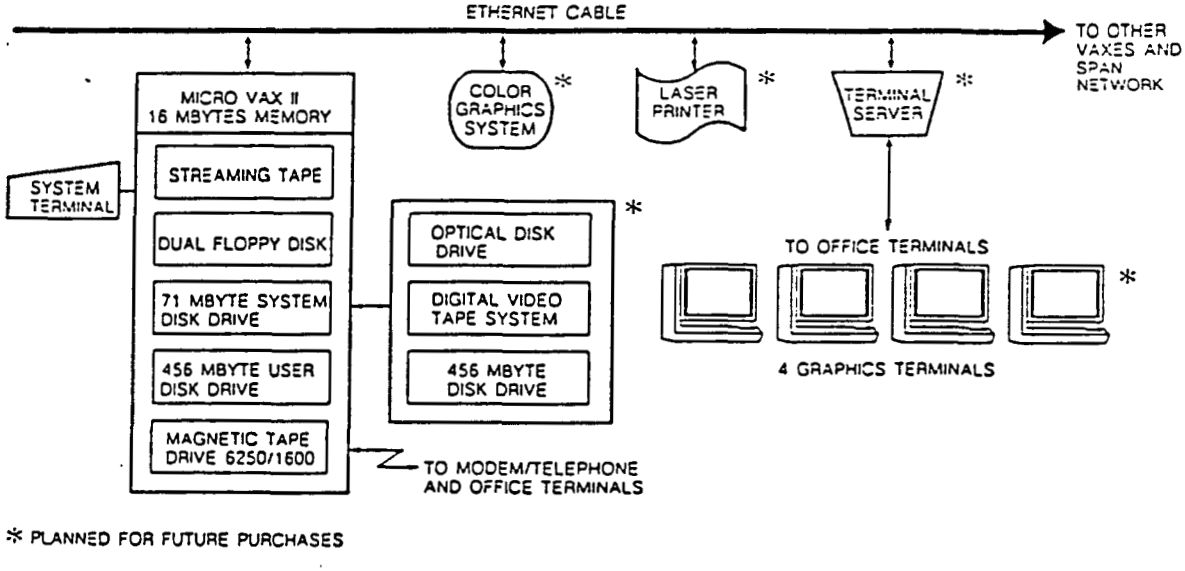

Figure 3-7. The *SMM*-XRP MicroVax computer system.

4. ACKNOWLEDGEMENTS

Construction and operation of an instrument of this complexity has depended on the commitment and efforts of a substantial team over a period of fourteen years. We acknowledge with sincere thanks the contributions of colleagues, subcontractors, suppliers, and especially the agencies and individuals sponsoring the research program. The two British groups have been supported by the UK Science and Engineering Council. The Lockheed program has been supported by the National Aeronautics and Space Administration through the Goddard Space Flight Center. Especially we wish to acknowledge our two British colleagues and co-Principal Investigators, J. L. Culhane and Alan H. Gabriel, whose enthusiasm and leadership made this mission possible.

The Appleton Laboratory team responsible for the FCS structure and mechanisms included B. A. Barker, J. E. Pateman, D. C. Tredgett, A. Wilson, R. F. Turner and J. Firth. W. G. Griffith was responsible for alignment of the FCS system and B. E. Patchett contributed to the evaluation of FCS optical systems. We are pleased to be working with K. J. H. Phillips as the current Rutherford Appleton Laboratory XRP Principal Investigator.

The Mullard Space Science Laboratory team responsible for the mechanical design and construction of the BCS and FCS gas systems and detectors included W. Gilford, J. Coker, R. Dryden and C. Dela Nougerade. Those responsible for electronic design, testing and construction work on BCS and FCS pulse height processing and gas control circuitry included M. Day, D. Hoyle and J. Ootes. In addition, we are grateful to Bob Nettleship and his colleagues at Pye Telecommunications for supplying several of the electronic subsystems for both instruments. Major parts of the X-ray detector construction were undertaken by John Leake and his associates at the UK Atomic Energy Research Establishment at Harwell and we are grateful to them for their skilled and dedicated work.

The Lockheed team responsible for the FCS collimator included T. Miller, R. Peterson, S. W. Salat, R. J. Salmon and J. R. Vieira. T. Pope was primarily responsible for the FCs alignment sensor. A. M. Cosner and S. R. Keith are acknowledged for their contributions to the design of XRP software, and B. C. Rix for his work on ground support equipment. Richard Deslattes, A. R. Burek and colleagues at the National Bureau of Standards provided invaluable counsel and assistance of all matters dealing with crystals.

For support of mission operations we acknowledge the Grumman Operations team under the direction of J. Harrison and the OAO Operations team under the direction of M. Sweetin and, more recently, W. Tittley. In particular we give special thanks to J. Barcus, G. Gavigan, J. Earp and E. Barksdale and the OCC team who

provided valuable real-time command assistance. We also make particular mention of S. Hammer, D. Simpson and M. Oben, whose assistance with OBC software and patches to the Flare Processor have helped maintain and improve the flexibility needed to obtain continued high quality observations. SMM remains a working, well-calibrated spacecraft largely due to the efforts of D. Douds, R. Shendock H. Wajsgras, and the Flight Dynamics team, especially F. Patt, J. Klein, D. Kulp, and D. Pittone. Thanks are due to V. Buczkowski and W. Palmer at IPD.

Technical support for planning of solar observations was provided by D. Speich and his colleagues at NOAA, and by J. Nelson, K. Kuehn and G. Einfault, of the the SMM Solar Forecast Team. The high quality of the XRP data in large measure reflects their coordination efforts and the spirit of cooperation and compromise in which the SMM instrument teams at the EOF work. We acknowledge the efficient work of the NASA SMM Project Team, initially under P. Burr and J. Donley, then headed by P. Corrigan, and more recently P. Pashby, G. Vincent and D. Dionisio, in carrying out the SMM Operations. Invaluable administrative assistance has been provided by G. Wharen, formerly of SASC, now of EER Systems. Special thanks are also due to the SMM Project Scientists: K. Frost, B. Woodgate and J. Gurman.

Other scientific and technical support has come from M. Kayat, R. D. Bentley, J. A. Bowles, M. L. Finch, C. W. Gilbreth, P. Guttridge, R. W. Hayes, E. G. Joki, B. B. Jones, B. J. Kent, J. W. Leibacher, R. A. Nobles, T. J. Patrick, C. G. Rapley, P. H. Sheather, J. C. Sherman, J. P. Stark, L. A. Springer and R. F. Turner. We also thank our secretaries, A. M. Green and R. S. Fielder, without whose efforts many things would surely grind to a halt.

The following high school students from the Palo Alto Unified School District and Fremont Union High School District have worked for this project: A. Gheorghiu, R. Fong, S. Lipscomb, K. Hill, K. Scott, M. Brown, M. Sanford and D. Conner.

Lastly, many of the observations described in this work were obtained in 1984 or later, with the fine-pointed instruments on SMM. These data were available only because of the repair of the SMM spacecraft, brought about through the efforts of the Satellite Servicing Project and the support of the solar physics community at large. The repair was carried out by the crew of the Challenger on mission 41-C. The pilot for that mission, and the commander of Challenger's last mission was Francis R. Scobee. This work is dedicated to his memory.

APPENDIX A: XRP BIBLIOGRAPHY

TABLE OF CONTENTS

A.1 Published Papers A–1
A.2 Reports and Popular Articles A–9
A.3 Talks A–9
A.4 Conference Proceedings A–14
A.5 Posters A–17

A.1 PUBLISHED PAPERS

The Soft X-Ray Polychromator for the Solar Maximum Mission: L.W. Acton, J.L. Culhane, A.H. Gabriel, R.D. Bentley, J.A. Bowles, J.G. Firth, M.L. Finch, C.W. Gilbreth, P. Guttridge, R.W. Hayes, E.G. Joki, B.B. Jones, B.J. Kent, J.W. Leibacher, R.A. Nobles, T.J. Patrick, K.J.H. Phillips, C.G. Rapley, P.H. Sheather, J.C. Sherman, J.P. Stark, L.A. Springer, R.F. Turner, and C.J. Wolfson, Sol. Phys., 65, 53, 1980.

Large-aperture High-Resolution X-Ray Collimator for the Solar Maximum Mission: R.A. Nobles, L.W. Acton, E.G. Joki, J.W. Leibacher and R.C. Peterson, Appl. Opt., 19, 2957, 1980.

Multitemperature Analysis of Solar X-Ray Line Emission: J. Sylwester, J. Schrijver and R. Mewe, Sol. Phys., 67, 285, 1980.

X-ray Spectra of Solar Flares: N.J. Veck, University College London, Department of Physics and Astronomy, Ph.D. thesis, 1980.

Dielectronic Satellite Spectra for Hydrogen-Like Iron in Low Density Plasmas: J. Dubau, A.H. Gabriel, M. Loulergue, L. Steenman-Clark and S. Volonte, M.N.R.A.S., 195, 705, 1981.

Observations of Transitions of Hydrogen-Like Fe XXVI in Solar Flare Spectra: A.N. Parmar, J.L. Culhane, C.G. Rapley, E. Antonucci, A.H. Gabriel and M. Loulergue, M.N.R.A.S., 29P, 1981.

Classification of the Spectra of Highly Ionized Atoms during the Last 7 Years: B.C. Fawcett, Physica Scr., 24, No. 4, 663, 1981.

Solar Flare Plasmas: A.H. Gabriel, Phil. Trans. R. Soc. Lond., A300, 497, 1981.

The Surface Preparation of Beryl Crystals for X-Ray Spectroscopy: R.W. Hayes and B.J. Kent, J. Phys. E: Sci. Instr., 14, 689, 1981.

Early Results from the Soft X-Ray Polychromator Experiment: A.H. Gabriel, J.L. Culhane, L.W. Acton, E. Antonucci, R.D. Bentley, C. Jordan, J.W. Leibacher, A.N. Parmar, K.J.H. Phillips, C.G. Rapley, C.J. Wolfson and K.T. Strong, Adv. Space Res., 1, 267, 1981.

X-Ray Line Widths and Coronal Heating: L.W. Acton, J.L. Culhane, A.H. Gabriel, C.J. Wolfson, C.G. Rapley, K.J.H. Phillips, E. Antonucci, R.D. Bentley, R.W. Hayes, E.G. Joki, C. Jordan, M. Kayat, B. Kent, J.W. Leibacher, R.A. Nobles, A.N. Parmar, K.T. Strong and N.J. Veck, Ap.J. (Letters), 244, L137, 1981.

X-Ray Spectra of Solar Flares Obtained with a High Resolution Bent Crystal Spectrometer: J.L. Culhane, A.H. Gabriel, L.W. Acton, C.G. Rapley, K.J.H. Phillips, C.J. Wolfson, E. Antonucci, R.D. Bentley, R.C. Catura, C. Jordan, M. Kayat, J.W. Leibacher, P. McWhirter, A.N. Parmar, J. Sherman, L. Springer, K.T. Strong and N.J. Veck, Ap.J. (Letters), 244, L141, 1981.

Observations of the Limb Solar Flare on 1980 April 30 with the SMM X-Ray Polychromator: A.H. Gabriel, L.W. Acton, J.L. Culhane, K.J.H. Phillips, C.J. Wolfson, C.G. Rapley, E. Antonucci, R.D. Bentley, C. Jordan, M. Kayat, J.W. Leibacher, M. Levay, J. Sherman, K.T. Strong and N.J. Veck, Ap.J. (Letters), 244, L147, 1981.

Relationship Between a Soft X-Ray Long Duration Event and an Intense Metric Noise Storm: P. Lantos, A. Kerdraon, C.G. Rapley and R.D. Bentley, Astron. and Astrophys., 101, 33, 1981.

Studies of X-ray Emission from Hercules X-1, OAO1653-40 and X-ray Spectroscopy of Solar Flares: A.N. Parmar, University College London, Department of Physics and Astronomy, Ph.D. thesis, 1981.

Simultaneous Radio, Optical, and Space Observation of AR 2490: F. Chiuderi-Drago, Proceedings of International Workshop on SOLAR MAXIMUM YEAR, Simferopol, Moscow, IZMIRAN V, 1, 1982.

Solar Observations Using the Soft X-Ray Polychromator Experiment on SMM: E. Antonucci, C.J. Wolfson, C.G. Rapley, L.W. Acton, J.L. Culhane, A.H. Gabriel, Proceedings of International Workshop on SOLAR MAXIMUM YEAR, Simferopol, Moscow, IZMIRAN V, 1, 62, 1982.

Observations of a Post-Flare Radio Burst in X-Rays: Z. Svestka, R.T. Stewart, P. Hoyng, W. Van Tend, L.W. Acton, A.H. Gabriel, C.G. Rapley, A. Boelee, E.C. Bruner, C. de Jager, H. Lafleur, G. Nelson, G.M. Simnett, H.F. Van Beek and W.J. Wagner, Sol. Phys., 75, 305, 1982.

Observation of Solar Flare Transition-Zone Plasmas from the Solar Maximum Mission: C-C. Cheng, E.C. Bruner, E. Tandberg-Hanssen, B.E. Woodgate, R.A. Shine, P.J. Kenny, W. Henze and G. Poletto, Ap.J., 253, 353, 1982.

Transition Region Oscillations in Sunspots: J. Gurman, J.W. Leibacher, R.H. Shine, B.E. Woodgate and W.E. Henze, Ap.J., 253, 939, 1982.

Solar Flare X-Ray Spectra from the SMM Flat Crystal Spectrometer: K.J.H. Phillips, J.W. Leibacher, C.J. Wolfson, J.H. Parkinson, B. Fawcett, B. Kent, H. Mason, L.W. Acton, J.L. Culhane and A.H. Gabriel, Ap.J., 256, 774, 1982.

Impulsive Phase of Flares in Soft X-Ray Emission: E. Antonucci, A.H. Gabriel, L.W. Acton, J.L. Culhane, C.J. Doyle, J.W. Leibacher, M. Machado, L.E. Orwig and C.G. Rapley, Sol. Phys., 78, 107, 1982.

Comparison of Observed Ca XIX and Ca XVII Relative Line Intensities With Current Theory: C. Jordan and N.J. Veck, Sol. Phys., 78, 125, 1982.

The Impulsive and Gradual Phases of a Solar Limb Flare as Observed from the Solar Maximum Mission Satellite: A.I. Poland, M.E. Machado, C.J. Wolfson, K.J. Frost, B.E. Woodgate, R.A. Shine, P.J. Kenny, C.C. Cheng, E.A. Tandberg-Hanssen, E.C. Bruner and W. Henze, Sol. Phys., 78, 201, 1982.

Multiple Wavelength Observations of a Solar Active Region: F. Chiuderi-Drago, R. Bandiera, F. Falciani, E. Antonucci, K.R. Lang, R.F. Willson, K. Shibaski and C. Slottje, Sol. Phys., 80, 71, 1982.

Unusual Coronal Activity Following the Flare of 6 November 1980: Z. Svestka, B.R. Dennis, M. Pick, A. Raoult, C.G. Rapley, R.T. Stewart and B.E. Woodgate, Sol. Phys., 80, 143, 1982.

Active Region Magnetic Fields Inferred from Simultaneous VLA Microwave Maps, X-Ray Spectroheliograms and Magnetograms: E. Schmahl, M. Kundu, K.T. Strong, R.D. Bentley, J.B. Smith, Jr., and K. Krall, Sol. Phys., 80, 233, 1982.

Soft X-Ray Discriminators of Flare Classification: E. Antonucci, The Observatory, 102, 121, August 1982.

Flare Classification - Fact or Fancy: L.W. Acton, The Observatory, 102, 123, August 1982.

Raies Satellites de Recombinaison Dielectronique: J. Dubau and S. Volonte, Ann. Phys. Fr., 7, 455, 1982.

Chromospheric Evaporation in a Well-Observed Compact Flare: L.W. Acton, R.C. Canfield, T.A. Gunkler, H.S. Hudson, A.L. Kiplinger and J.W. Leibacher, Ap.J. 263, 409, 1982.

Dielectronic Satellite Spectra for Highly-Charged Helium-Like Ions. VI. Iron Spectra with Improved Inner-shell and Helium-like Excitation Rates: F. Bely-Dubau, J. Dubau, P. Faucher, and A.H. Gabriel, M.N.R.A.S., 198, 239, 1982.

Dielectronic Satellite Spectra for Highly-Charged Helium-Like Ions. VII. Calcium Spectra - Theory and Comparison with SMM Observations: F. Bely-Dubau, J. Dubau, P. Faucher, A.H. Gabriel, M. Loulergue, L. Steenman-Clark, S. Volonte, E. Antonucci and C.G. Rapley, M.N.R.A.S., 201, 1155, 1982.

Chromospheric Evaporation in Soft X-Ray Flares: E. Antonucci, Mem. della Soc. Astron. Ital., 53(2), 495, 1982.

Solar Physics. Chapter 10 in Applied Atomic Collision Physics, Vol. 1: A.H. Gabriel and H.E. Mason, (ed. Massey and Bates, Academic Press) 1982.

Fluorescent Excitation of Photospheric Fe K-alpha Emission during Solar Flares: A.N. Parmar, J.L. Culhane, K.J.H. Phillips, C.J. Wolfson, L.W. Acton, B.R. Dennis, C. G. Rapley, Adv. Space Res., 2, No. 11, 151, 1982.

The Queens' Flare: Its Structure and Development; Precursors, Pre-Flare Brightenings, and Aftermaths: C. de Jager, M.E. Machado, A. Schadee, K.T. Strong, Z. Svestka, B.E. Woodgate and W. van Tend, Sol. Phys., 84, 205, 1983.

Magnetohydrodynamic Simulation of the Coronal Transient Associated with the Solar Limb Flare of 1980, June 29, 18:21 UT: S.T. Wu, S. Wang, M. Dryer, A.I. Poland, D.G. Sime, C.J. Wolfson, L.E. Orwig and A. Maxwell, Sol. Phys., 85, 351, 1983.

Inner Shell Transitions in Fe XIX-XXII in X-Ray Spectra of Solar Flares and Tokamaks: K.J.H. Phillips, J.R. Lemen, R.D. Cowan, G.A. Doschek and J.W. Leibacher, Ap.J., 265, 1120, 1983.

X-Ray Line Ratios from He-Like Ions: Updated Theory and SMM Flare Observations: C.J. Wolfson, J.G. Doyle, J.W. Leibacher and K.J.H. Phillips, Ap.J., 269, 319, 1983.

Closed Coronal Structures V. Gas-dynamic Models of Flaring Loops and Comparison with SMM Observations: R. Pallavicini, G. Peres, S. Serio, G. Vaiana, L.W. Acton, J.W. Leibacher and R. Rosner, Ap.J., 270, 270, 1983.

Non-Thermal and Non-Equilibrium Effects in Soft X-Ray Flare Spectra: A.H. Gabriel, E. Antonucci and L. Steenman-Clark, Sol. Phys., 86, 59, 1983.

Observation of Chromospheric Evaporation During the Solar Maximum Mission: E. Antonucci and B.R. Dennis, Sol. Phys., 86, 67, 1983.

Transport and Containment of Plasma, Particles and Energy within Flares: L.W. Acton, W.A. Brown, M.E.C. Bruner, B.M. Haisch and K.T. Strong, Sol. Phys., 86, 79, 1983.

Hydrodynamics of Flaring Loops: SMM Observations and Numerical Simulations: R. Pallavicini and G. Peres, Sol. Phys., 86, 147, 1983.

Microwave, Ultraviolet and Soft X-Ray Observations of Hale Region 16898: K. Shibasaki, F. Chiuderi-Drago, M. Melozzi, C. Slottje and E. Antonucci, Sol. Phys., 89, 307, 1983.

Bright Point Study: F. Tang, K. Harvey, M. Bruner, B.J. Kent, and E. Antonucci, Adv. Space Res., 2, 65, 1983.

SMM Flat Crystal Spectrometer Data Analysis of 7 April 1980 Flare: B. Sylwester, J. Sylwester, J. Jakimiec, R. Mewe and R.D. Bentley, Publ. Debrecen Obs., 5, 85, 1983.

Interpretation of Microwave Active Region Structures using SMM Soft X-Ray Observations: K.T. Strong, C. Alissandrakis and M. Kundu, Ap.J., 277, 865, 1984.

A Multiwavelength Study of a Double Impulsive Flare: K.T. Strong, A.O. Benz, B.R. Dennis, J.W. Leibacher, R. Mewe, A. Poland, J. Schrijver, G. Simnett, J.B. Smith, Jr., and J. Sylwester, Sol. Phys., 91, 325, 1984.

Derivation of Ionization Balance for Ca XVIII/XIX Using XRP Solar X-Ray Data: E. Antonucci, A.H. Gabriel, J.G. Doyle, J. Dubau, D. Foucher, C. Jordan and N.J. Veck., Astron. and Astrophys., 133, 239, 1984.

Interpretation of High Resolution X-Ray Observations of Coronal Plasmas: F. Bely-Dubau, Physica Scripta, Vol T7, 34, 1984.

Solar Research at RAL: A.H. Gabriel, J. Brit. Interplan. Soc., 37, 317, 1984.

SMM Observations of K-alpha Radiation from Fluorescence of Photospheric Iron by Solar X-Rays: A.N. Parmar, C.J. Wolfson, J.L. Culhane, K.J.H. Phillips, L.W. Acton, B.R. Dennis and C.G. Rapley, Ap.J., 279, 866, 1984.

Inner-Shell Transitions of Fe XXIII and Fe XXIV in the X-ray Spectra of Solar Flares: J.R. Lemen, K.J.H. Phillips, R.D. Cowan, J. Hata and I.P. Grant, Astron. and Astrophys., 135, 313, 1984.

Variation in the Observed Coronal Calcium Abundance of Various X-ray Flare Plasmas: J. Sylwester, J.R. Lemen, and R. Mewe, Nature, 310, 665, 1984.

Results from the X-Ray Polychromator on SMM: J.L. Culhane, L.W. Acton, and A.H. Gabriel, Mem. della Soc. Astron. Ital., 55, 673, 1984.

Analysis of the Magnetic Field Configuration of a Filament-associated Flare from X-ray, UV, and Optical Observations: C.C. Cheng and R. Pallavicini, Sol. Phys., 93, 337, 1984.

The Development and Cooling of a Solar Limb Flare: N.J. Veck, K.T. Strong, C. Jordan, G.M. Simnett, P.J. Cargill, and E.R. Priest, M.N.R.A.S., 210, 443, 1984.

Progress in the Study of Homologous Flares on the Sun: B.E. Woodgate, M.J. Matres, J.B. Smith, K.T. Strong, M.K. McCabe, M.E. Machado, V. Gaisauskas, R. Stewart, and P.A. Sturrock, Adv. Space Res., 4, No. 7, 11, 1984.

Homologous Flares and Evolution of NOAA Active Region 2372: K.T. Strong, J.B. Smith, Jr., M.K. McCabe, M.E. Machado, J.L.R. Saba, and G.M. Simnett, Adv. Space Res., 4, No.7, 23, 1984.

Relationship of a Growing Magnetic Flux Region to Flares: S.F. Martin, R.D. Bentley, A. Schadee, A. Antalova, A. Kucera, L. Dezso, L. Gesztelyi, K.L. Harvey, H. Jones, S.H.B. Livi, and J. Wang, Adv. Space Res., 4, No. 7, 61, 1984.

Origin and Location of Chromospheric Evaporation in Flares: E. Antonucci, D. Marocchi, G. M. Simnett, Adv. Space Res., 4, No.7, 111, 1984.

Differential Emission Measure Analysis of Hot-flare Plasma from Solar-Maximum Mission X-Ray Data: J. Jakimiec, J. Sylwester, J.R. Lemen, R. Mewe, R.D. Bentley, A. Fludra, J. Schrijver, and B. Sylwester, Adv. Space Res., 4, No. 7, 203, 1984.

Combined Analysis of Soft and Hard X-Ray Spectra from Flares: A.H. Gabriel, F. Bely-Dubau, J.C. Sherman, L.E. Orwig, H. Schrijver, Adv. Space Res., 4, No.7, 221, 1984.

The Impulsive Phase of a Solar Limb Flare: G.M. Simnett and K.T. Strong, Ap.J., 284, 839, 1984.

A.1 PUBLISHED PAPERS

A Consistent Picture of Coronal and Chromospheric Processes in a Well-Observed Solar Flare: T.A. Gunkler, R.C. Canfield, L.W. Acton, and A.L. Kiplinger, Ap.J., 285, 835, 1984.

The Energetics of Chromospheric Evaporation in Solar Flares: E. Antonucci, A.H. Gabriel and B.R. Dennis, Ap.J., 287, 917, 1984.

SMM Observations of a Compact Flare. Interpretation and Theoretical Implications for Flare Theory: J.G. Doyle and P.B. Byrne, Irish Astron. J., 16, 226, 1984.

Initial Phase of Chromospheric Evaporation in a Solar Flare: E. Antonucci, B.R. Dennis, A.H. Gabriel, and G.M. Simnett, Sol. Phys., 96, 129, 1985.

The X-ray Signature of Solar Coronal Mass Ejections: R.A. Harrison, P.W. Waggett, R.D. Bentley, K.J.H. Phillips, M. Bruner, and M. Dryer, Sol. Phys., 97, 387, 1985.

Properties of Solar Flare Plasmas Derived from Soft X-ray Line Emission: P.L. Bornmann, Ph.D. thesis, University of Colorado, 1985.

A New Method for Determining Temperature and Emission Measure During Solar Flares from Light Curves of Soft X-ray Fluxes: P.L. Bornmann, Ap.J., 293, 595, 1985.

Analysis of Loop Flows Observed on 27 March, 1980 by the UVSP Instrument during the Solar Maximum Mission: R.A. Kopp, G. Poletto, G. Noci, and M. Bruner, Sol. Phys., 98, 91, 1985.

Energetics of a Double Flare on November 8, 1980: J.G. Doyle, P.B. Byrne, B.R. Dennis, A.G. Emslie, A.I. Poland and G.M. Simnett, Sol. Phys., 98, 141, 1985.

X-ray Resonance Scattering in a Spherically Symmetric Coronal Model: B. Haisch and S. Claflin, Sol. Phys., 99, 101, 1985.

Multiwavelength Analysis of a Well Observed Flare from SMM: P. MacNeice, R. Pallavicini, H.E. Mason, G.M. Simnett, E. Antonucci, R.A. Shine, D.M. Rust, C. Jordan and B.R. Dennis, Sol. Phys., 99, 167, 1985.

Further Analysis of Temperature and Emission Measure during the Decay Phase of Solar Flares Derived from Soft X-ray Light Curves: P.L. Bornmann, Sol. Phys., 102, 111, 1985.

Energy Release Topology in a Multiple-Loop Solar Flare: C.-C. Cheng, R. Pallavicini, L.W. Acton and E. Tandberg-Hanssen, Ap.J., 298, 887, 1985.

Solar X-ray Spectrum Simulations for Flaring Loop Models with Emphasis on Transient Ionization Effects during the Impulsive Phase: R. Mewe, J.R. Lemen, G. Peres, J. Schrijver and S. Serio, Astron. and Astrophys., 152, 229, 1985.

The Excitation of the Iron K-alpha Feature in Solar Flares: A.G. Emslie, K.J.H. Phillips and B.R. Dennis, Sol. Phys., 103, 89, 1986.

Soft X-ray Observations of High-velocity Features in the 29 June 1980 Flares: R.D. Bentley, J.R. Lemen, K.J.H. Phillips, J.L. Culhane, Astron. and Astrophys., 154, 255, 1986.

Broadening of Soft X-ray Lines During the Impulsive Phase of Solar Flares: Random or Directed Mass Motions?: J.G. Doyle and R.D. Bentley, Astron. and Astrophys., 155, 278, 1986.

A Numerical Hydrodynamic Model of a Heated Coronal Loop: P. MacNeice, Sol. Phys., 103, 47, 1986.

Comparison of Three Methods Used for Calculation of the Differential Emission Measure: A. Fludra and J. Sylwester, Sol. Phys., 105, 323, 1986.

Plasma Densities from the He-like Ne IX Ion: J.G. Doyle and F.P. Keenan, Astron. and Astrophys., 157, 116, 1986.

A Comparison of Photospheric Electric Current and Ultraviolet and X-ray Emission in an Active Region: B. Haisch, M. Bruner, M. Hagyard and R. Bonnet, Ap.J., 300, 428, 1986.

On Magnetic Field Stochasticity and Nonthermal Line Broadening in Solar Flares: E. Antonucci, R. Rosner, K. Tsinganos, Ap.J., 301, 975, 1986.

Inner-shell X-ray Line Spectra of Highly Ionized Titanium, Chromium, Iron and Nickel and Their Application to Laboratory Plasmas: J.R. Lemen, K.J.H. Phillips, G.A. Doschek, R.D. Cowan, J. of Appl. Phys., 60 (6), 1960, 1986.

Variation in Calcium Abundance during Flares: J. Sylwester, J.R. Lemen, R. Mewe, R.D. Bentley, B. Sylwester, Solar Maximum Analysis, Proceedings of the SMA-SMY Workshop, Irkutsk, (eds. V.E. Stepanov and V.N. Obridko), Science Press, 1986.

High-temperature plasma diagnostics of solar flares and comparison with model calculations: J. Jakimiec, B. Sylwester, J. Sylwester, J.R. Lemen, R. Mewe, R.D. Bentley, G. Peres, S. Serio, and J. Schrijver, Solar Maximum Analysis, Proceedings of the SMA-SMY Workshop, Irkutsk, (eds. V.E. Stepanov and V.N. Obridko), Science Press, 1986.

Calculated X-radiation from Optically Thin Plasmas VI: Improved Calculations for Continuum Emission and Approximation Formulae for Nonrelativistic Average Gaunt Factors: R. Mewe, J.R. Lemen, G.H.J. and van den Oord, Astron. Astrophys. Suppl. Ser., 65, 511, 1986.

Thematic Observations of Solar Flares: P.W. Waggett, University College London, Department of Physics and Astronomy, Ph.D. thesis, 1986.

Soft X-ray Emission from Solar Flares and Active Regions: R.D. Bentley, University College London, Department of Physics and Astronomy, Ph.D. thesis, 1986.

Preflare Magnetic and Velocity Fields: M. Hagyard, G. Chapman, A. de Loach, F. Drago, A. Gary, B. Haisch, W. Henze, V. Gaizauskas, H. Jones, J. Karpen, M. Martres, J. Porter, E. Reichmann, B. Schmeider, G. Simon, G. Simon, J. Smith, Jr., J. Toomre, in PREFLARE ACTIVITY, Chapter 1 of ENERGETIC PHENOMENA ON THE SUN, Proceedings of the Solar Maximum Mission Workshop, (eds. M.R. Kundu and B. Woodgate), NASA CP 2439, 1986.

Coronal Manifestations of Pre-flare Activity: E. Schmahl, D. Webb, R. Bentley, F. Drago, S. Enome, V. Gaizauskas, R. Harrison, G. Hurford, B. Jackson, T. Kosugi, M. Kundu, K. Lang, A. Magun, P. Martens, G. Pneuman, E. Reichmann, A. Schadee, J. Schrijver, B. Schmieder, G. Simon, J. Smith, Jr., K. Strong, P. Waggett and B. Woodgate, in PREFLARE ACTIVITY, Chapter 1 of ENERGETIC PHENOMENA ON THE SUN, Proceedings of the Solar Maximum Mission Workshop, (eds. M.R. Kundu and B. Woodgate), NASA CP 2439, 1986.

Impulsive Phase Transport: R.C. Canfield, F. Bely-Dubau, J.C. Brown, G.A. Dulk, A.G. Emslie, S. Enome, A.H. Gabriel, M.R. Kundu, D. Melrose, D.F. Neidig, K. Ohki, V. Petrosian, A. Poland, E. Rieger, K. Tanaka, H. Zirin, Chapter 3 of ENERGETIC PHENOMENA ON THE SUN, Proceedings of Solar Maximum Mission Workshop, (eds. M.R. Kundu and B. Woodgate), NASA CP 2439, 1986.

Chromospheric Explosions: G.A. Doschek, S. K. Antiochos, E. Antonucci, C.-C. Cheng, J.L. Culhane, G.H. Fisher, C. Jordan, J.W. Leibacher, P. MacNeice, R.W.P. MacWhirter, R.L. Moore, D.M. Rabin, D.M. Rust, and R.A. Shine, Chapter 4 of ENERGETIC PHENOMENA ON THE SUN, Proceedings of Solar Maximum Mission Workshop, (eds. M.R. Kundu and B. Woodgate), NASA CP 2439, 1986.

Flare Energetics: S.T. Wu, C. de Jager, B.R. Dennis, H.S. Hudson, G.M. Simnett, K.T. Strong, R.D. Bentley, P.L. Bornmann, M.E. Bruner, P.J. Cargill, C.J. Crannell, J.G. Doyle, C.L. Hyder, R.A. Kopp, J.R. Lemen, S.F. Martin, R. Pallavicini, G. Peres, S. Serio, J. Sylwester, and N.J. Veck, Chapter 5 of ENERGETIC PHENOMENA ON THE SUN, Proceedings of Solar Maximum Mission Workshop, (eds. M.R. Kundu and B. Woodgate), NASA CP 2439, 1986.

Coronal Mass Ejections and Coronal Structures: E. Hildner, J. Bassi, J.L. Bougeret, R.A. Duncan, D.E. Gary, T.E. Gergely, R.A. Harrison, R.A. Howard, R.M.E. Illing, B.V. Jackson, S.W. Kahler, R. Kopp, B.C. Low, P. Lantos, K.J.H. Phillips, G. Poletto, N.R. Sheely, Jr., R.T. Stewart, Z. Svestka, P.W. Waggett, S.T. Wu, Chapter 6 of ENERGETIC PHENOMENA ON THE SUN, Proceedings of Solar Maximum Mission Workshop, (eds. M.R. Kundu and B. Woodgate), NASA CP 2439, 1986.

Coronal Response to Energy Release During Solar Flares: E. Antonucci, Highlights of Astronomy, (ed. J.-P. Schwings), 731, 1986.

Energetics of the Gradual Phase of Solar Flares: K.T. Strong, Adv. Space Res., 6, No.6, 257, 1986.

Evidence for Explosive Chromospheric Evaporation in a Solar Flare Observed with SMM: D.M. Zarro, K.T. Strong, R.C. Canfield, T. Metcalf, and J.L.R. Saba, Adv. Space Res., 6, No. 6, 61, 1986.

X-ray Imaging of a Filament Eruption with the Solar Maximum Mission Satellite: G.L. Slater and J.L.R. Saba, Adv. Space Res., 6, No. 6, 37, 1986.

Evidence for Coronal Turbulence in a Quiescent Active Region: J.L.R. Saba and K.T. Strong, Adv. Space Res., 6, No. 6, 37, 1986.

Determination of the Calcium Elemental Abundance for 43 Flares from SMM-XRP Solar X-Ray Spectra: J.R. Lemen, J. Sylwester, and R.D. Bentley, Adv. Space Res., 6, No. 6, 245, 1986.

Observations at the Onset of a Large Solar Flare and Their Relevance to Energy Transfer: G.M. Simnett, K.J.H. Phillips, and R.D. Bentley, Adv. Space Res., 6, No. 6, 109, 1986.

A Dynamic Flare with Anomalously Dense Flare Loops: Z. Svestka, J.M. Fontenla, M.E. Machado, S.F. Martin, D.F. Neidig, and G. Poletto, Adv. Space Res., 6, No. 6, 253, 1986.

Dynamical Behavior in Coronal Loops: B.M. Haisch, Adv. Space Res., 6, No. 6, 45, 1986.

Investigations of Turbulent Motions and Particle Acceleration in Solar Flares: J. Jakimiec, A. Fludra, J.R. Lemen, B.R. Dennis, and J. Sylwester, Adv. Space Res., 6, No. 6, 191, 1986.

Flare Onsets in Hard and Soft X-Rays: M.E. Machado, L.E. Orwig, E. Antonucci, Adv. Space Res., 6, No. 6, 101, 1986.

Hydrodynamics of Coronal Loops: a Comparison of Observed and Simulated Spectra Emitted from Flaring Coronal Loops: E. Antonucci, M.A. Dodero, G. Peres, and S. Serio, Adv. Space Res., 6, No. 6, 151, 1986.

Turbulence as a Proposed Intermediate Energy Storage During Solar Flares: P.L. Bornmann, Ap.J., 313, 449, 1987.

Hydrodynamic Flare Modelling: A Comparison of Numerical Calculations with SMM Observations of the 1980 November 12 17:00 UT Flare: G. Peres, F. Reale, S. Serio, and R. Pallavacini, Ap.J., 312, 895, 1987.

Nonpotential Features Observed in the Magnetic Field of an Active Region: A. Gary, R. Moore, M. Hagyard, and B. Haisch, Ap.J., 314, 782, 1987.

A Novel Observational Test of Momentum Balance in a Solar Flare: R.C. Canfield, T.R. Metcalf, K.T. Strong, and D.M. Zarro, Nature, 326, 165, 1987.

New Spectral Line Identifications in High Temperature Flares: B.C. Fawcett, C. Jordan, J.R. Lemen, K.J.H. Phillips, M.N.R.A.S., 225, 1013, 1987.

Solar Active Region Physical Parameters Inferred from a Thermal Cyclotron Line and Soft X-ray Spectral Lines: K.R. Lang, R.F. Willson, K.L. Smith and K.T. Strong, Ap.J., 322, 1044, 1987.

Simultaneous SMM Flat Crystal Spectrometer and Very Large Array Observations of Solar Active Regions: K.R. Lang, R.F. Willson, K.L. Smith and K.T. Strong, Ap.J., 322, 1035, 1987.

A Further Investigation of the Mg XII 8.42A doublet in a Solar Flare Spectrum: R.W.P. McWhirter and P.J. MacNeice, Sol. Phys., 107, 323, 1987.

Multi-thermal Observations of Newly Formed Loops in a Dynamic Flare: Z. Svestka, J.M. Fontenla, M.E. Machado, S.F. Martin, D. Neidig, G. Poletto, Sol. Phys., 108, 237, 1987.

Explosive Plasma Flows in a Solar Flare: D.M. Zarro, R.C. Canfield, K.T. Strong, and T.R. Metcalf, Ap.J., 324, 582, 1988.

Line Broadening and Shifts during the Impulsive Phase of Flares: E. Antonucci, Mem. della Soc. Astron. Ital., 1984, in press.

Interpretation of spectra emitted from the solar coronal plasmas: E. Antonucci, M.A. Dodero, D. Marochi, Mem. della Astron. Soc. Ital., 1986, in press.

Ionization Balance for Iron XXV, XXIV, and XXIII derived from Solar Flare X-ray Spectra: E. Antonucci, M.A. Dodero, A.H. Gabriel, K. Tanaka, J. Dubau, Astron. and Astrophys., 1986, in press.

X-ray Photographs of a Solar Active Region Using a Multilayer Telescope at Normal Incidence: J.H. Underwood, M.E. Bruner, B.M. Haisch, W.A. Brown, L.W. Acton, Science, 283, 61, 1987.

Post-Flare Coronal Arches Observed with the SMM/XRP Flat Crystal Spectrometer: P. Hick, Z. Svestka, K.L. Smith, and K.T. Strong, Sol. Phy., in press, 1988.

A Study of Solar Preflare Activity Using Two-Dimensional Radio and SMM-XRP Observations: M.R. Kundu, N. Gopalswamy, J.L.R. Saba, J.T. Schmelz, and K.T. Strong, Sol. Phys., in press, 1988.

Conduction-Driven Chromospheric Evaporation in a Solar Flare: D.M. Zarro, and J.R. Lemen, Ap. J., in press, June 1988.

Relationships among Flare Images at Different Wavelengths: Z. Svestka, Sol. Phys., in press, 1988.

Properties of an Impulsive Compact Solar Flare Determined by SMM X-ray Measurements: G.A. Linford and C.J. Wolfson, Ap. J., in press, 1988.

Active Region Coronal Loops: Structure and Variability: B.M. Haisch, K.T. Strong, R. Harrison, and G.A. Gary, Ap. J. Suppl., in press, 1988.

Energetics of a Two-Ribbon Flare on November 1, 1980: J. Doyle, submitted to Astron. and Astrophys., 1988.

Flares to Coronal Mass Ejections: A Proposed Activity Classification: P.L. Bornmann, submitted to Ap. J., 1988.

Calcium Ionization Balance and Argon/Calcium Abundance in Solar Flares: E. Antonucci, D. Marocchi, A.H. Gabriel, G.A. Doschek, Astron. and Astrophys., 1988, submitted.

Simulations of the Ca XIX Spectral Emission from a Flaring Loop: I. Thermal Case: E. Antonucci, M.A. Dodero, G. Peres, S. Serio, R. Rosner, Ap. J., 1988, submitted.

Investigations of Turbulent and Directed Motions in Solar Flares: A. Fludra, J.R. Lemen, J. Jakimiec, R.D. Bentley, and J. Sylwester, draft, 1988.

A Comparison of Theoretical and Solar Flare Intensity Ratios for the Fe XIX X-ray Lines: A.K. Bhatia, J.R. Lemen, H.E. Mason, K.J.H. Phillips, draft, 1988.

Momentum Balance in Four Solar Flares: R.C. Canfield, D.M. Zarro, T.R. Metcalf, and J.R. Lemen, submitted, 1988.

Coordinated Soft X-Ray and Hα Observations of Solar Flares: D.M. Zarro, R.C. Canfield, and T.R. Metcalf, in preparation, 1988.

A.2 REPORTS AND POPULAR ARTICLES

An Analysis of the XRP Raster Mechanism: D.M. Simpson, Appleton Laboratory, Report AL-R-6, June 1979.

Solar Maximum Mission: E. Antonucci, L'Astronomia No.l6, 1982.

Towards Understanding Solar Flares: L.W. Acton, Lockheed Horizons, Issue 10, 38-45, 1982.

Las Fulguraciones Solares (Solar Flares): J.I. Garcia de la Rosa, F. Herrera and M. Vazques, Investigacion Y Ciencia No.75, December 1982.

Stellar Coronae, X-rays and Einstein: R.A. Stern, Sky and Tel., 68, 24-28, 1984.

Astronomy from a Reconditioned Satellite: P.W. Waggett, R.D. Bentley, and J.R. Lemen, New Scientist, 1425, 14, 1984.

Solar Science from On High - The Flight of Spacelab 2: L.W. Acton, S.J. Pehanich, Lockheed Horizons, 19, 1985.

MAX '91: An Advanced Payload for the Exploration of High-Energy Processes on the Active Sun: B. Dennis, E. Chupp, C.J. Crannell, G. Doschek, H. Hudson, G. Hurford, S. Kane, R. Lin, T. Prince, R. Ramaty, G. Share, E. Tandberg-Hanssen, D. Bohlin, M. Bruner, F. Cepollina, T. Cline, L. Culhane, J. Dabbs, J. Davis, P. Dunphy, G. Emslie, D. Forrest, T. Gergely, L. Golub, R. Hoover, K. Hurley, S. Jordan, G. Kanbach, A. Kiplinger, J. Lemen, E. Maier, R. Novick, L. Orwig, G. Simnett, S. Sofia, D. Spicer, K. Strong, R. Thomas, F. van Beek, A. Walker, P. Willmore, R. Willson, K. Wood, Report of the MAX '91 NASA Science Study Committee.

NASA's Solar Maximum Mission: A Look at the New Sun, prepared by the SMM Principal Investigator Teams, ed. J. B. Gurman, NASA publication, June 1987.

Successful Solar Rocket Launched by AS&E Scientists: D. Moses, American Science and Engineering, Inc. NEWS, 1988.

A.3 TALKS

Preliminary Results from Ca and Fe Solar Flare Spectra from a Bent Crystal Spectrometer: E. Antonucci for the XRP Team, 156th A.A.S. Meeting, College Park, MD, Abstract in B.A.A.S., 12, 533, 1980.

Morphology of Active Regions and Flares: R.D. Bentley for the XRP Team, 156th A.A.S. Meeting, College Park, MD, Abstract in B.A.A.S., 12, 533, 1980.

Search for Flare Non-Thermal Electrons in Fe and Ca BCS Spectra: M.A. Kayat, A.H. Gabriel, K.J.H. Phillips for the XRP Team, 156th A.A.S. Meeting, College Park, MD, Abstract in B.A.A.S., 12, 533, 1980.

Dynamics of the High Temperature Flare: J.W. Leibacher for the XRP Team, 156th A.A.S. Meeting, College Park, MD, Abstract in B.A.A.S., 12, 531, 1980.

A Presentation of Some BCS Spectra: A. Parmar for the XRP Team, 156th A.A.S. Meeting, College Park, MD, Abstract in B.A.A.S., 12, 531, 1980.

Inner-Shell Ionization (K-alpha) Lines in Flare Impulsive Phases: K.J.H. Phillips for the XRP and HXRBS Teams, 156th A.A.S. Meeting, College Park, MD, Abstract in B.A.A.S., 12, 534, 1980.

Continuum Emission Observed with the BCS: C.G. Rapley for the XRP and HXRBS Teams, 156th A.A.S. Meeting, College Park, MD, Abstract in B.A.A.S., 12, 534, 1980.

Observations from the FCS on the SMM: K.T. Strong for the XRP Team, 156th A.A.S. Meeting, College Park, MD, Abstract in B.A.A.S., 12, 533, 1980.

Temporal Comparison of Fe K-alpha and Hard X-Ray Emission During Several Solar Flares: C.J. Wolfson for the XRP and HXRB Teams, 156th A.A.S. Meeting, College Park, MD, Abstract in B.A.A.S., 12, 534, 1980.

Soft X-Ray Line Spectra from SMM: J.W. Leibacher - Talk at Solar Neighborhood Meeting in Palo Alto, CA, 13 Nov 1981.

When the Sun Flares, All Hell Breaks Loose: L.W. Acton - Media talk at Lockheed Technology Symposium III, Washington, DC, 16 Sep 1981.

The Solar Flare Plasma Machine: L.W. Acton - Invited talk to Plasma Physics Division of American Physical Society, NY, 12 Oct 1981.

Flare Densities from Iron K-alpha Lines: J.R. Lemen, K.J.H. Phillips and the XRP Team, 159th AAS Meeting, Boulder, CO, Abstract in B.A.A.S., 13, 543, 1981.

SMM Observations of Soft X-Ray Line Spectra: J.W. Leibacher, K.J.H. Phillips, C.J. Wolfson and XRP the Team, 159th AAS Meeting, Boulder, CO, Abstract in B.A.A.S., 13, 555, 1981.

The Relation between Fluxes of Soft and Hard X-rays and Its Relevance to Flare Energetics: B.R. Dennis and K.J.H. Phillips. 159th AAS Meeting, Boulder, CO, Abstract in B.A.A.S., 13, 555, 1981.

The Significance of Multiple Flares: K.T. Strong, B. Dennis, J.W. Leibacher, and C.J. Wolfson, 159th AAS Meeting, Boulder, CO, Abstract in B.A.A.S., 13, 820, 1981.

Direct Evidence for Chromospheric Evaporation in a Well-Observed Compact Flare: R.C. Canfield, L.W. Acton, T.A. Gunkler, H.S. Hudson, A. Kiplinger and J.W. Leibacher, 159th AAS Meeting, Boulder, CO, Abstract in B.A.A.S., 13, 819, 1981.

X-Ray Spectroscopic Observations from the Solar Maximum Mission: K.J.H. Phillips - Invited talk - Third Topical Conference of the American Physical Society: ATOMIC PROCESSES IN HIGH TEMPERATURE PLASMAS, Baton Rouge, Louisiana, February 1981. Abstract in B.A.P.S., 26, 808, 1981.

Solar Flares Observed with the SMM: K.J.H. Phillips - Talk at Fitzharry's Astronomical Society, Abingdon, 9 Feb 1982.

Observational Studies of Chromospheric Evaporation: L.W. Acton, Symposium on Hinotori and SMM Results, Tokyo, Jan 1982.

Some Spectroscopic Results From the X-Ray Polychromator on SMM: K.J.H. Phillips, Symposium on Hinotori and SMM Results, Tokyo, Jan 1982.

The Effect of Fe XXIII in Fe XXIV Satellite Line Ratios: J.R. Lemen, K.J.H. Phillips, G.A. Doschek, R.D. Cowan, 160th AAS meeting, Troy, NY, Abstract in B.A.A.S., 14, 608, 1982.

C-2

SMM Observations of a Coronal Archade at the Onset of a Flare: K.T. Strong, M.E. Bruner, G. Poletto and R. Kopp, S.P.D. Meeting of the A.A.S., Pasadena, CA, Abstract in B.A.A.S., 15, 715, 1983.

An X-Ray Empirical Model of a Solar Flare Loop: M.E. Bruner, W.A. Brown, L.W. Acton and K.T. Strong. S.P.D. Meeting of the A.A.S., Pasadena, CA, Abstract in B.A.A.S., 15, 708, 1983.

The 12 November 1980 Flare at 17:00 UT: Analysis of Observations by the XRP: R. Pallavicini and L.W. Acton, UK SMM Workshop, May 1983.

Active Region Soft X-Ray Line Profiles: K.T. Strong, J.R. Lemen, and K.J.H. Phillips, 164th A.A.S. Meeting, Baltimore, MD, Abstract in B.A.A.S., 16, 730, 1984.

Recent Soft X-Ray Spectra During a Flare Decay: K.J.H. Phillips, J.R. Lemen, and K.T. Strong, 164th A.A.S. Meeting, Baltimore, MD, Abstract in B.A.A.S., 16, 730, 1984.

A New Method for Determining Temperature and Emission Measure Variations During Solar Flares: P.L. Bornmann, 164th A.A.S. Meeting, Baltimore, MD, Abstract in B.A.A.S., 16, 545, 1984.

Variation in the Observed Coronal Calcium Abundance for Various X-ray Flare Plasmas: J.R. Lemen, J. Sylwester, R. Mewe., 164th A.A.S. Meeting, Baltimore, MD, Abstract in B.A.A.S., 16, 545, 1984.

Filament Activations as Coronal Flare Precursors: D.F. Webb and E.J. Schmahl, 164th A.A.S. Meeting, Baltimore, MD, Abstract in B.A.A.S., 16, 536, 1984.

Electron Beam Heating during a Well-Observed Compact Flare: R.C. Canfield and T.A. Gunkler, 164th A.A.S. Meeting, Baltimore, MD, Abstract in B.A.A.S., 16, 544, 1984.

Progress in the Study of Homologous Flares on the Sun: B.E. Woodgate, M.J. Matres, J.B. Smith, K.T. Strong, M.K. McCabe, M.E. Machado, V. Gaisauskas, R. Stewart, and P.A. Sturrock, COSPAR 25th Plenary Meeting, Graz, Austria, 25 June - 7 July 1984.

Homologous Flares and Evolution of NOAA Active Region 2372: K.T.Strong, J.B. Smith, Jr., M.K. McCabe, M.E. Machado, J.L.R. Saba, and G.M. Simnett, COSPAR 25th Plenary Meeting, Graz, Austria, 25 June - 7 July 1984.

Relationship of a Growing Magnetic Flux Region to Flares: S.F. Martin, R.D. Bentley, A. Schadee, A. Antalova, A. Kucera, L. Dezso, L. Gesztelyi, K.L. Harvey, H. Jones, S.H.B. Livi, and J. Wang, COSPAR 25th Plenary Meeting, Graz, Austria, 25 June - 7 July 1984.

Origin and Location of Chromospheric Evaporation in Flares: E. Antonucci, D. Marocchi, G. M. Simnett, COSPAR 25th Plenary Meeting, Graz, Austria, 25 June - 7 July 1984.

Differential Emission Measure Analysis of Hot-flare Plasma from Solar-Maximum Mission X-ray Data: J. Jakimiec, J. Sylwester, J.R. Lemen, R. Mewe, R.D. Bentley, A. Fludra, J. Schrijver, and B. Sylwester, COSPAR 25th Plenary Meeting, Graz, Austria, 25 June - 7 July 1984.

Combined Analysis of Soft and Hard X-Ray Spectra from Flares: A.H. Gabriel, F. Bely-Dubau, J.C. Sherman, L.E. Orwig, H. Schrijver, COSPAR 25th Plenary Meeting, Graz, Austria, 25 June - 7 July 1984.

An Overview of the Results and Observations from the X-Ray Polychromator on the Solar Maximum Mission: K.T. Strong, P.J. MacNeice, J.R. Lemen, A.H. Gabriel, J.L. Culhane, and L.W. Acton - invited talk - A.G.U. Meeting, San Francisco, CA, abstract in EOS, 65, No. 45, 1067, 1984.

Dynamics of the Non-flaring Solar Atmosphere: Results from the Solar Maximum Mission: K.T. Strong and J.B. Gurman, talk presented at the Advanced Solar Observatory Workshop, Carmel, CA, 1985.

X-ray, Ultraviolet, Optical, and Magnetic Structure in and Near an Active Region: B.M. Haisch, T.D. Tarbell, M.E.Bruner, L.W.Acton, R.M. Bonnet, M.J. Hagyard, 165th AAS Meeting, Tucson, AZ, Abstract in B.A.A.S., 16, 1002, 1985.

Coronal Response to Energy Release during Solar Flares: E. Antonucci, invited talk, New Delhi, India, 1985, Published in Highlights of Astronomy, (ed. J.-P. Schwings), 731, 1986.

Plasma Parameters from the Helium-like Ion Mg XI During a Small Impulsive Flare: G.A. Linford and C.J. Wolfson, 167th AAS Meeting, Houston, TX, Abstract in B.A.A.S., 17, 905, 1986.

Rapid Fluctuations in Solar Flares Observed with the SMM Soft X-ray Polychromator: D.M. Zarro, K.T. Strong, and J.L.R. Saba, 168th AAS Meeting, Ames, IA, Abstract in B.A.A.S., 18, 638, 1986.

Non-potential Features Observed in the Magnetic Field of an Active Region: G.A. Gary, R.L. Moore, M.J. Hagyard, B.M. Haisch, 168th AAS Meeting, Ames, IA, Abstract in B.A.A.S., 18, 709, 1986.

Solar Burst Precursors and Energy Build-Up at Microwave Wavelengths: K.R. Lang and R.F. Willson, the XXVIth COSPAR Plenary Meeting, Symposium 5: SYNOPSIS OF THE SOLAR MAXIMUM ANALYSIS, Toulouse, France, July 1986.

Hydrodynamics of Coronal Loops: A Comparison of Observed and Simulated Spectra Emitted from Coronal Loops: E. Antonucci and M.A. Dodero, the XXVIth COSPAR Plenary Meeting, Symposium 5: SYNOPSIS OF THE SOLAR MAXIMUM ANALYSIS, Toulouse, France, July 1986.

Energetics of the Gradual Phase: K.T. Strong, invited talk given at the XXVIth COSPAR Plenary Meeting, Symposium 5: SYNOPSIS OF THE SOLAR MAXIMUM ANALYSIS, Toulouse, France, July 1986.

Evidence for Coronal Turbulence in a Quiescent Active Region: J.L.R. Saba and K.T. Strong, the XXVIth COSPAR Plenary Meeting, Symposium 5: SYNOPSIS OF THE SOLAR MAXIMUM ANALYSIS, Toulouse, France, July 1986.

A Dynamic Flare with Anomalously Dense Flare Loops: Z. Svestka, J.M. Fontenla, M.E. Machado, S.F. Martin, D.F. Neidig, and G. Poletto, the XXVIth COSPAR Plenary Meeting, Symposium 5: SYNOPSIS OF THE SOLAR MAXIMUM ANALYSIS, Toulouse, France, July 1986.

Dynamical Behavior in a Coronal Loop: B.M. Haisch, the XXVIth COSPAR Plenary Meeting, Symposium 5: SYNOPSIS OF THE SOLAR MAXIMUM ANALYSIS, Toulouse, France, July 1986.

How Empty is a Coronal Hole?: K.T. Strong and D. Sime, AGU Meeting, San Francisco, CA, Abstract in EOS, 67, No. 44, 1142, 1986.

Flares: The Solar-Stellar Perspective and Opportunities: B.M. Haisch, invited talk given at the Rutherford Appleton Laboratory Workshop on Flares: Solar and Stellar, 1986.

Variability in Active Region Coronal Loops: B.M. Haisch, 169th AAS Meeting, Pasadena, CA, Abstract in B.A.A.S., 18, 901, 1987.

Action and Reaction in a Solar Flare: D.M. Zarro, R.C. Canfield, K.T. Strong, and T.R. Metcalf, 169th AAS Meeting, Pasadena, CA, Abstract in B.A.A.S., 18, 966, 1987.

Simultaneous SMM and VLA Observations of Coronal Loops: R.F. Willson, K.R. Lang, K.L. Smith, and K.T. Strong, 169th AAS Meeting, Pasadena, CA, Abstract in B.A.A.S., 18, 1042, 1987.

An Overview of SMM/XRP (X-Ray Polychromator) Science, Projects, and Plans: K.T. Strong, Symposium on Solar Physics at Goddard, 18 Feb 1987.

Coronal Dynamics: XRP Observations of Nonthermal Motions in Active Regions: J.L.R. Saba, Symposium on Solar Physics at Goddard, 18 Feb 1987.

Coronal Dynamics: XRP Observations of Chromospheric Evaporation in Solar Flares: D.M. Zarro, Symposium on Solar Physics at Goddard, 18 Feb 1987.

A Review of the SMM Workshop on Thermal/Nonthermal Interactions in Flares: K.T. Strong, U.S.–Japan Seminar on Solar Flare Research, University of Hawaii, 08-10 Apr 1987.

Spectroscopic Techniques for Determining the Electron Densities in the Solar Atmosphere: H. Mason, IAU Colloquuium No. 102, UV and X-Ray Spectroscopy of Astrophysical and Laboratory Plasmas, Beaulieu-Sur-Mer, France, 09-11 Sep 1987.

Explosive Mass Motions in the Flare of 1456 UT 7 May 1980: R.C. Canfield and D.M. Zarro, S.P.D. Meeting of the A.A.S., Honolulu, HI, Abstract in B.A.A.S., 19, 921, 1987.

Coronal Explosions in Solar Flares: D.M. Zarro and R.C. Canfield, A.G.U. Meeting, San Francisco, CA, Abstract in EOS, 68, No. 44, 1409, 1987.

Soft X-ray Spectroscopy at a Loop Footpoint: G.L. Slater, D.M. Zarro, and S.L. Freeland, A.G.U. Meeting, San Francisco, CA, Abstract in EOS, 68, No. 44, 1409, 1987.

Investigations of Turbulent and Directed Motions in Solar Flares: J.R. Lemen, A. Fludra, and J. Jakimec, A.G.U. Meeting, San Francisco, CA, Abstract in EOS, 68, No. 44, 1409, 1987.

Variability of Active Region Coronal Loops: B.M. Haisch and K.T. Strong, A.G.U. Meeting, San Francisco, CA, Abstract in EOS, 68, No. 44, 1409, 1987.

Properties of a Compact Solar Flare Determined by X-ray Measurements: G.A. Linford and C.J. Wolfson, A.G.U. Meeting, San Francisco, CA, Abstract in EOS, 68, No. 44, 1409, 1987.

Coordinated Soft X-ray and H-alpha Observations of Solar Flares: D.M. Zarro, R.C. Canfield, and T.R. Metcalf, XXVIIth COSPAR meeting, Workshop XV: SCIENTIFIC PLANNING FOR THE SOLAR MAXIMUM AND BEYOND, Espoo, Finland, 18-29 Jul 1988, submitted.

Preliminary Results from the Coronal Magnetic Structures Observing Campaign (CoMStOC): J.T. Schmelz, J.L.R. Saba, K.T. Strong, and G.D. Holman, XXVIIth COSPAR meeting, Workshop XV: SCIENTIFIC PLANNING FOR THE SOLAR MAXIMUM AND BEYOND, Espoo, Finland, 18-29 Jul 1988, submitted.

A Statistical Study of Coronal Densities From X-Ray Line Ratios of Helium-Like Ions: Ne IX and Mg XI: G.A. Linford, J.R. Lemen, and K.T. Strong, XXVIIth COSPAR meeting, Workshop XV: SCIENTIFIC PLANNING FOR THE SOLAR MAXIMUM AND BEYOND, Espoo, Finland, 18-29 Jul 1988, submitted.

Coronal Temperature Diagnostic from High Resolution Soft X-Ray Spectra: K.T. Strong, E.S. Claflin, J.R. Lemen, and G.A. Linford, XXVIIth COSPAR meeting, Workshop XV: SCIENTIFIC PLANNING FOR THE SOLAR MAXIMUM AND BEYOND, Espoo, Finland, 18-29 Jul 1988, submitted.

Investigations of Turbulent and Directed Motions in Solar Flares: J.R. Lemen, A. Fludra, and J. Jakimiec, XXVIIth COSPAR meeting, Workshop XV: SCIENTIFIC PLANNING FOR THE SOLAR MAXIMUM AND BEYOND, Espoo, Finland, 18-29 Jul 1988, submitted.

SMM-XRP Observations of the X-4 Flare on 19 May 1984: J.T. Schmelz, J.L.R. Saba, and K.T. Strong, A.G.U. Meeting, Baltimore, MD, Abstract in EOS, Vol. 69, submitted.

A.4 CONFERENCE PROCEEDINGS

A Two Axis Pointing System for an Orbiting Astronomical Instrument: R.F. Turner and J.G. Firth, Proc. 13th Aerospace Mechanisms Symposium, NASA Conf. Pub. 2031, JSC Houston, 26-27 Apr 1979.

Observational Insights Into Solar/Stellar Problems from the Solar Maximum Mission: L.W. Acton for the SMM Team, NATO Advanced Study on Solar Phenomena in Stars and Stellar Systems, France, 1980.

Early Results from the SMM: C.G. Rapley for the SMM Teams, Sixth International Colloquium on Ultraviolet and X-Ray Spectroscopy of Astrophysical and Laboratory Plasmas, I.A.U. Colloquium No. 55, Toronto, Canada, 1980.

Preliminary Soft X-Ray Spectroscopy and Imagery from the SMM X-Ray Polychromator: J.W. Leibacher for the XRP Team, Sixth International Colloquium on Ultraviolet and X-Ray Spectroscopy of Astrophysical and Laboratory Plasmas, I.A.U. Colloquium No. 55, Toronto, Canada, 1980.

Velocities Observed with the X-Ray Polychromator on Board the Solar Maximum Mission: J.W. Leibacher and the XRP Team, S.P.D. Meeting of the A.A.S., Taos, NM, Abstract in B.A.A.S., 12, 906, 1980.

Changes in the Characteristics of the Coronal Plasma During Two Impulsive Flares: K.T. Strong, J. Sylwester, A. Parmar, B. Dennis, A. Poland and the XRP Team, S.P.D. Meeting of the A.A.S., Taos, NM, Abstract in B.A.A.S., 12, 911, 1980.

A Study of a Soft X-Ray Slow Event Associated with the Commencement of a Type 1 Noise Storm: C.G. Rapley, R.D. Bentley, P. Lantos, A. Kerdraon, S.P.D. Meeting of the A.A.S., Taos, NM, Abstract in B.A.A.S., 12, 912, 1980.

Coronal Flare Densities: C.J. Wolfson, J.G. Doyle, K.J.H. Phillips and the XRP Team, S.P.D. Meeting of the A.A.S., Taos, NM, Abstract in B.A.A.S., 12, 912, 1980.

A Small Impulsive Flare: L.W. Acton, J.W. Leibacher and the XRP Team, S.P.D. Meeting of the A.A.S., Taos, NM, Abstract in B.A.A.S., 12, 904, 1980.

Soft X-Ray Emission During the Impulsive Phase of a Flare: E. Antonucci, A.H. Gabriel, J.G. Doyle and the XRP Team, S.P.D. Meeting of the A.A.S., Taos, NM, Abstract in B.A.A.S., 12, 900, 1980.

Interpretation of the Ca XIX, Fe XXV, and Fe XXVI BCS Spectra: A.H. Gabriel, E. Antonucci, J. Dubau and the XRP Team, S.P.D. Meeting of the A.A.S., Taos, NM, Abstract in B.A.A.S., 12, 912, 1980.

Control of the Soft X-Ray Polychromator on the Solar Maximum Mission Satellite: L.A. Springer, M. Levay, C.W. Gilbreth, M.L. Finch, R.D. Bentley and J.G. Firth, AIAA 19th Aerospace Science Meeting, St. Louis, MO, 12-15 Jan 1981.

Solar Flare Diagnostics Using the SMM: A.H. Gabriel, lst European Conference on Atomic Physics. Heidelberg, Germany, April 1981.

Early Results from the XRP and UVSP Experiments on the SMM: A.H. Gabriel, Third European Solar Meeting, Solar Section, Astronomy and Astrophys. Div. of EPS., Oxford, England, 1981.

Relationship Between a Soft X-Ray Long Duration Event and an Intense Noise Storm: C.G. Rapley, Third European Solar Meeting, Solar Section, Astronomy and Astrophys. Div. of EPS., Oxford, England, 1981.

The Excitation of Fe K-alpha Radiation in Flares: J.L. Culhane, Third European Solar Meeting, Solar Section, Astronomy and Astrophys. Div. of EPS., Oxford, England, 1981.

A.4 CONFERENCE PROCEEDINGS

Analysis of the XRP Ca and Fe Spectra: J. Dubau, Third European Solar Meeting, Solar Section, Astronomy and Astrophys. Div. of EPS., Oxford, England, 1981.

Analysis of X-Ray Flare on 7 April 1980 Based on SMM Data: B. Sylwester, J. Sylwester, J. Jakimiec, R. Mewe, J. Schrijver, K.T. Strong, C. Rapley, Third European Solar Meeting, Solar Section, Astronomy and Astrophys. Div. of EPS., Oxford, England, 1981.

Determination of the Energy Balance During a Solar Flare, From Soft X-Ray Observations: N.J. Veck and C. Jordan, Third European Solar Meeting, Solar Section, Astronomy and Astrophys. Div. of EPS., Oxford, England, 1981.

Analysis of Soft X-Ray Ca and Fe Spectra: M. Loulergue, L. Faucher, L. Steenman-Clark, European Phys. Soc. Meeting, Istanbul, Turkey, Sep 1981.

Analysis of X-Ray Spectra Emitted by High Temperature Plasmas: Solar Flares, Tokamak and Laser Fusion: F. Bely-Dubau and J. Dubau, European Phys. Soc. Meeting, Istanbul, Turkey, Sep 1981.

X-Ray Observations of Flares and Active Regions with the Flat Crystal Spectrometer on SMM: R. Pallavicini, G. Poletto and the XRP Team, Annual Meeting of Italian Astr. Soc. Modena, Italy, 01-04 Oct 1981.

Hydrodynamics of Solar Flares: Observations and Numerical Modeling: R. Pallavicini, G. Peres, G. Vaiana and XRP Team, Annual Meeting of Italian Astr. Soc., Modena, Italy, 01-04 Oct 1981.

Ground-Based and SMM Observations of a Filament-Associated Event on November 22, 1980: R. Pallavicini, L.W. Acton, C-C. Cheng, G. Nelson and A. Zappala, Annual Meeting of Italian Astr. Soc., Modena, Italy, 01-04 Oct 1981.

Space-Borne and Ground-Based Observations of a Solar Active Region and a Flare: F. Chiuderi-Drago, Proceedings Vl ERMA Meeting, Dubrovnic, Yugoslavia, 1981.

SMM Soft X-Ray and UV Observations of Solar Flares for the XRP Team: J.W. Leibacher, Tokyo, Japan, Nov 1981.

X-Ray Classification of Flares in Large and Small Magnetic Structures: C.G. Rapley, R.A.S. Discussion Meeting on Solar Flares, London, England, 11 Dec 1981.

Soft X-Ray Discriminators of Flare Classifications: E. Antonucci, R.A.S. Discussion Meeting on Solar Flares, London, England, 11 Dec 1981.

Flare Classification - Fact or Fancy: L.W. Acton, R.A.S. Discussion Meeting on Solar Flares, London, England, 11 Dec 1981.

Osservazioni SMM Radio and Ottiche di Regioni Attive Solar: E. Antonucci, R. Bandiera, F. Chiuderi-Drago and R. Falciani, S.I.F. Meeting, Pisa, Italy, 1981.

The XRP Experiment: E. Antonucci and C.J. Wolfson, Crimea SMM Workshop, Crimea, U.S.S.R., Mar 1981.

Direct Evidence for Chromospheric Evaporation in a Well Observed Compact Flare: R.C. Canfield, T.A. Gunkler, H.S. Hudson, L.W. Acton, J.W. Leibacher and A. Kiplinger, Symposium on SMY. COSPAR, Ottawa, Canada, 1982.

Observational Studies of Chromospheric Evaporation: L.W. Acton, Hinotori Symposium on Solar Flares, Jan 1982.

Some Spectroscopic Results from the X-Ray Polychromator on SMM: K.J.H. Phillips, Hinotori Symposium on Solar Flares, Jan 1982.

Correlations Between Soft X-Ray Long Duration Events and Metric Noise Storms: C.G. Rapley, Hinotori Symposium on Solar Flares, Jan 1982.

Inner-shell Transitions in Fe XIX-XXIII in the X-ray Spectra of Solar Flares and Tokamaks: J.R. Lemen, K.J.H. Phillips, R.D. Cowan, G.A. Doschek, I.A.U. Colloquium No. 73, Dublin, Ireland, Aug 1982.

Evidence for Simultaneous Presence of Large and Small Loops in Solar Flares: A.O. Benz, B.R. Dennis, J.W. Leibacher, R. Mewe, A. Poland, J. Schrijver, G. Simnett, J.B. Smith, K.T. Strong and J. Sylwester, Presented at I.A.U. in Petrak, 1982.

Soft X-Ray Spectroscopy from the X-Ray Polychromator on the Newly Repaired Solar Maximum Mission: K.T. Strong, J.R. Lemen, and K.J.H. Phillips, Proceedings of the Eighth International Colloquium on Ultraviolet and X-Ray Spectroscopy of Astrophysical and Laboratory Plasmas, I.A.U. Colloquium No.86, Washington, DC, 27-29 Aug 1984.

Derivation of the Ionization Balance for Fe XXIV / Fe XXV Using Solar X-ray Data: E. Antonucci, M.A. Dodero, A.H. Gabriel and K. Tanaka, Proceedings of the Eighth International Colloquium on Ultraviolet and X-Ray Spectroscopy of Astrophysical and Laboratory Plasmas, I.A.U. Colloquium No.86, Washington, DC, 27-29 Aug 1984.

Variation of the Observed Coronal Calcium Abundance for Various X-ray Flare Plasmas: J. Sylwester, J.R. Lemen and R. Mewe, Proceedings of the Eighth International Colloquium on Ultraviolet and X-Ray Spectroscopy of Astrophysical and Laboratory Plasmas, I.A.U. Colloquium No.86, Washington, DC, 27-29 Aug 1984 (short abstract).

New Calculations of Inner-Shell X-ray Lines in Ti, Cr, and Ni as Density Diagnostics: J.R. Lemen, K.J.H. Phillips, G.A. Doschek and R.D. Cowan, Proceedings of the Eighth International Colloquium on Ultraviolet and X-Ray Spectroscopy of Astrophysical and Laboratory Plasmas, I.A.U. Colloquium No.86, Washington, DC, 27-29 Aug 1984 (short abstract).

Atomic Calculations for the Highly Ionized Iron Atoms Produced in Solar Flares: H.E. Mason and A.K. Bhatia, Proceedings of the Eighth International Colloquium on Ultraviolet and X-Ray Spectroscopy of Astrophysical and Laboratory Plasmas, I.A.U. Colloquium No.86, Washington DC, 27-29 Aug 1984.

Solar Flares: Thermal Phase Models: P. MacNeice, Proceedings of a Workshop on FLARES: SOLAR AND STELLAR, Cosener's House, Abingdon, England, May 1986.

Flares: The Solar-Stellar Perspective and Opportunities: B.M. Haisch Proceedings of a Workshop on FLARES: SOLAR AND STELLAR, Cosener's House, Abingdon, England, May 1986.

Rapid Fluctuations in Solar Flares Observed in Soft X-rays: D. Zarro, K.T. Strong, and J.L.R. Saba, Proceedings of the SMM Topical Workshop on RAPID FLUCTUATIONS IN SOLAR FLARES, NASA CP 2449, 289-298, 1986.

Turbulence as a Proposed Intermediate Energy Storage Mechanism during Solar Flares: P.L. Bornmann, in THE LOWER ATMOSPHERE IN SOLAR FLARES: RELATIONSHIP BETWEEN LOW TEMPERATURE PLASMAS AND HIGH ENERGY EMISSIONS, Proceedings of the National Solar Observatory/Solar Maximum Mission Symposium, 20-24 Aug 1985, Sacramento Peak Observatory, NM, (ed. D.F. Neidig), p.428, 1986.

Dynamic Conditions of Thermal Plasma in Large Flares: E. Antonucci and M.A. Dodero, in THE LOWER ATMOSPHERE IN SOLAR FLARES: RELATIONSHIP BETWEEN LOW TEMPERATURE PLASMAS AND HIGH ENERGY EMISSIONS, Proceedings of the National Solar Observatory/Solar Maximum Mission Symposium, 20-24 Aug 1985, Sacramento Peak Observatory, NM, (ed. D.F. Neidig), p.363, 1986.

On Chromospheric Heating During Solar Flares: E. Antonucci, Proc. of the International Symposium on Space Physics Chinese Society of Space Research, Beijng, China, p.10, 1986.

Line Broadening and Magnetic Reconnection at Flare Onset: E. Antonucci, R. Rosner, K. Tsinganos, Proc. of the Solar Maximum Analysis Workshop, Irkutsk, U.S.S.R., 1986, in press.

A.5 POSTERS

Simultaneous Observations of AR2490 Performed in X-UV, Optical and Radio Wavelength Domain: Franca Chiuderi Drago, SOLAR PHYSICS FROM SPACE Meeting, Zurich, 1980, Abstract in Space Sci. Rev. 29, 439, 1981.

A Study of a Double Impulsive Flare Event: K.T. Strong, R. Mewe, B. Dennis, J.W. Leibacher, A. Parmar, A. Poland, J. Schrijver and J. Sylwester, Third European Solar Meeting, Solar Section, Astronomy and Astrophys. Div. of EPS., Oxford, England, 1981.

Bent Crystal Spectrometer Results on the Soft X-Ray Emission During the Impulsive Phase of Flares: E. Antonucci, Third European Solar Meeting of Solar Section, Astronomy and Astrophys. Division of EPS., Oxford, England, 1981.

Characteristics of the Soft X-Ray Long Duration Events Observed by the SMM X-Ray Polychromator: R.D. Bentley, C.G. Rapley and the XRP Team, S.P.D. Meeting of the A.A.S., Taos, NM, Abstract in B.A.A.S., 12, 904, 1980.

Analysis of XRP Bent Crystal Spectra of Hydrogen-Like Fe 26: A. Parmar, Third European Solar Meeting, Solar Section, Astronomy and Astrophys. Div. of EPS., Oxford, England, 1981.

Active Region Magnetic Fields: J.B. Smith, K.T. Strong, E. Schmahl, M. Kundu and R.D. Bentley, 159th AAS Meeting, Boulder, CO, Abstract in B.A.A.S., 13, 881, 1981.

The Decay of a Large Limb Flare: P.J. Cargill, N.J. Veck, C. Jordan, K.T. Strong, G. Simnett and E.R. Priest. S.P.D. Meeting of the A.A.S., Pasadena, CA, Abstract in B.A.A.S., 15, 712, 1983.

Recent Solar Observations from the X-Ray Polychromator on the Repaired SMM Satellite: J.L.R. Saba, G.L. Slater, M.X. Levay, K.L. Smith, K.T. Strong, R.D. Bentley, J.R. Lemen, R.R. Caffey, S.L. Freeland, D.P. Mathur, K.J.H. Phillips, and T.A. Waters, 164th A.A.S. Meeting, Baltimore, MD, Abstract in B.A.A.S., 16, 726, 1984.

Timing and Energetics of Associated Coronal Mass Ejections and X-ray Events: P.W. Waggett, R.D. Bentley, G.M. Simnett, R.A. Harrison, P. Lantos, A.G.U. Meeting, San Francisco, CA, Abstract in EOS, 65, No. 45, 1070, 1984.

Soft X-ray Observations of the Sun from the X-Ray Polychromator on SMM: J.L.R. Saba, L.W. Acton, R.D. Bentley, R.R. Caffey, J.L. Culhane, S.L. Freeland, Jr., A.H. Gabriel, J.R. Lemen, M. X Levay, P. MacNeice, D.P. Mathur, K.J.H. Phillips, J.M. Repace, G.L. Slater, K.L. Smith, K.T. Strong, P.W. Waggett, and T.A. Waters, A.G.U. Meeting, San Francisco, CA, Abstract in EOS, 65, No. 45, 1071, 1984.

Rapid Fluctuations in Solar Flares observed in Soft X-rays: D. Zarro, K.T. Strong and J.L.R. Saba, SMM Topical Workshop on RAPID FLUCTUATIONS IN SOLAR FLARES, Lanham, MD, 30 Sep-04 Oct 1985.

X-ray Imaging of a Filament Eruption with the Solar Maximum Mission Satellite: G.L. Slater and J.L.R. Saba, poster presented at the XXVIth COSPAR Plenary Meeting, Symposium 5: SYNOPSIS OF THE SOLAR MAXIMUM ANALYSIS, Toulouse, France, Jul 1986.

Investigations of Turbulent Motions and Particle Acceleration in Solar Flares: J. Jakimiec, A. Fludra, J.R. Lemen, B.R. Dennis and J. Sylwester, poster presented at the XXVIth COSPAR Plenary Meeting, Symposium 5: SYNOPSIS OF THE SOLAR MAXIMUM ANALYSIS, Toulouse, France, Jul 1986.

Evidence for Chromospheric Evaporation and Condensation in a Solar Flare Observed with SMM: D.M. Zarro, K.T. Strong, R.C. Canfield, T. Metcalf, and J.L.R. Saba, poster presented at the XXVIth COSPAR Plenary Meeting, Symposium 5: SYNOPSIS OF THE SOLAR MAXIMUM ANALYSIS, Toulouse, France, Jul 1986.

Determination of the Calcium Elemental Abundance for 43 Flares from SMM-XRP Solar X-ray Spectra: J.R. Lemen, J. Sylwester, and R.D. Bentley, poster presented at the XXVIth COSPAR Plenary Meeting, Symposium 5: SYNOPSIS OF THE SOLAR MAXIMUM ANALYSIS, Toulouse, France, Jul 1986.

Magnetic Morphology of Explosive Chromospheric Evaporation in a Solar Flare Observed with SMM: R.C. Canfield, and D.M. Zarro, presented at the SMM topical workshop on Thermal-Nonthermal Interactions in Solar Flares, New Carrollton, MD, 23-27 Mar 1987.

SMM-XRP Observations of Chromospheric Evaporation in Solar Flares: D.M. Zarro, and J.R. Lemen, presented at SMM topical workshop on Thermal-Nonthermal Interactions in Solar Flares, New Carrollton, MD, 23-27 Mar 1987.

A Study of Solar Preflare Activty Using Two-Dimensional Radio and SMM-XRP Observations: M.R. Kundu, N. Gopalswamy, J.L.R. Saba, and K.T. Strong, presented at SMM topical workshop on Thermal-Nonthermal Interactions in Solar Flares, New Carrollton, MD, 23-27 Mar 1987.

Flare Heating of the Temperature Minimum Region of the Solar Atmosphere: T.R. Metcalf, R.C. Canfield, and J.L.R. Saba, presented at SMM topical workshop on Thermal-Nonthermal Interactions in Solar Flares, New Carrollton, MD, 23-27 Mar 1987.

The Flare, Coronal Mass Ejection Relationship: Initial Results of the CME Onset Program: R.A. Harrison and K.J.H. Phillips, presented at SMM topical workshop on Thermal-Nonthermal Interactions in Solar Flares, New Carrollton, MD, 23-27 Mar 1987.

Post-Burst Increase of the X1 Flare Observed Using the VLA at 6 cm, 1984 May 19: E.J. Schmahl, presented at SMM topical workshop on Thermal-Nonthermal Interactions in Solar Flares, New Carrollton, MD, 23-27 Mar 1987.

Geometry of Chromospheric Evaporation: A.H. Gabriel and F. Millier, presented at SMM topical workshop on Thermal-Nonthermal Interactions in Solar Flares, New Carrollton, MD, 23-27 Mar 1987.

Two Component Analysis of Soft X-ray Line Emission: P.L. Bornmann, presented at SMM topical workshop on Thermal-Nonthermal Interactions in Solar Flares, New Carrollton, MD, 23-27 Mar 1987.

Compact Solar Flare Loops with Inverted Temperature Gradients: G.A. Linford, presented at SMM topical workshop on Thermal-Nonthermal Interactions in Solar Flares, New Carrollton, MD, 23-27 Mar 1987.

SMM-FCS Observations of Nonthermal X-ray Line Broadening in Quiescent Coronal Loops: Setting the Stage for Thermal/Nonthermal Processes in Solar Flares: J.L.R. Saba and K.T. Strong, presented at SMM topical workshop on Thermal-Nonthermal Interactions in Solar Flares, New Carrollton, MD, 23-27 Mar 1987.

Use of Generalized Differential Emission Measure to Study Nonthermal Energy Dissipation: F. Bely-Dubau and A.H. Gabriel, presented at SMM topical workshop on Thermal-Nonthermal Interactions in Solar Flares, New Carrollton, MD, 23-27 Mar 1987.

Soft X-Ray Images of the Solar Corona Using Normal Incidence Optics: M.E. Bruner, B.M. Haisch, W.A. Brown, L.W. Acton, J.H. Underwood, I.A.U. Colloquuium No. 102, UV and X-Ray Spectroscopy of Astrophysical and Laboratory Plasmas, Beaulieu-Sur-Mer, France, 09-11 Sep 1987.

Time Variation of the Calcium Elemental Abundance in Flares from NOAA Active Region 2779: J. Sylwester, J.R. Lemen, R.D. Bentley, I.A.U. Colloquuium No. 102, UV and X-Ray Spectroscopy of Astrophysical and Laboratory Plasmas, Beaulieu-Sur-Mer, France, 09-11 Sep 1987.

Results of the LEBAN Diagnostic Procedure Applied to Two SMM Observed Flares: B. Sylwester, J. Sylwester, J. Jakimiec, G. Peres, S. Serio, I.A.U. Colloquuium No. 102, UV and X-Ray Spectroscopy of Astrophysical and Laboratory Plasmas, Beaulieu-Sur-Mer, France, 09-11 Sep 1987.

Localisation of Chromospheric Evaporation by the Analysis of Solar Flare X-Ray Spectra: F. Millier, N. Lizambert, A.H. Gabriel, I.A.U. Colloquuium No. 102, UV and X-Ray Spectroscopy of Astrophysical and Laboratory Plasmas, Beaulieu-Sur-Mer, France, 09-11 Sep 1987.

The Comparison of Helium-Like Ion Emission Line Ratios with Solar X-Ray Spectral Data: S.M. Mc Cann, F.P. Keenan, I.A.U. Colloquuium No. 102, UV and X-Ray Spectroscopy of Astrophysical and Laboratory Plasmas, Beaulieu-Sur-Mer, France, 09-11 Sep 1987.

SMM, VLA, and VMG Observations of a Solar Active Region: K.L. Smith, K.T. Strong, R.F. Willson, and M.J. Hagyard, A.G.U. Meeting, San Francisco, CA, Abstract in EOS, 68, No. 44, 1408, 1987.

A Catalogue of the SOON H-alpha Patrol Films: A New Resource for Solar Physics: O.C. St.Cyr, K.T. Strong, D. Speich, R. Murphy, A.G.U. Meeting, San Francisco, CA, Abstract in EOS, 68, No. 44, 1408, 1987.

Comparison of SMM/FCS Solar X-Ray Spectra with Simulated Single- and Multi-Temperature Spectra: E.S. Claflin, J.R. Lemen, K.T. Strong, A.G.U. Meeting, San Francisco, CA, Abstract in EOS, 68, No. 44, 1408, 1987.

Microwave Observations of the X-Flare of May 19, 1984: E.J. Schmahl, M.R. Kundu, J.T. Schmelz, J.L.R. Saba, K.T. Strong, 171st A.A.S. Meeting, Austin, TX, Abstract in B.A.A.S, 19, 1122, 1987.

The Effect of a Large Flare on the Solar Corona: J.T. Schmelz, J.L.R. Saba, K.T. Strong, E.J. Schmahl, M.R. Kundu, 171st A.A.S. Meeting, Austin, TX, Abstract in B.A.A.S, 19, 1122, 1987.

Coronal Diagnostics of New Cycle Solar Active Regions: J.L.R. Saba, J.T. Schmelz, G.D. Holman, H.S. Bawa, S.U. Rehman, D.L. Kemp, D.P. Mathur, G.L. Slater, D.M. Zarro, S.L. Freedman, K.L. Smith, and K.T. Strong, A.G.U. Meeting, Baltimore, MD, Abstract in EOS, 69, submitted.

APPENDIX B: FCS SPECTROSCOPIC DATA

TABLE OF CONTENTS

B.1 Introduction B–1
B.2 Key to Abbreviations B–2
B.3 1980 Spectroscopic Data B–2
B.4 1984 Spectroscopic Data B–2
B.5 1985 Spectroscopic Data B–3
B.6 1986 Spectroscopic Data B–4
B.7 1987 Spectroscopic Data B–6
B.8 1988 Spectroscopic Data B–11

B.1 INTRODUCTION

This appendix lists all of the significant FCS spectroscopic data obtained since the launch of *SMM*. The FCS suffered a failure of its prime wavelength drive during the check-out tests following the launch of *SMM*, hence all but one of these data sets have been taken on the remaining B-drive. This meant that we have had to be very cautious in the use of this system. It is a remarkable achievement to have obtained over 400 such scans since the *SMRM* (especially considering most of them have been taken in solar minimum conditions!). Each scan had to be custom designed to minimize the risk to the FCS and, hence, represents a great deal of work by the XRP instrument operations team and EOF scientists. Many of these observations would not have been possible to obtain without the cooperation of the other *SMM* experiment teams.

This list is meant as a beginner's guide to the available data. **It is not complete.** There are many engineering, calibration and low-quality (partially complete or problem) data sets not included in this list. A more detailed and comprehensive list is being prepared as part of the XRP archiving effort.

For each entry the date and time (UT) of the start of the observation are listed as well as its duration and the *GOES* classification of the event (if any) that triggered it. Then follow some important engineering data: the crystal encoder address at which the drive was located at the onset of the observation; the temperatures of the crystal drives (which is needed to determine the absolute wavelength calibration of the FCS); and a brief comment on the scientific objective of each experimental sequence.

B.2 KEY TO ABBREVIATIONS

AR	Active Region target
Atlas	λ scan over full FCS crystal address range
BP	Bright Point find algorithm used
CH	Coronal Hole target
Doy	Day of year
FL	Flare
HP	Home Position (O VIII, Ne IX, Mg XI, Si XIII, S XV, Fe XXV)
Quad	Map in 4 different soft X-ray lines
Quint	Map in 5 different soft X-ray lines
QS	Quiet Sun target
Sextet	Map in 6 different soft X-ray lines
Short atlas	Atlas over restricted λ range
Trip.	Triplet
UVSP	Uses UVSP BP
(2)	Ne IX observed in Channel 2

B.3 1980 SPECTROSCOPIC SCANS

DATE	Doy	Start Time	On Time	GOES Event	Xtal on Address	Xtal Temps. T1	T2	Comments
03 Mar 80	063	07:00:00	29:00		6367	19.44	19.09	HP Profiles
25 Aug 80	238	13:01:39	27:34		6356	15.22	15.93	HP Profiles+Atlas
23 Sep 80	267	20:14:09	10:06		6358	14.87	15.58	Line profiles in AR
05 Nov 80	310	22:28:52	15:17		6354	15.93	16.63	Ne IX trip.

B.4 1984 SPECTROSCOPIC SCANS

DATE	Doy	Start Time	On Time	GOES Event	Xtal on Address	Xtal Temps. T1	T2	Comments
28 Apr 84	119	21:53:00	59:29		6353	16.8	18.0	HP profiles in AR map
30 Apr 84	121	18:02:00	58:00	C3	6357	15.6	16.3	Ne IX trip. map (2)
02 May 84	123	22:02:00	54:00		6356	16.1	16.8	Ch 1/2 cross calibration
19 May 84	140	15:26:00	56:00		6357	15.1	15.8	Ne IX trip. map (2)
21 May 84	142	14:40:00	15:00		6358	14.5	15.4	Ne IX trip. map (2)
26 May 84	147	13:19:00	21:16	C5	6359	15.1	15.9	HP profiles in AR map
20 Sep 84	264	17:26:00	54:26		6357	17.0	17.7	HP profiles in CH

B.5 1985 SPECTROSCOPIC SCANS

DATE	Doy	Start Time	On Time	GOES Event	Xtal on Address	Xtal Temps. T1	T2	Comments
21 Jan 85	021	02:19:00	10:19	C2	6360	17.3	18.1	Mg XI trip. at FL BP
23 Jan 85	023	07:29:00	28:00	M1	6357	17.3	18.3	HP profiles at FL BP
19 Feb 85	050	18:29:00	40:00	C2	6358	17.7	18.7	HP profiles at FL BP
23 Apr 85	113	00:36:00	06:00		6356	17.0	17.7	Ne IX trip. in AR
24 Apr 85	114	01:52:00	44:00	C9	6358	17.0	17.8	Ne IX trip. at FL BP
24 Apr 85	114	09:41:00	60:00	X2	6358	17.1	18.0	Ne IX trip. at FL BP
24 Apr 85	114	23:41:00	37:00		6358	17.2	18.0	Ne IX trip. AR map
26 Apr 85	116	21:18:00	47:00		6358	17.3	18.0	Ne IX trip. AR map
27 Apr 85	117	20:54:00	34:00	C1	6359	17.3	18.0	HP profiles map
28 Apr 85	118	20:30:00	33:00	B7	6361	17.3	18.1	Ne IX trip. map at FL BP
29 Apr 85	119	20:06:00	53:00		6361	17.3	18.3	HP profiles AR map
30 Apr 85	120	18:02:00	58:00		6357	15.6	16.3	Ne IX trip. AR map
30 Apr 85	120	21:17:00	33:00		6361	17.3	18.3	Ne IX trip. map at FL BP
30 Apr 85	120	23:45:00	06:00	C2	6350	17.5	18.4	Ne IX trip. at FL BP
01 May 85	121	20:53:00	34:00		6361	17.3	18.2	Ne IX trip. AR map
02 May 85	122	20:29:00	34:00		6361	17.3	18.3	Ne IX trip. AR map
02 May 85	122	22:00:00	57:40		6356	16.1	16.8	Chan. 1/2 cross calibration
15 May 85	135	04:13:00	39:00		6361	17.0	17.7	HP profiles in AR
16 May 85	136	04:58:00	57:00		6363	17.0	17.7	HP profiles in AR
17 May 85	137	05:09:00	42:00		6361	16.5	17.3	HP+Fe XVII map
19 May 85	139	07:18:00	42:00		6364	16.8	17.5	Ne IX trip. AR map
20 May 85	140	06:54:00	42:00		6363	17.0	17.7	HP profiles
21 May 85	141	09:54:00	39:00	C4	6364	17.0	17.7	Mg XI trip. at FL BP
04 Jun 85	155	02:43:00	07:00		6365	16.9	17.3	Ne IX trip. AR map
04 Jun 85	155	10:09:00	35:00		6364	17.0	17.7	Ne IX trip. AR map
04 Jun 85	155	11:43:00	38:00		6365	17.0	18.8	Ne IX trip. AR map
06 Jun 85	157	09:19:00	26:59		6365	15.9	16.6	Ne IX trip. AR map
06 Jun 85	157	10:54:00	34:00		6366	16.3	17.3	HP profiles in AR
17 Jun 85	168	00:18:00	41:00	C2	6367	18.0	18.7	Mg XII Lα/β
02 Jul 85	183	21:15:00	30:00	M5	6367	15.9	16.6	Atlas
07 Jul 85	188	05:38:00	10:00	C3				FL DEM at BP
02 Aug 85	214	13:26:00	24:00		6366	17.7	18.4	HP profiles AR map
03 Aug 85	217	21:05:00	61:00		6365	17.3	18.4	HP+Ne IX scans in AR
03 Aug 85	217	23:02:00	61:00		6365	17.7	19.1	HP+Ne IX scans in AR
05 Aug 85	217	18:04:00	16:00		6365	17.3	18.0	HP profiles AR map
05 Aug 85	217	19:03:00	60:00		6364	17.3	18.4	HP+Ne IX scans in AR
08 Aug 85	220	21:02:00	58:00		6365	16.2	17.3	HP+Ne IX scans in AR
09 Aug 85	221	21:00:00	58:00		6365	16.6	17.3	HP+Ne IX scans in AR
24 Oct 85	297	04:51:00	57:00	C1		16.9	18.3	HP profile map at FL BP
25 Oct 85	298	01:53:00	57:00	C1	6367	16.9	17.6	HP profile map at FL BP
26 Oct 85	299	04:37:00	47:00	M2	6367	16.9	17.6	HP profile map at FL BP
27 Oct 85	300	02:38:00	57:00		6367	16.9	17.6	HP profile map at AR BP
28 Oct 85	301	02:13:00	57:00		6367	16.9	17.6	HP profile map at AR BP
29 Oct 85	302	03:22:00	57:00		6367	17.3	17.6	O/Ne Abundance
29 Oct 85	302	08:05:00	57:00		6366	17.3	18.0	Mg XII Lα/β
16 Nov 85	320	14:44:00	58:00		6368	16.9	17.6	Short atlas

B.6 1986 SPECTROSCOPIC SCANS

DATE	Doy	Start Time	On Time	GOES Event	Xtal on Address	Xtal Temps. T1	T2	Comments
01 Feb 86	032	22:08:00	57:00		6369	15.2	15.9	HP profiles at FL BP
02 Feb 86	033	21:43:00	57:00	C3	6368	14.8	15.5	HP profiles at FL BP
04 Feb 86	035	00:26:00	57:00	C1	6367	14.8	15.5	HP profiles at FL BP
04 Feb 86	035	20:52:00	63:00		6368	14.8	15.5	HP profiles at AR BP
05 Feb 86	036	20:27:00	57:00	C1	6366	14.8	15.5	HP profiles at FL BP
06 Feb 86	037	20:02:00	47:00		6366	16.2	16.9	HP profiles at AR BP
07 Feb 86	038	05:45:00	39:00	B7	6365	16.6	17.3	Short atlas
07 Feb 86	038	19:37:00	57:00	C1	6368	16.9	17.6	HP profile map at FL BP
08 Feb 86	039	19:12:00	57:00		6366	16.9	17.6	HP profile map at AR BP
13 Feb 86	044	04:48:00	40:00	C7	6366	16.9	18.0	Atlas
13 Feb 86	044	17:21:00	11:00	C2	6367	17.3	18.0	Atlas
14 Feb 86	045	04:23:00	40:00		6368	17.3	18.0	Short atlas
15 Feb 86	046	03:41:00	57:00	C9	6369	17.3	18.0	HP profile map at FL BP
27 Feb 86	058	00:11:00	58:00		6369	17.6	18.3	Atlas
03 Mar 86	062	12:52:00	50:00	M1	6371	17.3	18.0	Mg XII Lα at FL BP
03 Mar 86	062	14:24:00	53:00	C5	6372	17.3	18.7	Atlas
03 Mar 86	062	20:35:00	41:00		6373	17.3	18.3	Ne IX trip. map at FL BP
04 Mar 86	063	23:19:00	41:00		1078	16.9	18.0	Ne IX trip. map at FL BP
07 Mar 86	066	00:07:00	37:00	C2	6374	16.9	17.6	Fe Kα at FL BP
28 Apr 86	118	03:15:00	40:00		6374	16.6	17.3	Ne IX trip. AR map
18 May 86	138	20:02:00	56:00		6375	16.6	17.3	Short atlas
20 May 86	140	00:19:00	53:00		6377	16.9	17.6	Short atlas
21 May 86	141	14:02:00	53:00		6380	16.9	17.6	Short atlas
22 May 86	142	02:36:00	57:00		6381	16.6	17.3	HP+Fe XVII map in FL
23 May 86	143	02:11:00	52:00		6379	16.6	17.6	Short atlas
24 May 86	144	04:54:00	52:00		6381	16.9	17.3	Short atlas
24 May 86	144	17:28:00	53:00		2322	16.9	17.6	HP+Fe XVII AR map
25 May 86	145	21:59:00	53:00		2307	16.9	17.6	Fe Kα/β at FL BP
08 Jul 86	189	01:34:00	57:00		2308	16.6	17.3	DEM at QS BP
10 Jul 86	190	18:07:00			2309	16.6	17.3	Atlas
11 Jul 86	192	05:10:00	47:00	C1	2310	16.6	17.3	Atlas
13 Jul 86	194	01:08:00	49:00		2300	16.6	17.3	Atlas
13 Jul 86	194	02:42:00	49:00	C1	2306	16.9	18.0	Atlas
13 Jul 86	194	04:16:00	49:00	C2	2309	17.3	18.3	Atlas
14 Jul 86	195	00:49:00	49:00	C1	2303	16.9	17.6	Atlas
14 Jul 86	195	02:16:00	50:00	C1	2302	16.9	18.0	Atlas
14 Jul 86	195	14:51:00	49:00		2297	16.9	17.6	Atlas
30 Aug 86	242	15:10:00	53:00		2283	16.6	17.6	HP+Fe XVII profiles
08 Oct 86	281	18:57:00	57:00		2284	16.6	16.9	HP+Fe XVII AR map
09 Oct 86	282	18:31:00	58:00		4338	16.6	17.3	HP+Fe XVII AR map
10 Oct 86	283	19:40:00	58:00		4338	16.9	17.6	HP+Fe XVII AR map
13 Oct 86	286	18:23:00	59:00		4355	17.3	18.0	HP+Fe XVII AR map
14 Oct 86	287	14:49:00	59:00	C2	4352	17.3	18.0	HP+Fe XVII FL map
16 Oct 86	289	15:33:00	59:00	C3	4351	17.3	18.3	HP+Fe XVII FL map
16 Oct 86	289	22:05:00	34:00	C1	4351	17.6	18.3	Mg XII Lα
17 Oct 86	290	05:50:00	51:00		4352	17.6	18.3	Atlas

1986 SPECTROSCOPIC SCANS (continued)

DATE	Doy	Start Time	On Time	GOES Event	Xtal on Address	Xtal Temps. T1	T2	Comments
17 Oct 86	290	15:08:00	59:00		4355	17.6	18.3	HP+Fe XVII scans at BP
18 Oct 86	291	14:43:00	59:00		4354	17.6	18.3	HP+Fe XVII scans at BP
19 Oct 86	292	01:49:00	56:00	M5	4353	17.6	18.3	Atlas
19 Oct 86	292	03:24:00	58:00	M5	4357	17.6	18.7	Atlas
19 Oct 86	292	04:58:00	52:00	M5	4359	17.6	19.0	Atlas
19 Oct 86	292	14:18:00	58:00		4360	17.6	18.3	HP+Fe XVII AR map
20 Oct 86	293	13:52:00	59:00		4358	17.3	18.3	HP+Fe XVII AR map
21 Oct 86	294	13:27:00	58:00		4358	17.3	18.0	HP+Fe XVII AR map
22 Oct 86	295	19:19:00						HP+Fe XVII AR map
22 Oct 86	295	20:53:00						HP+Fe XVII AR map
23 Oct 86	296	14:10:00	58:00		4358	17.3	18.0	HP+Fe XVII AR map
23 Oct 86	296	23:36:00			4358	17.3	18.0	HP+Fe XVII AR map
24 Oct 86	297	01:29:00	39:00		4359	17.6	18.3	HP profiles (UVSP)
24 Oct 86	297	05:59:00	51:00		4358	17.3	18.3	Atlas
24 Oct 86	297	12:40:00	38:00	C1	4361	17.3	18.3	Atlas
26 Oct 86	299	03:28:00	54:00		4363	16.9	18.0	HP+Fe XVII AR map
27 Oct 86	300	03:02:00	56:00		4362	17.3	18.0	HP+Fe XVII AR map
28 Oct 86	301	02:36:00	57:00		4362	17.3	18.0	HP+Fe XVII AR map
29 Oct 86	302	02:10:00	57:00		4362	16.9	18.0	HP+Fe XVII AR map
30 Oct 86	303	01:44:00	57:00		4362	16.9	17.6	HP+Fe XVII AR map
30 Oct 86	303	09:55:00	37:00	C1	4362	17.3	17.6	Atlas
31 Oct 86	304	01:19:00	56:00		4364	16.9	18.0	HP+Fe XVII AR map
06 Nov 86	310	05:38:00	19:00	C1	4363	16.9	17.6	Fe Kα/β

B.7 1987 SPECTROSCOPIC SCANS

DATE	Doy	Start Time	On Time	GOES Event	Xtal on Address	Xtal Temps. T1	T2	Comments
23 Jan 87	023	23:45:04	21:09	C1	4364	14.52	15.22	Fe Kα/β
05 Apr 87	095	19:35:03	09:01	M1	6333	15.58	16.28	Fe Kα/β
06 Apr 87	096	04:29:35	40:00	C9	6334	15.58	16.28	Short atlas
07 Apr 87	097	18:48:40	02:44	C1	6333	16.28	16.98	HP Line Profiles
07 Apr 87	097	19:29:13	55:10		2301	16.28	17.33	HP+Fe XVII AR map
08 Apr 87	098	17:28:41	56:15		2298	16.98	18.04	HP+Fe XVII AR map
08 Apr 87	098	21:21:36	11:53	C1	2295	16.98	17.69	Mg XI/Ne IX trip.(UVSP)
09 Apr 87	099	17:02:21	55:17		2293	16.63	17.33	HP+Fe XVII AR map
09 Apr 87	099	18:36:33	55:26		2299	17.33	18.39	HP+Fe XVII AR map
09 Apr 87	099	21:45:06	55:18		2297	16.98	18.04	Short atlas
10 Apr 87	100	18:10:13	55:18		2296	16.98	17.69	HP+Fe XVII AR map
10 Apr 87	100	19:44:50	55:02		2295	17.33	18.39	HP Scans+Fe XVII map
10 Apr 87	100	21:18:46	55:17		2301	17.33	18.74	Short atlas
11 Apr 87	101	16:09:41	55:26		2298	16.98	17.69	HP+Fe XVII AR map
11 Apr 87	101	19:18:06	55:34		2296	17.33	18.04	Quad map HP/Ne IX/Fe XVII
11 Apr 87	101	22:26:39	55:26		2299	17.33	18.04	Short atlas
12 Apr 87	102	15:43:21	55:34		2299	16.98	17.69	HP+Fe XVII AR map
12 Apr 87	102	18:51:46	55:42		2297	17.33	18.04	Quad map HP/Ne IX/Fe XVII
13 Apr 87	103	01:08:52	55:34		2300	17.33	18.04	Short atlas
13 Apr 87	103	18:25:34	55:42		2300	16.98	18.04	HP+Fe XVII AR map
14 Apr 87	104	14:50:57	55:43		2301	16.98	17.69	Short atlas
14 Apr 87	104	17:59:22	55:34		2302	17.33	18.04	HP+Fe XVII AR map
15 Apr 87	105	00:17:42	54:37		2304	17.33	18.04	Quad map HP/Fe XVII
15 Apr 87	105	02:32:28	14:04	C2	2304	17.33	18.39	Mg XI/Ne IX trip.(UVSP)
15 Apr 87	105	11:50:29	20:26	C4	2302	16.98	18.04	HP profiles (UVSP)
15 Apr 87	105	12:48:06	58:16	C4	2302	17.33	18.39	HP profiles (UVSP)
15 Apr 87	105	15:58:58	55:51		4753	17.33	18.39	Short atlas
15 Apr 87	105	17:33:11	55:50		2304	17.68	18.74	Quad map HP/Fe XVII/Ne IX
15 Apr 87	105	20:40:14	54:12	C2	2303	17.69	18.74	Mg XI/Ne IX trip.(UVSP)
15 Apr 87	105	22:18:56	52:59	B5	2305	17.69	19.09	Atlas
15 Apr 87	105	23:45:00	32:27		2306	18.04	19.44	HP profiles (UVSP)
16 Apr 87	106	07:56:29	31:22	C1	2303	16.98	18.04	Atlas
16 Apr 87	106	17:12:27	50:39	C7	2303	16.63	17.33	Atlas
16 Apr 87	106	18:46:47	31:08	C7	2306	16.98	18.04	Atlas
17 Apr 87	107	02:37:58	50:47	C2	2304	16.63	17.33	Atlas
17 Apr 87	107	17:26:15	10:47	C2	2304	16.98	17.69	Atlas
17 Apr 87	107	19:54:56	43:17	C1	2304	16.98	17.69	Atlas
17 Apr 87	107	23:39:16	11:11	C5	2304	16.98	17.69	Atlas
18 Apr 87	108	02:06:43	55:51		2304	16.98	17.69	HP+Fe XVII AR map
18 Apr 87	108	05:23:03	48:04	C2	2299	17.33	18.04	Atlas
18 Apr 87	108	13:56:41	06:06	C4	2304	17.33	18.39	Atlas
18 Apr 87	108	16:15:00	55:59		2304	17.33	18.04	HP+Fe XVII AR map
18 Apr 87	108	21:32:10	13:06	C2	2297	17.33	18.04	S XV map+Atlas
18 Apr 87	108	22:31:58	50:23		2303	17.33	18.39	Short atlas
19 Apr 87	109	14:41:30	29:04	C2	2303	16.98	17.69	Atlas
19 Apr 87	109	15:48:48	55:59		2304	17.33	18.39	Short atlas

1987 SPECTROSCOPIC SCANS (continued)

DATE	Doy	Start Time	On Time	GOES Event	Xtal on Address	Xtal Temps. T1	T2	Comments
20 Apr 87	110	01:14:28	55:50		2301	16.98	18.04	Short atlas
20 Apr 87	110	04:23:01	55:50		2302	17.33	18.04	HP+Fe XVII AR map
15 May 87	135	02:51:44	61:02		2301	17.33	18.04	Ne IX trip. map
16 May 87	136	11:12:58	05:03	C2	2304	17.33	18.04	S XV map+Atlas
16 May 87	136	16:34:55	19:31		2301	17.33	18.04	Ne IX trip. map
19 May 87	139	12:53:47	13:23	C3	2301	16.98	17.69	S XV map+Atlas
21 May 87	141	19:13:23	51:12	C2	2301	16.63	17.69	Atlas
22 May 87	142	12:57:40	23:49	C5	2302	16.63	17.33	Atlas
22 May 87	142	20:21:16	50:55	B8	2302	16.63	17.33	Atlas
24 May 87	144	09:06:49	12:34	C2	2303	16.63	17.33	Mg XI/Ne IX trip.(UVSP)
24 May 87	144	15:21:28	14:45	M1	2302	16.63	17.33	HP profiles (UVSP)
24 May 87	144	17:59:10	45:28	C2	2302	16.98	16.69	Mg XI/Ne IX trip.(UVSP)
24 May 87	144	21:12:38	41:35	C3	2303	16.98	17.69	HP profiles (UVSP)
25 May 87	145	05:04:21	39:52	C2	2303	16.98	17.69	HP profiles (UVSP)
25 May 87	145	16:14:36	29:13	C4	2303	16.98	17.33	Mg XI/Ne IX trip.(UVSP)
25 May 87	145	18:55:34	56:40		2303	16.98	17.69	Ne IX trip. map
26 May 87	146	01:12:34	56:40		2304	16.98	17.69	HP+Fe XVII AR map
26 May 87	146	17:20:01	31:24	C3	2304	16.63	17.69	Mg IX/Ne IX trip.(UVSP)
26 May 87	146	20:09:35	50:15	C8	2304	16.98	17.69	Atlas
26 May 87	146	23:11:52	56:23	C3	2305	16.98	18.04	HP+Fe XVII AR map
27 May 87	147	00:46:04	56:32	C2	2305	17.33	18.74	Mg XI/Ne IX trip.(UVSP)
27 May 87	147	16:28:26	56:21		2305	16.98	17.69	HP+Fe XVII AR map
27 May 87	147	19:36:51	56:23		2305	17.33	18.04	Ne IX trip. map+Atlas
28 May 87	148	16:01:49	57:28		2305	16.63	17.33	HP+Fe XVII AR map
28 May 87	148	19:10:22	56:24		2306	16.98	18.04	Ne IX trip. map+Atlas
28 May 87	148	23:53:00	56:23		2306	16.98	17.69	AR Poly map+Ne IX scan
29 May 87	149	02:17:35	06:01	C2	2307	17.33	18.39	S XV map+Atlas
29 May 87	149	16:18:22	13:22	B9	2305	16.63	17.33	S XV map+Atlas
29 May 87	149	18:43:46	56:32		2305	16.98	17.69	HP+Fe XVII AR map
29 May 87	149	21:52:19	56:24		2306	16.98	18.04	Poly map+Ne IX scan
10 Jun 87	161	14:59:56	56:32		2306	16.63	17.33	Quint AR map
10 Jun 87	161	16:34:17	35:14		2307	16.98	18.04	HP+Fe XVII+Ne IX map
11 Jun 87	162	02:25:20	30:35	C5	2305	16.63	17.33	Mg XI/Ne IX trip. (FCS)
11 Jun 87	162	23:58:35	56:42		2305	16.63	17.33	Quint AR map
13 Jun 87	164	01:06:11	56:24		2306	16.63	17.33	Quint AR map
13 Jun 87	164	02:40:24	56:31		2304	16.98	18.04	Quint AR map
14 Jun 87	165	11:38:46	56:56		2306	16.63	17.33	Quint AR map
15 Jun 87	166	03:20:51	57:04		2306	16.63	17.33	Quint AR map
16 Jun 87	167	02:53:58	57:29		2305	16.98	17.33	Quint AR map
17 Jun 87	168	08:45:25	56:32		2304	15.58	16.28	Quint AR map
18 Jun 87	169	03:34:33	58:18		2305	15.93	16.63	Sextet AR map
19 Jun 87	170	04:42:01	57:51		2306	16.28	16.98	Sextet AR map
23 Jun 87	174	20:22:41	31:40		2304	17.33	18.04	Sextet AR map
24 Jun 87	175	02:29:24	62:57		6341	17.33	18.39	Sextet AR map
26 Jun 87	177	22:02:38	64:10		2304	17.69	18.74	Quad AR map
26 Jun 87	177	23:37:50	64:11		2306	18.04	19.04	Quad AR map

1987 SPECTROSCOPIC SCANS (continued)

DATE	Doy	Start Time	On Time	GOES Event	Xtal on Address	Xtal Temps. T1	T2	Comments
27 Jun 87	178	21:38:15	64:45		2305	17.69	18.39	Quad AR map
27 Jun 87	178	23:12:36	63:56		2306	18.04	19.44	Quad AR map
28 Jun 87	179	00:46:48	64:02		2307	18.39	19.80	Quad AR map
28 Jun 87	179	00:02:21	64:02		2307	18.39	19.80	Ne IX trip. map
23 Jul 87	204	09:22:25	14:29	C3	6342	16.63	17.69	Fe Kα/β
23 Jul 87	204	18:15:35	30:43	C3	6341	16.63	17.33	Fe Kα/β
24 Jul 87	205	00:35:09	43:58	C2	6341	16.63	17.33	Fe Kα/β
24 Jul 87	205	09:56:43	47:47	M3	6342	16.98	17.33	Fe Kα/β
27 Jul 87	208	18:11:34	17:04	M3	6342	16.63	17.33	S XV map+Atlas
07 Aug 87	219	15:26:58	06:17	C5	6342	16.98	17.33	S XV map+Atlas
07 Aug 87	219	17:04:52	02:44	C9	6342	16.98	17.69	S XV map+Atlas
07 Aug 87	219	19:44:37	08:44	M1	6342	16.98	17.69	S XV map+Atlas
08 Aug 87	220	01:32:05	61:10	M1	6342	16.98	17.69	S XV map+Atlas
08 Aug 87	220	03:35:06	32:30	M1	6344	17.33	18.39	S XV map+Atlas
08 Aug 87	220	14:05:54	18:58	M1	6344	16.98	18.04	S XV map+Atlas
08 Aug 87	220	20:43:20	21:27	C1	6345	16.98	17.69	S XV map+Atlas
08 Aug 87	220	22:22:44	21:51	C3	6345	17.33	18.04	S XV map+Atlas
09 Aug 87	221	06:21:58	28:16	C1	6344	17.33	18.04	S XV map+Atlas
10 Aug 87	222	22:05:42	01:22	C4	6346	17.33	18.04	S XV map+Atlas
11 Aug 87	223	11:16:31	05:44	C3	6347	16.98	17.69	S XV map+Atlas
13 Aug 87	225	15:58:29	07:56	C4	6347	16.98	18.04	Fe XXV Ion Equilibrium
23 Aug 87	235	23:15:19	57:53	M1	6345	16.28	17.23	Fe XXV Ion Equilibrium
05 Sep 87	248	00:19:18	50:31	C3	6346	16.98	17.69	Fe XXV Ion Equilibrium
07 Sep 87	250	07:37:04	30:43	C3	6347	16.98	17.69	Fe XXV Ion Equilibrium
07 Sep 87	250	12:02:21	48:11	C3	6348	16.98	17.69	Fe XXV Ion Equilibrium
08 Sep 87	251	08:41:15	34:16	C2	6348	16.98	17.69	Fe XXV Ion Equilibrium
15 Oct 87	287	11:10:30	23:53	C5	6348	16.98	17.69	Fe XXV Ion Equilibrium
02 Nov 87	306	18:16:25	29:29	C8	6356	17.33	17.69	HP Poly map
04 Nov 87	308	17:22:06	25:57	M2	6349	16.98	18.04	S XV map+Atlas
04 Nov 87	308	23:38:56	50:39	M2	6349	16.98	18.04	S XV map+Atlas
05 Nov 87	309	04:57:20	21:26	M3	6356	16.98	18.04	S XV map+Atlas
12 Nov 87	316	20:34:21	03:17	C2	6350	16.98	17.69	Atlas (UVSP)
18 Nov 87	322	03:17:21	50:23	M1	6350	16.28	16.98	Atlas (UVSP)
20 Nov 87	324	04:14:36	32:10	M1	6351	16.98	17.69	HP Profiles+Atlas
20 Nov 87	324	23:33:14	03:57	M1	6350	16.98	17.69	HP Profiles+Atlas
21 Nov 87	325	00:14:03	57:21	M1	6349	16.98	18.04	HP Profiles+Atlas
21 Nov 87	325	17:58:11	29:05	M4	6350	17.33	18.04	HP Profiles+Atlas
26 Nov 87	330	03:18:03	18:51	C4	6348	17.33	18.04	Mg XI/ Ne IX trip.
27 Nov 87	331	00:38:28	57:04		6350	17.33	18.04	Quint map
27 Nov 87	331	14:45:47	57:21		2306	17.33	18.39	AR scans
27 Nov 87	331	16:20:00	57:21		2308	17.69	18.74	Short atlas
28 Nov 87	332	15:52:26	57:58		2307	17.69	18.39	Quint map
28 Nov 87	332	20:34:56	58:09		2307	17.69	18.74	Quint map
28 Nov 87	332	22:09:00	58:18		2308	18.04	19.09	Quint map
29 Nov 87	333	01:17:17	58:18		2307	18.04	19.09	AR Scans
29 Nov 87	333	13:50:40	58:35		2307	17.69	18.74	Short atlas

1987 SPECTROSCOPIC SCANS (continued)

DATE	Doy	Start Time	On Time	GOES Event	Xtal on Address	Xtal Temps. T1	T2	Comments
29 Nov 87	333	15:24:44	58:51		2308	18.39	19.80	AR Scans
29 Nov 87	333	16:58:57	58:55		2308	18.39	19.44	Quint map
29 Nov 87	333	20:07:22	58:51		2308	18.04	19.44	Short atlas
30 Nov 87	334	14:57:27	59:16		2307	17.69	18.74	Quint map
30 Nov 87	334	19:39:56	59:32		2307	18.04	19.09	Short atlas
01 Dec 87	335	16:04:14	60:13		2308	17.69	18.74	Quint map of AR
01 Dec 87	335	20:46:43	60:30		0848	18.04	19.09	Short atlas
02 Dec 87	336	17:08:26	63:28		2304	18.04	19.09	Quint map of AR
02 Dec 87	336	21:53:47	61:01		2308	18.04	19.09	Short atlas
04 Dec 87	338	03:03:45	62:16		2308	18.04	18.74	Quint map of AR
04 Dec 87	338	11:34:55	62:24		2308	17.69	18.39	Short atlas
04 Dec 87	338	14:43:20	62:32		2309	18.04	18.74	Quint map of AR
04 Dec 87	338	19:26:05	55:00		2309	18.04	19.09	Quint map of AR
05 Dec 87	339	00:08:35	62:48		2308	18.39	19.09	Quint map of AR
05 Dec 87	339	01:42:47	62:49		2309	18.39	19.80	Quint map of AR
05 Dec 87	339	15:50:56	62:00		2308	18.39	19.09	Short atlas
06 Dec 87	340	12:16:11	62:57		2309	18.39	19.09	AR scan map
06 Dec 87	340	16:58:48	63:05		2309	18.74	19.44	Short atlas
07 Dec 87	341	10:15:30	62:27		0858	18.39	19.09	Short atlas
07 Dec 87	341	14:58:16	63:00		2310	18.74	19.09	Short atlas
08 Dec 87	342	03:32:20	62:32		2310	18.39	19.44	Short atlas
08 Dec 87	342	09:49:27	62:14		2310	18.39	19.44	Short atlas
08 Dec 87	342	16:06:25	62:07		2311	18.74	19.44	Short atlas
09 Dec 87	343	03:06:09	61:59		2311	18.39	19.44	Short atlas
09 Dec 87	343	07:48:54	61:43		2311	18.39	19.44	Short atlas
10 Dec 87	344	02:39:57	61:02		2311	18.39	19.09	Short atlas
10 Dec 87	344	10:31:08	60:45		2311	18.39	19.09	Short atlas
10 Dec 87	344	13:39:33	60:45		2312	18.39	19.44	Quint map of AR
10 Dec 87	344	23:04:56	47:31		2311	18.39	19.09	AR scan map
11 Dec 87	345	02:13:29	60:13		2310	18.39	19.44	Short atlas
11 Dec 87	345	10:04:40	59:56		2312	18.39	19.09	Short atlas
11 Dec 87	345	13:13:13	59:40		2312	18.39	19.44	Quint map of AR
11 Dec 87	345	17:55:42	35:40		2311	18.39	19.44	Quint map of AR
11 Dec 87	345	19:29:54	37:57		2311	18.74	19.80	AR line profiles
12 Dec 87	346	00:12:32	52:01		2310	18.39	19.44	AR scan map
12 Dec 87	346	14:20:24	59:16		2310	17.33	18.39	Quint map of AR
13 Dec 87	347	02:54:04	58:51		2311	17.33	18.39	AR scan map
13 Dec 87	347	09:10:54	58:35		2310	17.69	18.39	Short atlas
13 Dec 87	347	13:53:32	58:26		2311	17.69	18.74	AR scan map
14 Dec 87	348	02:27:11	58:00		2310	17.69	18.39	Quint map of AR
14 Dec 87	348	04:23:06	36:44	C9	2311	18.04	19.09	Mg XI/Ne IX trip. at FL BP
14 Dec 87	348	08:44:01	57:43		2310	18.04	18.74	Short atlas
14 Dec 87	348	13:26:39	57:38		2311	18.04	18.74	Quint map of AR
15 Dec 87	349	03:34:15	57:29		2310	17.69	18.74	Short atlas
15 Dec 87	349	08:16:44	60:00		2311	18.04	18.74	Short atlas
16 Dec 87	350	03:06:58	57:06		2311	17.69	18.39	Quint map of AR

1987 SPECTROSCOPIC SCANS (continued)

DATE	Doy	Start Time	On Time	GOES Event	Xtal on Address	Xtal Temps. T1	T2	Comments
16 Dec 87	350	07:49:27	57:04		2311	17.69	18.74	Short atlas
16 Dec 87	350	12:32:04	56:48		2311	17.69	18.74	AR scan map
17 Dec 87	351	12:04:39	56:31		2311	17.69	18.39	AR scan map
18 Dec 87	352	03:46:19	56:23		2311	17.69	18.39	Short atlas
18 Dec 87	352	06:54:36	56:23		2311	17.69	18.74	AR line profile map
18 Dec 87	352	11:37:05	56:23		2311	17.69	18.74	Quint map of AR
18 Dec 87	352	22:36:16	48:14		2311	17.69	18.39	Quint map of AR
19 Dec 87	353	01:44:33	56:15		2311	17.69	18.74	Quint map of AR
19 Dec 87	353	11:09:40	56:07		2311	17.69	18.39	AR scan map
20 Dec 87	354	02:51:12	55:59		2311	17.69	18.39	Quint map of AR
20 Dec 87	354	05:56:45	91:20		2304	18.04	19.09	Quint map of AR
20 Dec 87	354	09:07:54	55:58		2310	18.04	19.09	Short atlas

B.8 1988 SPECTROSCOPIC SCANS

DATE	Doy	Start Time	On Time	GOES Event	Xtal on Address	Xtal Temps. T1	T2	Comments
02 Jan 88	002	21:57:38	58:38	X1	6346	16.98	17.69	FL Atlas (UVSP)
02 Jan 88	002	23:31:51	58:37	X1	6349	17.69	18.74	FL Atlas (UVSP)
03 Jan 88	003	01:06:03	57:29	X1	6349	17.69	19.09	FL Atlas (UVSP)
26 Jan 88	026	11:09:25	50:29	C6	6350	17.33	18.39	FL Atlas (UVSP)
27 Jan 88	027	23:06:39	46:25	C5	6350	17.69	18.39	FL Atlas (UVSP)
28 Jan 88	028	06:07:02	14:45	C7	6350	17.69	18.39	FL Atlas (UVSP)
28 Jan 88	028	08:48:00	42:04	C9	6350	17.69	18.39	FL Atlas (UVSP)
29 Jan 88	029	14:31:16	00:18		6351	17.33	18.04	FL Atlas (UVSP)
20 Feb 88	050	04:15:14	48:27	M1	6351	16.98	17.69	FL Atlas (UVSP)
12 Mar 88	072	04:25:27	00:16	C7	6351	16.98	18.04	FL Ar XVII (UVSP)
12 Mar 88	072	15:16:18	00:24	C6	6350	17.33	18.04	FL Ar XVII (UVSP)
14 Mar 88	074	08:16:06	00:10	C9	6350	16.98	17.69	FL Ar XVII (UVSP)
15 Mar 88	075	21:10:40	00:40	M4	6350	16.28	16.98	FL Ar XVII (UVSP)
16 Mar 88	076	00:56:21	00:15	C4	6351	16.28	17.33	FL Ar XVII (UVSP)
16 Mar 88	076	01:56:10	00:30	C8	6351	16.28	17.33	FL Ar XVII (UVSP)
16 Mar 88	076	04:19:39	00:04	M1	6350	16.63	17.69	FL Ar XVII (UVSP)
16 Mar 88	076	05:55:06	00:03	M3	6350	16.63	17.69	FL Ar XVII (UVSP)
16 Mar 88	076	09:46:56	00:43	M1	6350	16.63	17.33	FL Ar XVII (UVSP)
16 Mar 88	076	19:36:21	00:06	M9	6349	16.98	17.69	FL Ar XVII (UVSP)
16 Mar 88	076	20:55:40	00:25	C4	6350	16.98	17.69	FL Ar XVII (UVSP)
16 Mar 88	076	22:36:50	00:25	C6	6350	16.98	17.69	FL Atlas (UVSP)
17 Mar 88	077	02:08:12	00:13	C3	6349	16.98	17.69	FL Atlas (UVSP)
17 Mar 88	077	03:23:21	00:32	C3	6350	17.33	18.04	FL Atlas (UVSP)
17 Mar 88	077	04:32:39	00:57	C8	6351	17.33	18.39	FL Atlas (UVSP)
17 Mar 88	077	17:28:01	00:07	C2	6350	16.98	17.69	FL Atlas (UVSP)
17 Mar 88	077	18:48:02	00:24	C2	6350	16.98	17.69	FL Atlas (UVSP)
17 Mar 88	077	20:48:11	00:02	C1	6350	16.98	18.04	FL Atlas (UVSP)
17 Mar 88	077	22:27:18	00:04	C5	6351	16.98	18.04	FL Atlas (UVSP)
17 Mar 88	077	23:44:02	00:28	C3	6350	16.98	17.69	FL Atlas (UVSP)
09 Apr 88	101	21:18:47	00:01	C6	6350	16.28	16.98	FL S XV
13 Apr 88	104	18:33:31	00:51	C5	6349	16.63	17.33	FL S XV
14 Apr 88	105	19:39:29	00:50	X1	6350	16.98	17.69	FL S XV (UVSP)
15 Apr 88	106	21:14:48	00:20	M2	6350	16.98	17.69	FL S XV
16 Apr 88	107	22:13:07	00:27	M1	6198	16.98	17.69	FL S XV
17 Apr 88	108	01:04:12	00:44	C6	6350	16.98	17.69	FL S XV
17 Apr 88	108	04:30:13	00:27	M1	6350	16.98	18.04	FL S XV
17 Apr 88	108	22:06:27	00:05	C8	6197	16.63	17.69	FL S XV
18 Apr 88	109	04:12:46	00:16	C5	6349	16.98	17.69	FL S XV
18 Apr 88	109	05:21:27		M1	6350	16.98	17.69	FL S XV
20 Apr 88	111	10:35:14	00:46	M1	6350	16.98	17.69	FL S XV
21 Apr 88	111	10:04:32	00:48	M2	6349	16.63	17.69	FL S XV
22 Apr 88	113	14:12:46	00:54	M1	6349	16.63	17.69	FL S XV
24 Apr 88	115	01:14:50	00:21	M1	6349	16.98	17.69	FL S XV

APPENDIX C: XRP FLARE CATALOGUE

TABLE OF CONTENTS

C.1 Introduction C–1
C.2 1984 Flare listing C–2
C.3 1985 Flare listing C–4
C.4 1986 Flare listing C–6
C.5 1987 Flare listing C–7
C.6 1988 Flare listing C–9

C.1 INTRODUCTION

The following listings contain all the flare events observed by the Bent Crystal Spectrometer (BCS) at a count rate exceeding 50 cnts/s in its Ca XIX channel (which is approximately equivalent to an *GOES* class C1 event). As the field of view of the BCS is only 6 arcmin and the duty cycle of the *SMM* spacecraft is about 60 percent (allowing for spacecraft night and SAA passage) it means that this can not be a comprehensive list of all such events on the Sun. However, the fact that it was observed by the BCS implies that the *SMM* was looking at the active region that produced the flare. It is probable, therefore, that the Flat Crystal Spectrometer (FCS) will either have images and/or spectra of these events. For more comprehensive information on what all the other *SMM* instruments observed throughout this period (1984–1988) one should refer to the *SMM* Flare Catalogue which is being prepared at the EOF by the NOAA team.

The start, stop and peak Ca XIX flux times are all measured in Universal Time and are **determined from the BCS data only**, hence may not agree with the actual times from *GOES*. This can be the result of a number of reasons:

(1) The flare started, peaked, or ended during spacecraft night.

(2) The observation was interrupted by SAA passage.

(3) The flare was either very soft (cool) or very hard (hot), hence, the response to it would have been different in the two instruments.

(4) If different regions flare at the same time their lightcurves are superimposed in the *GOES* instrument, and as it has no spatial information the timing can be misleading.

(5) The fundamental integration time is different for BCS and *GOES*.

C.2 1984 XRP Flare Listing

Event #	Event Start Time (U.T.)	Date	Event Stop Time (U.T.)	Date	Peak Ca XIX Cts/s	(U.T.)
411502	23:53	24 Apr 84	08:15	25 Apr 84	8220	00:22
411632	06:00	25 Apr 84	06:10	25 Apr 84	82	06:05
411613	11:00	25 Apr 84	11:25	25 Apr 84	64	11:07
411631	15:08	25 Apr 84	15:11	25 Apr 84	64	15:09
411614	17:43	25 Apr 84	19:10	25 Apr 84	148	18:19
411714	05:19	26 Apr 84	05:30	26 Apr 84	126	00:00
411732	05:30	26 Apr 84	06:19	26 Apr 84	178	05:40
411716	07:16	26 Apr 84	07:45	26 Apr 84	122	07:16
411719	08:57	26 Apr 84	09:28	26 Apr 84	1788	09:03
411721	11:37	26 Apr 84	12:37	26 Apr 84	54	12:20
411731	13:11	26 Apr 84	14:12	26 Apr 84	668	13:11
411811	05:34	27 Apr 84	05:55	27 Apr 84	700	05:40
411815	16:43	27 Apr 84	16:58	27 Apr 84	391	16:58
411900	20:19	28 Apr 84	20:49	28 Apr 84	196	20:22
412000	02:43	29 Apr 84	02:55	29 Apr 84	341	02:50
412002	06:28	29 Apr 84	06:46	29 Apr 84	87	06:45
412012	18:49	29 Apr 84	19:16	29 Apr 84	109	18:55
412101	05:43	30 Apr 84	06:23	30 Apr 84	319	05:57
412105	11:41	30 Apr 84	12:40	30 Apr 84	477	12:13
412203	00:28	01 May 84	04:25	01 May 84	727	01:52
412201	20:45	01 May 84	21:01	01 May 84	50	20:46
412320	14:05	02 May 84	15:03	02 May 84	69	15:02
412300	16:12	02 May 84	17:28	02 May 84	417	16:17
412316	19:12	02 May 84	21:21	02 May 84	1889	19:25
412319	21:57	02 May 84	22:56	02 May 84	92	22:37
412411	03:13	03 May 84	03:31	03 May 84	403	03:18
412503	06:05	04 May 84	06:22	04 May 84	104	06:06
412508	23:33	04 May 84	23:43	04 May 84	55	23:35
412601	01:05	05 May 84	01:18	05 May 84	304	01:07
412611	18:10	05 May 84	21:24	05 May 84	6017	18:24
412700	01:43	06 May 84	01:53	06 May 84	167	01:45
412705	08:21	06 May 84	08:39	06 May 84	220	08:23
412718	16:23	06 May 84	16:28	06 May 84	202	16:25
412722	19:02	06 May 84	19:12	06 May 84	231	19:04
413009	15:29	09 May 84	16:06	09 May 84	92	15:47
413100	03:19	10 May 84	03:35	10 May 84	95	03:22
413111	15:43	10 May 84	15:59	10 May 84	143	15:53
413200	07:42	11 May 84	07:56	11 May 84	117	07:42
413210	20:34	11 May 84	21:01	11 May 84	306	20:38
413300	05:39	12 May 84	05:58	12 May 84	574	05:39
413504	18:01	14 May 84	18:17	14 May 84	116	18:16
413503	22:15	14 May 84	22:39	14 May 84	184	22:21
413602	04:55	15 May 84	05:00	15 May 84	141	04:58
413900	02:01	18 May 84	02:02	18 May 84	64	02:02
413904	05:34	18 May 84	05:39	18 May 84	95	05:35
413906	07:06	18 May 84	07:09	18 May 84	82	07:07

C.2 1984 XRP Flare Listing (continued)

Event #	Event Start Time (U.T.)	Date	Event Stop Time (U.T.)	Date	Peak Ca XIX Cts/s	(U.T.)
413908	09:33	18 May 84	10:02	18 May 84	208	09:37
413918	22:05	18 May 84	22:22	18 May 84	101	22:07
413925	23:39	18 May 84	00:06	19 May 84	70	23:47
414013	03:04	19 May 84	04:52	19 May 84	188	03:31
414029	12:28	19 May 84	12:54	19 May 84	58	12:40
414008	20:28	19 May 84	20:53	19 May 84	251	20:46
414010	21:48	19 May 84	22:30	19 May 84	7785	21:55
414134	00:51	20 May 84	01:48	20 May 84	2047	01:29
414129	02:49	20 May 84	03:23	20 May 84	3078	03:01
414100	04:00	20 May 84	04:31	20 May 84	457	04:08
414130	04:31	20 May 84	04:49	20 May 84	63	04:35
414135	05:36	20 May 84	06:31	20 May 84	3102	05:42
414131	06:15	20 May 84	06:31	20 May 84	442	06:20
414108	08:50	20 May 84	09:30	20 May 84	325	09:04
414132	15:13	20 May 84	15:30	20 May 84	551	15:16
414133	19:45	20 May 84	20:27	20 May 84	139	19:45
414121	21:53	20 May 84	21:59	20 May 84	407	21:53
414124	22:53	20 May 84	00:41	21 May 84	4672	22:53
414200	02:21	21 May 84	02:21	21 May 84	77	02:21
414202	13:26	21 May 84	13:57	21 May 84	87	13:32
414207	16:12	21 May 84	16:52	21 May 84	165	16:25
414208	17:46	21 May 84	18:27	21 May 84	1113	18:10
414216	19:21	21 May 84	20:03	21 May 84	205	20:01
414209	20:55	21 May 84	23:19	21 May 84	532	20:56
414320	06:22	22 May 84	07:00	22 May 84	850	06:38
414329	09:31	22 May 84	09:42	22 May 84	95	09:31
414332	11:12	22 May 84	11:17	22 May 84	145	11:14
414334	14:52	22 May 84	16:22	22 May 84	3152	15:01
414400	02:57	23 May 84	03:02	23 May 84	58	02:58
414413	04:51	23 May 84	05:22	23 May 84	1409	05:12
414406	12:16	23 May 84	12:32	23 May 84	121	12:20
414414	23:32	23 May 84	00:11	24 May 84	137	23:50
414504	12:47	24 May 84	12:50	24 May 84	62	12:49
414600	04:22	25 May 84	04:31	25 May 84	115	04:26
414602	14:57	25 May 84	15:12	25 May 84	89	15:02
414604	21:29	25 May 84	21:40	25 May 84	152	21:32
414703	13:16	26 May 84	13:38	26 May 84	170	13:23
416603	14:52	14 Jun 84	15:02	14 Jun 84	70	14:55
416606	20:14	14 Jun 84	20:25	14 Jun 84	252	20:14
418700	15:08	05 Jul 84	15:29	05 Jul 84	91	15:16
423107	22:41	18 Aug 84	23:00	18 Aug 84	400	22:47
423106	22:59	18 Aug 84	23:22	18 Aug 84	949	23:05
425200	23:57	08 Sep 84	00:05	09 Sep 84	125	00:00
431503	20:02	10 Nov 84	21:18	10 Nov 84	1748	20:07
431700	10:28	12 Nov 84	11:00	12 Nov 84	130	10:29
433200	02:18	27 Nov 84	02:26	27 Nov 84	139	02:21

C.2 1984 XRP Flare Listing (continued)

Event #	Event Start Time (U.T.)	Date	Event Stop Time (U.T.)	Date	Peak Ca XIX Cts/s	(U.T.)
433201	04:50	27 Nov 84	05:10	27 Nov 84	69	04:52
433206	06:22	27 Nov 84	06:41	27 Nov 84	134	06:30
433208	10:54	27 Nov 84	11:27	27 Nov 84	586	10:58
433300	01:04	28 Nov 84	01:32	28 Nov 84	186	01:04

C.3 1985 XRP Flare Listing

Event #	Event Start Time (U.T.)	Date	Event Stop Time (U.T.)	Date	Peak Ca XIX Cts/s	(U.T.)
501500	19:38	15 Jan 85	20:11	15 Jan 85	79	19:39
502000	20:45	20 Jan 85	21:25	20 Jan 85	2882	20:52
502134	00:05	21 Jan 85	00:18	21 Jan 85	63	00:12
502132	02:10	21 Jan 85	02:24	21 Jan 85	80	02:19
502139	03:17	21 Jan 85	04:00	21 Jan 85	1489	03:52
502140	04:37	21 Jan 85	05:34	21 Jan 85	717	05:08
502130	07:06	21 Jan 85	07:09	21 Jan 85	67	07:08
502131	09:54	21 Jan 85	10:18	21 Jan 85	248	10:10
502123	14:04	21 Jan 85	15:01	21 Jan 85	1521	14:19
502114	15:38	21 Jan 85	15:55	21 Jan 85	70	15:38
502118	17:12	21 Jan 85	18:10	21 Jan 85	738	17:19
502144	18:47	21 Jan 85	19:18	21 Jan 85	100	19:00
502121	21:56	21 Jan 85	22:38	21 Jan 85	132	22:22
502122	23:30	21 Jan 85	00:18	22 Jan 85	8246	00:10
502200	01:04	22 Jan 85	02:02	22 Jan 85	306	01:53
502203	02:39	22 Jan 85	03:28	22 Jan 85	51	02:41
502201	11:07	22 Jan 85	11:18	22 Jan 85	98	11:07
502300	04:11	23 Jan 85	04:18	23 Jan 85	55	04:13
502303	07:25	23 Jan 85	07:55	23 Jan 85	1314	07:29
504900	23:20	18 Feb 85	23:49	18 Feb 85	263	23:27
505013	01:29	19 Feb 85	01:47	19 Feb 85	86	01:39
505000	02:22	19 Feb 85	02:35	19 Feb 85	64	02:24
505005	18:24	19 Feb 85	18:45	19 Feb 85	203	18:29
508000	22:25	21 Mar 85	22:40	21 Mar 85	91	22:29
511205	09:03	22 Apr 85	09:09	22 Apr 85	72	09:05
511209	16:39	22 Apr 85	17:03	22 Apr 85	862	16:40
511206	19:51	22 Apr 85	19:57	22 Apr 85	149	19:53
511311	10:16	23 Apr 85	10:49	23 Apr 85	71	10:27
511305	19:20	23 Apr 85	19:59	23 Apr 85	141	19:24
511313	20:54	23 Apr 85	21:39	23 Apr 85	307	21:11
511401	01:48	24 Apr 85	02:21	24 Apr 85	767	01:52
511409	03:41	24 Apr 85	04:10	24 Apr 85	107	03:51
511403	04:46	24 Apr 85	05:45	24 Apr 85	432	05:00
511404	09:29	24 Apr 85	10:28	24 Apr 85	13694	09:41
511410	11:03	24 Apr 85	12:02	24 Apr 85	657	11:04
511411	12:38	24 Apr 85	13:37	24 Apr 85	67	12:39

C.3 1985 XRP Flare Listing (continued)

Event #	Event Start Time (U.T.)	Date	Event Stop Time (U.T.)	Date	Peak Ca XIX Cts/s	(U.T.)
511413	16:06	24 Apr 85	16:46	24 Apr 85	97	16:45
511412	17:21	24 Apr 85	17:52	24 Apr 85	100	17:22
511408	20:50	24 Apr 85	22:05	24 Apr 85	57	20:57
511512	07:30	25 Apr 85	08:00	25 Apr 85	238	07:32
511509	20:40	25 Apr 85	20:47	25 Apr 85	68	20:47
511701	20:51	27 Apr 85	21:34	27 Apr 85	70	21:00
511801	22:12	28 Apr 85	22:17	28 Apr 85	288	22:13
512002	23:44	30 Apr 85	23:48	30 Apr 85	122	23:44
512104	14:32	01 May 85	14:47	01 May 85	188	14:33
512201	08:19	02 May 85	08:50	02 May 85	682	08:20
512204	09:25	02 May 85	10:26	02 May 85	56	09:26
512701	08:08	07 May 85	08:12	07 May 85	93	08:08
512704	20:01	07 May 85	20:19	07 May 85	67	20:03
513100	06:03	11 May 85	06:15	11 May 85	58	06:03
513303	10:05	13 May 85	10:23	13 May 85	111	10:05
513305	18:23	13 May 85	18:32	13 May 85	126	18:29
513400	00:12	14 May 85	00:39	14 May 85	72	00:26
513902	17:31	19 May 85	17:38	19 May 85	54	17:38
514100	09:53	21 May 85	10:00	21 May 85	520	09:54
516800	00:13	17 Jun 85	00:26	17 Jun 85	161	00:18
516802	12:06	17 Jun 85	12:09	17 Jun 85	94	12:09
518000	23:35	29 Jun 85	00:12	30 Jun 85	65	23:36
518303	21:07	02 Jul 85	21:44	02 Jul 85	3273	21:24
518304	22:21	02 Jul 85	23:18	02 Jul 85	293	22:21
518802	00:11	07 Jul 85	00:14	07 Jul 85	67	00:12
518800	05:26	07 Jul 85	05:31	07 Jul 85	155	05:28
518815	20:18	07 Jul 85	20:32	07 Jul 85	153	20:28
518913	15:58	08 Jul 85	16:07	08 Jul 85	160	16:05
519002	02:10	09 Jul 85	03:07	09 Jul 85	677	02:10
519116	10:21	10 Jul 85	10:29	10 Jul 85	73	10:23
519118	16:46	10 Jul 85	16:51	10 Jul 85	102	16:47
519200	13:56	11 Jul 85	14:03	11 Jul 85	91	13:56
519304	06:11	12 Jul 85	06:17	12 Jul 85	185	06:17
519400	06:56	13 Jul 85	07:37	13 Jul 85	126	06:59
519407	13:19	13 Jul 85	13:30	13 Jul 85	128	13:21
522000	07:43	08 Aug 85	08:04	08 Aug 85	284	07:47
529501	04:39	22 Oct 85	05:13	22 Oct 85	58	04:41
529506	07:55	22 Oct 85	08:07	22 Oct 85	50	07:58
529601	15:15	23 Oct 85	15:24	23 Oct 85	50	15:15
529705	11:51	24 Oct 85	12:24	24 Oct 85	215	11:53
529902	04:34	26 Oct 85	05:12	26 Oct 85	497	04:34
534900	06:06	15 Dec 85	06:14	15 Dec 85	55	06:10

C.4 1986 XRP Flare Listing

Event #	Event Start Time (U.T.)	Date	Event Stop Time (U.T.)	Date	Peak Ca XIX Cts/s	(U.T.)
603303	21:40	02 Feb 86	21:54	02 Feb 86	75	21:43
603401	21:15	03 Feb 86	22:13	03 Feb 86	200	21:20
603506	07:01	04 Feb 86	07:38	04 Feb 86	2686	07:37
603719	23:08	06 Feb 86	23:43	06 Feb 86	66	23:27
603810	10:40	07 Feb 86	11:05	07 Feb 86	2406	10:56
603811	11:43	07 Feb 86	12:39	07 Feb 86	419	11:43
603812	13:17	07 Feb 86	13:17	07 Feb 86	89	13:17
603813	14:51	07 Feb 86	15:48	07 Feb 86	55	14:53
604100	12:01	10 Feb 86	12:48	10 Feb 86	96	12:01
604106	19:54	10 Feb 86	20:50	10 Feb 86	429	20:39
604109	21:27	10 Feb 86	22:24	10 Feb 86	125	21:28
604200	00:39	11 Feb 86	01:27	11 Feb 86	201	01:02
604201	00:43	11 Feb 86	01:31	11 Feb 86	19	00:43
604202	00:45	11 Feb 86	00:45	11 Feb 86	201	01:02
604207	03:54	11 Feb 86	04:41	11 Feb 86	452	03:54
604211	13:10	11 Feb 86	14:07	11 Feb 86	59	13:46
604218	23:00	11 Feb 86	23:33	11 Feb 86	634	23:18
604404	01:19	13 Feb 86	02:16	13 Feb 86	200	02:16
604405	03:01	13 Feb 86	03:01	13 Feb 86	374	03:01
604406	04:42	13 Feb 86	05:25	13 Feb 86	265	04:54
604505	15:03	14 Feb 86	15:45	14 Feb 86	68	15:45
604514	20:36	14 Feb 86	20:37	14 Feb 86	56	20:37
604607	17:46	15 Feb 86	17:53	15 Feb 86	99	17:48
604707	11:33	16 Feb 86	12:01	16 Feb 86	52	11:48
604710	22:38	16 Feb 86	22:47	16 Feb 86	50	22:46
604712	23:38	16 Feb 86	00:37	16 Feb 86	592	23:38
604800	01:14	17 Feb 86	02:18	17 Feb 86	208	01:14
605900	20:21	28 Feb 86	20:29	28 Feb 86	54	20:29
606001	15:50	01 Mar 86	15:53	01 Mar 86	53	15:53
606104	05:41	02 Mar 86	05:42	02 Mar 86	60	05:42
606103	20:58	02 Mar 86	20:58	02 Mar 86	103	20:58
606200	04:59	03 Mar 86	04:59	03 Mar 86	70	04:59
606501	04:15	06 Mar 86	04:16	06 Mar 86	68	04:15
611402	06:29	24 Apr 86	07:08	24 Apr 86	359	06:30
611406	14:20	24 Apr 86	14:40	24 Apr 86	181	14:21
612300	09:43	03 May 86	09:57	03 May 86	63	09:55
612301	10:30	03 May 86	11:26	03 May 86	55	10:37
619200	05:03	11 Jul 86	05:38	11 Jul 86	673	05:10
625900	09:26	16 Sep 86	09:40	16 Sep 86	54	09:27
628710	13:44	14 Oct 86	14:11	14 Oct 86	50	13:50
628705	14:46	14 Oct 86	15:04	14 Oct 86	63	14:50
629105	03:41	18 Oct 86	03:46	18 Oct 86	64	03:42
629206	00:07	19 Oct 86	01:02	19 Oct 86	2943	00:45
629207	01:40	19 Oct 86	02:40	19 Oct 86	635	01:40
629205	21:09	19 Oct 86	21:16	19 Oct 86	172	21:15
629702	12:38	24 Oct 86	12:44	24 Oct 86	871	12:40

C.4 1986 XRP Flare Listing (continued)

Event #	Event Start Time (U.T.)	Date	Event Stop Time (U.T.)	Date	Peak Ca XIX Cts/s	(U.T.)
630300	09:52	30 Oct 86	10:18	30 Oct 86	117	09:55
631000	05:36	06 Nov 86	05:40	06 Nov 86	54	12:35

C.5 1987 XRP Flare Listing

Event #	Event Start Time (U.T.)	Date	Event Stop Time (U.T.)	Date	Peak Ca XIX Cts/s	(U.T.)
709501	19:34	05 Apr 87	19:41	05 Apr 87	251	19:38
709600	04:28	06 Apr 87	04:41	06 Apr 87	594	04:33
709700	18:44	07 Apr 87	18:48	07 Apr 87	51	18:48
709800	21:15	08 Apr 87	21:29	08 Apr 87	51	21:22
710501	11:43	15 Apr 87	12:10	15 Apr 87	104	12:07
710502	12:47	15 Apr 87	13:44	15 Apr 87	69	12:48
710504	20:38	15 Apr 87	20:48	15 Apr 87	177	20:40
710710	02:29	17 Apr 87	02:54	17 Apr 87	90	02:33
710702	17:16	17 Apr 87	17:35	17 Apr 87	59	17:27
710712	23:35	17 Apr 87	23:50	17 Apr 87	253	23:48
710801	13:55	18 Apr 87	14:01	18 Apr 87	173	13:59
710800	14:37	18 Apr 87	15:34	18 Apr 87	139	14:45
710805	21:25	18 Apr 87	21:44	18 Apr 87	73	21:32
710900	14:40	19 Apr 87	15:09	19 Apr 87	71	14:42
712200	02:11	02 May 87	02:31	02 May 87	99	02:14
713901	12:52	19 May 87	13:05	19 May 87	119	12:57
714406	09:05	24 May 87	09:18	24 May 87	63	09:07
714427	15:18	24 May 87	15:24	24 May 87	55	15:21
714428	15:24	24 May 87	15:35	24 May 87	796	15:28
714424	17:57	24 May 87	18:09	24 May 87	68	18:00
714431	20:54	24 May 87	21:23	24 May 87	104	21:18
714500	03:17	25 May 87	03:24	25 May 87	51	03:18
714503	03:40	25 May 87	04:00	25 May 87	793	03:43
714505	04:59	25 May 87	05:16	25 May 87	85	05:09
714508	16:12	25 May 87	16:42	25 May 87	178	16:23
714511	18:53	25 May 87	19:16	25 May 87	297	19:00
714603	01:11	26 May 87	01:37	26 May 87	64	01:21
714608	06:05	26 May 87	06:28	26 May 87	124	06:13
714610	07:43	26 May 87	07:56	26 May 87	57	07:49
714617	20:01	26 May 87	20:51	26 May 87	137	20:10
714621	23:12	26 May 87	00:07	27 May 87	98	23:56
714702	00:44	27 May 87	01:18	27 May 87	51	01:13
714705	01:27	27 May 87	01:41	27 May 87	108	01:30
714706	18:00	27 May 87	18:09	27 May 87	66	18:01
714904	01:48	29 May 87	02:22	29 May 87	51	02:18
714900	16:16	29 May 87	16:27	29 May 87	87	16:22
716200	01:58	11 Jun 87	02:55	11 Jun 87	108	02:40
720300	15:24	22 Jul 87	15:43	22 Jul 87	58	15:31

C.5 1987 XRP Flare Listing (continued)

Event #	Event Start Time (U.T.)	Date	Event Stop Time (U.T.)	Date	Peak Ca XIX Cts/s	(U.T.)
720402	03:12	23 Jul 87	03:18	23 Jul 87	68	03:15
720403	07:15	23 Jul 87	07:33	23 Jul 87	104	07:24
720406	09:19	23 Jul 87	09:35	23 Jul 87	168	09:24
720411	18:13	23 Jul 87	18:28	23 Jul 87	127	18:16
720415	19:38	23 Jul 87	19:52	23 Jul 87	79	19:38
720500	00:37	24 Jul 87	01:17	24 Jul 87	167	00:37
720501	09:55	24 Jul 87	10:43	24 Jul 87	2324	10:01
721904	15:26	07 Aug 87	15:31	07 Aug 87	736	15:27
721905	17:04	07 Aug 87	17:05	07 Aug 87	172	17:05
721906	17:53	07 Aug 87	18:03	07 Aug 87	51	17:56
721909	19:35	07 Aug 87	19:52	07 Aug 87	819	19:46
721910	22:26	07 Aug 87	22:38	07 Aug 87	53	22:30
722001	01:31	08 Aug 87	02:02	08 Aug 87	1048	01:33
722004	03:34	08 Aug 87	04:05	08 Aug 87	1221	03:36
722006	04:52	08 Aug 87	05:25	08 Aug 87	77	05:08
722010	09:26	08 Aug 87	09:58	08 Aug 87	58	09:30
722011	10:20	08 Aug 87	10:23	08 Aug 87	80	10:22
722012	10:56	08 Aug 87	11:40	08 Aug 87	82	10:56
722013	12:31	08 Aug 87	12:44	08 Aug 87	71	12:37
722014	14:05	08 Aug 87	14:16	08 Aug 87	244	14:06
722016	17:18	08 Aug 87	17:33	08 Aug 87	50	17:25
722020	20:41	08 Aug 87	20:56	08 Aug 87	162	20:44
722023	22:20	08 Aug 87	22:33	08 Aug 87	155	22:24
722105	03:03	09 Aug 87	03:18	09 Aug 87	56	03:08
722107	06:11	09 Aug 87	06:43	09 Aug 87	96	06:21
722200	21:34	10 Aug 87	22:05	10 Aug 87	145	22:05
722300	11:12	11 Aug 87	11:54	11 Aug 87	120	11:18
722301	22:12	11 Aug 87	22:25	11 Aug 87	61	22:13
722500	02:54	13 Aug 87	03:16	13 Aug 87	62	03:01
722502	15:56	13 Aug 87	16:05	13 Aug 87	188	16:02
723302	05:31	21 Aug 87	05:39	21 Aug 87	76	05:31
723303	05:55	21 Aug 87	06:13	21 Aug 87	96	06:01
723500	02:53	23 Aug 87	03:13	23 Aug 87	54	02:54
723502	12:44	23 Aug 87	13:12	23 Aug 87	83	12:51
723503	23:14	23 Aug 87	23:55	23 Aug 87	640	23:15
723700	05:42	25 Aug 87	06:01	25 Aug 87	50	05:47
723800	00:48	26 Aug 87	00:52	26 Aug 87	71	00:51
724400	16:04	01 Sep 87	16:34	01 Sep 87	60	16:05
724600	15:39	03 Sep 87	15:48	03 Sep 87	55	15:42
724802	00:10	05 Sep 87	00:29	05 Sep 87	159	00:20
725000	07:35	07 Sep 87	07:43	07 Sep 87	166	07:38
725003	12:00	07 Sep 87	12:23	07 Sep 87	208	12:04
725012	19:55	07 Sep 87	20:06	07 Sep 87	52	19:57
725101	03:33	08 Sep 87	03:36	08 Sep 87	60	03:34
725103	08:39	08 Sep 87	08:40	08 Sep 87	92	08:40
725401	04:17	11 Sep 87	04:29	11 Sep 87	61	04:21

C.5 1987 XRP Flare Listing (continued)

Event #	Event Start Time (U.T.)	Date	Event Stop Time (U.T.)	Date	Peak Ca XIX Cts/s	(U.T.)
725402	18:10	11 Sep 87	18:26	11 Sep 87	65	18:16
728800	11:07	15 Oct 87	11:19	15 Oct 87	278	11:11
730812	17:21	04 Nov 87	17:38	04 Nov 87	888	17:22
730810	23:38	04 Nov 87	23:55	04 Nov 87	405	23:38
730900	04:56	05 Nov 87	05:17	05 Nov 87	2140	05:01
730903	18:32	05 Nov 87	18:57	05 Nov 87	50	18:49
731601	20:31	12 Nov 87	20:56	12 Nov 87	143	20:35
732200	03:16	18 Nov 87	03:24	18 Nov 87	610	03:19
732400	04:12	20 Nov 87	04:46	20 Nov 87	713	04:20
732405	23:30	20 Nov 87	23:36	20 Nov 87	444	23:35
732500	00:13	21 Nov 87	01:10	21 Nov 87	367	00:14
732504	17:56	21 Nov 87	18:26	21 Nov 87	2300	18:06
732505	19:03	21 Nov 87	19:43	21 Nov 87	71	19:04
733000	03:12	26 Nov 87	03:32	26 Nov 87	105	03:18
734400	14:06	10 Dec 87	14:16	10 Dec 87	59	14:09
734700	03:39	13 Dec 87	03:52	13 Dec 87	59	03:45
734701	06:28	13 Dec 87	06:53	13 Dec 87	59	06:32
734801	04:22	14 Dec 87	04:33	14 Dec 87	809	04:24
734800	21:15	14 Dec 87	21:26	14 Dec 87	56	21:21
735100	07:49	17 Dec 87	08:01	17 Dec 87	50	07:53
736400	01:42	30 Dec 87	02:18	30 Dec 87	202	01:52

C.6 1988 XRP Flare Listing

Event #	Event Start Time (U.T.)	Date	Event Stop Time (U.T.)	Date	Peak Ca XIX Cts/s	(U.T.)

(1988 listing was not yet compiled when this report was prepared.)